PH.D. DISSERTATION

# Human glutamate carboxypeptidases II and III

Michal Navrátil, MSc

Supervisor: Associate professor Jan Konvalinka, PhD

Department of Biochemistry

Faculty of Science

Charles University


Institute of Organic Chemistry and Biochemistry

Gilead Sciences & IOCB Research Centre

Academy of Sciences of the Czech Republic

# ACKNOWLEDGEMENTS

My gratitude and thanks go to:

- Associate professor Jan Konvalinka for providing a solid working environment and his freedom-spirited leadership and for critical evaluation of this Ph.D. dissertation.
- Dr. Petra "Mlochova" Mlčochová for initial supervision during my GCPII, and later GCPIII, project.
- Dr. Cyril Bařinka for growing larger crystals of GCPII-$FolGlu_n$ complexes, kindly introducing me into the crystallographic refinement procedure and sharing the two times cheaper variant of the radiometric GCPII assay.
- Dr. Jiří Schimer for the fast synthesis of β-citryl-L-glutamate (BCG), (S)-2-(3-(1,3-dicarboxypropan-2-yl)ureido)pentanedioic acid, and (2S,2'S)-2,2'-(carbonylbis(azanediyl))dipentanedioic acid.
- Prof. Barbara Slusher for her kind gift of the 2-PMPA inhibitor.
- Prof. Neil Harrison Bander for his kind gift of the monoclonal murine antibodies J415 and J591.
- Prof. David Spiegel for his ARM-P2,4,8 inhibitors, and especially for his excusing us not having him acknowledged by mistake in our publication.
- Prof. Clifford E. Berkman for 2-(sulfamoylamino)pentanedioic acid.
- Dr. Jacek Lubkowski for collecting data at the Advanced Photon Source of the Argonne National Laboratory.
- Dr. Evžen Bouřa for donating one aliquot of TEV protease.
- Dr. Lubomír Rulíšek, Dr. Tibor András Rokob and Dr. Ondřej Gutten for QM/MM calculations.
- Dr. Ondřej Přenosil for docking N-acetyl-L-aspartate into the N-acetyl binding site of GCPII.
- Dr. Jan Tykvart for his numerous aliquots of recombinant human GCPII and GCPIII.
- Dr. Pavlína Řezářová, Dr. Sebastian Zoll, Dr. Petr Pachl for collectind data at the Berlin BESSY synchrotron radiation facility, scaling them and creating an initial model by the molecular replacement method.
- Dr. Petr Pachl for helping me with the PDB syntax.
- Dr. Jan Hradílek for the synthesis of NAAG2 and other peptides.
- Associate professor Jiří Brynda, Dr. Pavlína Řezáčová and Dr. Petr Pachl for teaching me how to properly refine an X-ray model.

- Dr. Pavel Šácha for recloning the GCPII Glu424Ala sequence into the vector pMT/Bip/AviTEV/rhGCPII and helping me with the Ph.D. dissertation.
- Tomáš Knedlík for helping me with the Ph.D. dissertation.
- Dr. Hillary Hoffman for language help with our manusripts.
- Dr. Radko Souček for amino acid analysis of proteins and advice during the develepoment of my novel glutamate quantification methods.
- Mass Spectrometry laboratory for their competent sample analysis.
- Jana Starková for S2 cell cultivations.
- Karolína Šrámková for her excellent technical assistance.

Finally, I also thank my parents for coming to the bold conclusion that it is worth sponsoring my whole master studies. In my view, it has been an investition which makes a difference for me until present.

# CONTENTS

# ABSTRACT

The herein presented Ph.D. dissertation describes kinetic and structural characterization of human glutamate carboxypeptidases II and III (GCPII and GCPIII) using a complete panel of their natural substrates. These enzymes hydrolyze C-terminal glutamate from their substrates. They share 67 % sequence identity and also similar enzymatic activities.

This thesis quantitatively compares human GCPII and GCPIII in terms of their ability to hydrolyze the substrates N-acetyl-L-aspartyl-L-glutamate (NAAG), folyl-poly-γ-L-glutamic acids ($FolGlu_n$) and β-citryl-L-glutamate (BCG). We demonstrated that GCPIII hydrolyzes its substrates in a metal-dependent manner, that BCG is a specific substrate of GCPIII, and that NAAG and $FolGlu_n$ are specific substrates of GCPII. We also provide indirect biochemical evidence that GCPIII might feature a heterometallic active-site cluster. Additionally, we characterized the relevance of a surface exosite of GCPII, the arene-binding site (ABS), for the hydrolysis of $FolGlu_n$ substrates using mutagenesis and enzyme kinetics and showed that polymorphic His475Tyr variant of GCPII hydrolyzes $FolGlu_n$ substrates with the same kinetic parameters as the wild-type enzyme.

Furthermore, this thesis focuses on structural aspects of the substrate specificities of GCPII and GCPIII: we present the X-ray structures of inactive mutant of GCPII, Glu424Ala, in complex with its substrates $FolGlu_{1-3}$ and BCG. The $FolGlu_{1-3}$ complexes show how ABS residues of GCPII - Arg463, Arg511 and Trp 541 - participate in binding the aromatic pteridine ring of these substrates. These findings are complemented by high-level quantum mechanics/molecular mechanics (QM/MM) calculations which reveal how BCG probably binds to the active site of GCPIII and how a calcium-zinc heterometallic active-site cluster of GCPIII might look like.

Finally, we also quantified the kinetics of the N-acetyl-L-aspartyl-L-glutamyl-L-glutamate (NAAG2)-hydrolyzing activity of GCPII and GCPIII. Further, we quantified the tissue distribution of GCPII and GCPIII (in human tissues) both at the mRNA and the protein level, showing highest expression of GCPIII in testes and discussing its possible role as an iron chelator. The thesis is rounded off with structural characterizatin of lipophilic inhibitors of GCPII and the discovery of a moderately specific inhibitor of GCPIII.

# ABBREVIATIONS

| | |
|---|---|
| 2-PMPA | 2-(phosphonomethyl)pentanedioic acid |
| AAS | atomic absorbtion spectroscopy |
| ABS | arene-binding site |
| AP | action potential |
| ATP | adenosin triphosphate |
| BCG | β-citryl-L-glutamate |
| CNS | central nervous system |
| DISC1 | disrupted in schizophrenia 1 gene |
| DNA | deoxyribonucleic acid |
| dNTP | deoxynucleoside triphospates |
| EAAC1 | excitatory amino-acid transporter 3 |
| EAAT | excitatory acidic amino acid transporter |
| $EC_{50}$ | constant of 50 % effect |
| EDTA | ethylenediaminetetraacetic acid |
| EPE | (2S,3′S)-{[(3′-amino-3′-carboxy-propyl)-hydroxyphosphinoyl]methyl}-pentanedioic acid |
| FGCP | folyl-poly-γ-glutamate carboxypeptidase |
| $FolGlu_n$ | poly-γ-L-glutamylated folic acids (oxidized forms) |
| FOLH1 | folyl-poly-γ-glutamate hydrolase I |
| GABA | γ-aminobutyric acid |
| GCPII | glutamate carboxypeptidase II |
| GCPIII | glutamate carboxypeptidase III |
| $G_{i/o}$ | G protein inhibiting the production of cAMP from ATP |
| $G_{q/11}$ | G protein stimulating membrane bound phospholipase $C_\beta$ |
| GIRK channels | G protein-coupled inwardly-rectifying potassium channels |
| GLT-1 | solute carrier family 1 (glial high affinity glutamate transporter), member 2 |
| HO-1 | hemeoxygenase-1 |
| HPLC | High-performance liquid chromatography |
| HRP | horseradish peroxidase |
| $IC_{50}$ | constant of 50 % inhibition |
| IOCB | Institute of Organic Chemistry and Biochemistry |
| $k_{cat}$ | rate constant of enzymatic catalysis |

| | |
|---|---|
| $K_I$ | inhibition constant |
| $K_M$ | Michaelis-Menten constant |
| LTD | long-term depression |
| LTP | long-term potentiation |
| mGluR1/2/3/4/5/6/7/8/s | metabotropic glutamate receptor 1/2/3/4/5/6/7/8/a group |
| MnSOD | manganese superoxide dismutase |
| MPE | 2-[(3-{4-[(2-amino-4-hydroxy-pteridin-6-ylmethyl)-amino]-benzoylamino}-3-carboxy-propyl)-hydroxy-phosphinoylmethyl]-pentanedioic acid |
| OPA | orthophtalaldehyde |
| mRNA | messenger ribonucleid acid |
| NAA | N-acetyl-L-aspartate |
| NAAG | N-acetyl-L-aspartyl-L-glutamate |
| NAAG2 | N-acetyl-L-aspartyl-L-glutamyl-L-glutamate |
| NAAGS-I | NAAG synthetase I |
| NAAGS-II | NAAG synthetase II |
| NAALADase I | N-acetylated α-linked acidic dipeptidase I (GCPII) |
| NAALADase II | N-acetylated α-linked acidic dipeptidase II (GCPIII) |
| NAALA dipeptidase | N-acetylated α-linked acidic dipeptidase (GCPII) |
| NAALADase L | N-acetylated α-linked acidic dipeptidase L |
| NAALADase L2 | N-acetylated α-linked acidic dipeptidase L 2 |
| NMDA | N-methlyl-D-aspartate |
| NMDAR | N-methlyl-D-aspartate receptor |
| NMR | nuclear magnetic resonance |
| NR2A-NMDAR | NMDA receptor containing the variable NR2A subunit(s) |
| NR2B-NMDAR | NMDA receptor containing the variable NR2B subunit(s) |
| P1 | substrate's amino acid no. 1 (N-terminus) |
| P1' | substrate's amino acid no. 1 (C-terminus) |
| PAP | prostatic acidic phosphatase |
| PCP | phencyclidine |
| PCR | polymerase chain reaction |
| PDB | Protein Data Bank |
| PET/CT | combined positron emission tomografy and computer tomography imaging |

| | |
|---|---|
| PET/MRI | positron emission tomografy and magnetic resonance imaging |
| PDB | Protein Data Bank |
| PGCP | plasma glutamate carboxypeptidase |
| PSA | prostate specific antigen |
| PSM | prostate-specific membrane antigen |
| PSMA | prostate-specific membrane antigen |
| PSMAL | prostate-specific membrane antigen-like protein |
| PVDF | polyvinylidene fluoride |
| QM/MM | quantum mechanics and molecular mechanics |
| qPCR | quantitative polymerase chain reaction |
| RIMKLA | ribosomal modification protein K like protein A |
| RIMKLB | ribosomal modification protein K like protein B |
| ROS | reactive oxygen species |
| RPM | revolutions per minute |
| RT-PCR | reverse transcription polymerase chain reaction |
| S1 | site for amino acid no. 1 (N-terminus) |
| S1' | site for amino acid no. 1 (C-terminus) |
| SD | standard deviation |
| SDS | sodium dodecylsulfate |
| SDS-PAGE | sodium dodecylsulfate polyacrylamide gel electrophoresis |
| SPE | (2S)-2-{[(2-carboxy-ethyl)-hydroxy-phosphinoyl]methyl}-pentanedioic acid |
| TAE | Tris-Acetate-EDTA buffer |
| TGF-β | transforming growth factor β |
| TfR1 | transferrin receptor protein 1 |
| TfR2 | transferrin receptor protein 2 |
| $T_m$ | temperature midpoint for the unfolding transition |
| Tris | tris(hydroxymethyl)aminomethane |
| Tris-HCl | tris hydrochloride |
| UHPLC | ultra high performance liquid chromatography |
| xCT | cystine/glutamate transporter |
| X-ray | Röntgen radiation |

# 1. INTRODUCTION

## 1.1. Brief History of Glutamate Carboxypeptidases II and III

The discovery of glutamate carboxypeptidase II (GCPII) dates back to 1987 when an enzyme hydrolyzing N-acetyl-L-aspartyl-L-glutamate (NAAG) was isolated from rat forebrain synaptosomal membranes and called N-acetylated α-linked acidic dipeptidase (NAALA dipeptidase)[1]. First in 1993, the human orthologue of this enzyme was sequenced and cloned[2]. At that time, however, it was only called prostate-specific membrane antigen (PSM/PSMA) (according to its site of expression[3]) because its NAAG hydrolyzing activity became evident three years later[4]. Similarly, GCPII's capacity to hydrolyze poly-γ-L-glutamylated folic acids ($FolGlu_n$) in a carboxyexopeptidase manner was elucidated 1996[5], although the human protein capable of this reaction was isolated already in 1986[6].

Glutamate carboxypeptidase III (GCPIII), a less studied paralogue of GCPII, was likely discovered already 1983[7] in rat testes. Based on its capacity to hydrolyze β-citryl-L-glutamate (BCG) in a $Ca^{2+}$- and $Mn^{2+}$-dependent manner, researchers called it citrylglutamate hydrolyzing enzyme. Then, it took another 18 years to reveal that citrylglutamate hydrolyzing enzyme is in fact GCPIII[8].

## 1.2. Human Glutamate Carboxypeptidase II

Human glutamate carboxypeptidase II (GCPII) is also known as prostate-specific membrane antigen (PSMA), N-acetylated-alpha-linked acidic dipeptidase I (NAALADase I or NAALA dipeptidase), folyl-poly-γ-glutamate hydrolase I (FOLH1) and folyl-poly-γ-glutamate carboxypeptidase (FGCP). These names reflect gradual discovery of the individual enzymatic activities and tissue localizations and the fact that GCPII is a multifunctional protein (see following sections).

The coding sequence of GCPII (FOLH1 gene) localizes to the 11p11.2 locus[9] and consists of 19 exons spanning approximately 60 kb of genomic DNA[10]. Interestingly, the enhancer responsible for androgen-dependent down-regulation of expression of GCPII is located within the third intron[11,12].

### 1.2.1. GCPII mRNA and Splicing Variants

At the mRNA level, GCPII (PSMA) is most abundant in normal prostate and approximately 10 fold lower expression is also found in liver, kidney and brain[13]. At least five splice variants of GCPII are

known[14], but there is a number of other splice variants (Navratil, V. *et al.*, manuscript in preparation).

## 1.2.2. GCPII Protein

At the protein level, GCPII (EC 3.4.17.21) is a transmembrane type II glycoprotein[15]. It is a zinc-binuclear metaloprotease[16] which has to be glycosylated in order to maintain its activity[17]. Recombinant protein can be obtained at moderate to high yields using the S2 *Drosophila* expression system[18]. Its active form is a dimer[19] and each monomer consists of 750 amino acids[2]. Both active-site zinc atoms, in contrast to GCPIII (see section 1.3.3.2), have 100 % occupancy[16], and the enzyme shows no metal-dependent enzyme kinetics (Navratil, M., Tykvart. J., unpublished observation)[8].

### 1.2.2.1. Enzymatic Activities

GCPII possesses several enzymatic activities. The longest known activity is hydrolysis of NAAG (Figure 1A) to N-acetyl-L-aspartate (NAA) and L-glutamate[1]. Although less known, GCPII catalyzes also hydrolysis of C-terminal γ-linked L-glutamic acid units from dietary $FolGlu_n$[5] (Figure 1B). Very recently, it has also been shown that mouse GCPII hydrolyzes N-acetyl-L-aspartyl-L-glutamyl-L-glutamate (NAAG2, Figure 1C) to NAAG and L-glutamate[20]. As a result, it is no surprise that GCPII has several names (see 1.2). Since GCPII was found to be upregulated in cancerous prostate tissue[21] before the discovery of its NAAG and $FolGlu_n$ hydrolyzing activity[4,5], the name prostate-specific membrane antigen (PSMA or PSM) is the name of choice in medical literature[22].

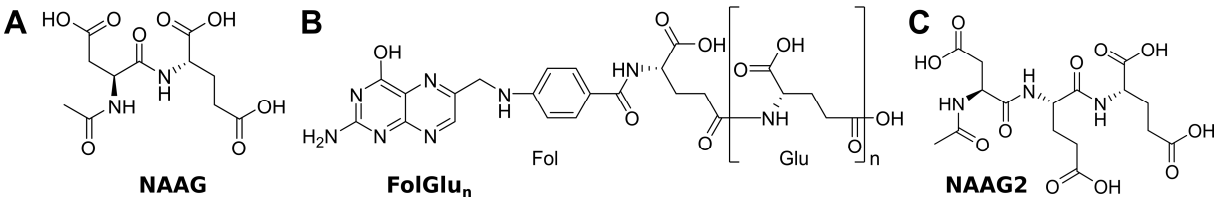


**Figure 1: Molecular structures of NAAG, $FolGlu_n$ and NAAG2.** (A) N-acetyl-L-aspartyl-L-glutamate (NAAG). (B) Folyl-poly-γ-L-glutamic acids ($FolGlu_n$). (C) N-acetyl-L-aspartyl-L-glutamyl-L-glutamate (NAAG2).

#### 1.2.2.1.1. NAAG-hydrolyzing Acitivity

NAAG-hydrolyzing activity of GCPII is the best studied one (structure of NAAG is shown in the Figure 1A). The $K_M$ value is reported to be around 0.4 - 1 μM and the $k_{cat}$ value around 0.6 - 1 $s^{-1}$ [17,23], depending on the buffer used for activity assay. Activity of GCPII has been quantified only

using a $^{3}$H-labelled NAAG (N-Acetyl-L-aspartyl-L-glutamate-3,4-$^{3}$H) in a sample-by-sample[1,24] or 96-well set-up[25]. pH optimum has been twice reported to lie around 7.5 - 8.0[17,26]. Using X-ray crystallography and quantum mechanics and molecular mechanics (QM/MM), the reaction mechanism underlying the hydrolysis of NAAG has been proposed[16]. According to this study, the two active-site zinc atoms function to bridge an activated water molecule (likely $OH^-$ [16,27]) and the key residue Glu424 serves as a "proton shuttle" to abstract one proton from the active-site catalytic water molecule and transfer it to the amide nitrogen of the C-terminal glutamic acid moiety whereby the $OH^-$ nucleophile is then free to attack the amidic α-carboxylate of the leaving N-acetyl-L-aspartate.

### 1.2.2.1.2. FolGlu$_n$-hydrolyzing Acitivity

Although the enzyme from human jejunum catalyzing the hydrolysis of FolGlu$_n$ (called also pteroyl-poly-γ-glutamates, see Figure 1B for structure) was isolated already 1986[6], the quesion of full enzymatic characterization of GCPII's FolGlu$_n$ hydrolyzing activity remains largely unaddressed: In the above mentioned study, the enzyme was called human jejunal brush-border pteroylpolyglutamate hydrolase and it was found out that this enzyme cleaves FolGlu$_1$, FolGlu$_2$ and FolGlu$_6$ with a $K_M$ value of 0.6 μM. The folyl-poly-γ-glutamate carboxypeptidase activity has been attributed to GCPII in 1996[5], but only the pH optimum curve of FolGlu$_n$ hydrolyzing activity has been determined. It is claimed to have two maxima at pH 5.0 and 8.0[5]. This is surprising, because one would expect the reaction mechanism to be identical to NAAG hydrolysis[16] and to have the same pH optimum of 7.5 - 8.0[17,26]. Furthermore, there is no follow-up study confirming whether the enzyme isolated in 1986 was GCPII.

### 1.2.2.1.3. NAAG2-hydrolyzing Acitivity

While NAAG is known since 1965[28] (see also section 1.1), NAAG2 and its cleavage by mouse GCPII has only been described 2011[20] (structure of NAAG2 is shown in the Figure 1C). Kinetic parameters of this enzymatic reaction catalysed by mouse GCPII were determined 2013[29], but using only thin-layer chromatography as a quantification method. NAAG2 hydrolyzing activity of human GCPII has not been investigated so far.

### 1.2.2.1.4. BCG-hydrolyzing Acitivity

The long-known dipeptide β-citryl-L-glutamate (BCG, Figure 2)[30] is cleaved by mouse GCPIII in a $Ca^{2+}$ and $Mn^{2+}$ dependent manner[8]. It has also been established that mouse GCPII does not hydrolyze BCG[8].

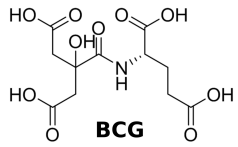


**Figure 2: β-citryl-L-glutamate (BCG).**

## 1.2.2.2. Inhibitors

Inhibitors of GCPII feature a noncleavable peptidomimetic connected mostly to glutamate in the P1' position. The peptidomimetic can be a sulfate[31], hydroxamate[32], phosphate, phosphoramidate[33] or urea derivative[34]. Although glutamate in the P1' position is a simple and usually high affinity choice[32], other quite different moieties are also possible[32] (see below, section 1.2.2.3.2.2). In the opposite direction, for the P1 position and beyond, GCPII does not require stringent structural features, although one addtional carboxyl group significantly enhances the inhibitor's binding[32] (likely due to favourable interactions with Arg534 and Arg536 which, for example, bind the β-carboxylate of aspartate moiety of NAAG in the x-ray structrure of GCPII in complex with NAAG, PDB entry 3BXM[16]).

## 1.2.2.3. X-ray Structures with Substrates and Inhibitors

For GCPII, one low-resolution[35], two medium-resolution[36,37], and one high-resolution crystallization conditions are known[38]., The low-resolution condition was published in 2005 and since that time, a plethora of GCPII structures with various inhibitors appeared in the scientific literature[16,18,39–45].

Structure of the extracellular portion of GCPII reveals that the protein is composed of three domains (Figure 3), the protease domain (amino acid no. 57 – 116 and 352 – 590), the apical domain (amino acid no. 117 – 351) and the C-terminal domain (also dimerization domain, amino acid no. 591 – 750, Figure 3)[35]. There is also a short disordered stretch (amino acid no. 44 - 56) tethering the protein to the membrane via a single pass transmembrane helix (amino acid no. 20 - 43), and a short cytoplasmic part (amino acid no. 1 - 19)[15].

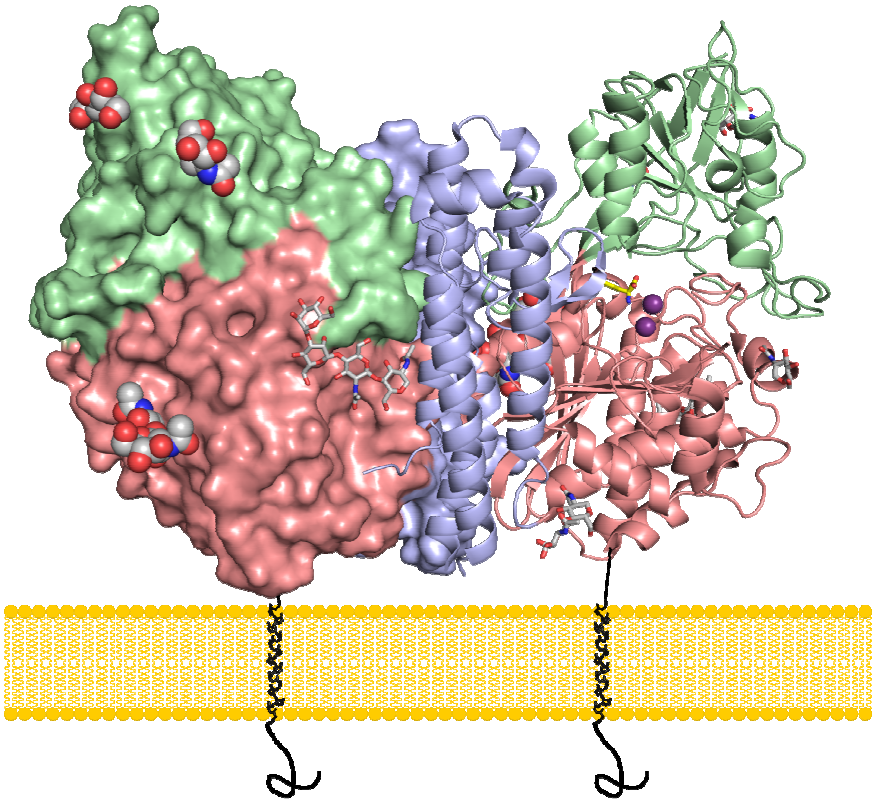

**Figure 3: Domain organization of GCPII and its topology.** GCPII is a transmembrane type II glycoprotein, with its monomers consisting of three domains, from N-terminus to C-terminus: The protease domain (pink), apical domain (green) and dimerization domain/C-terminal (blue). Left monomer is shown in surface representation (saccharides as gray spheres), right monomer in cartoon representation (saccharides as gray sticks). Active-site zinc atoms (right monomer) are shown as purple spheres. Right monomer is depicted with glutamate bound in the active site (yellow sticks). Please note the short intracellular N-termal part. Structural image was created using PyMol[46].

The protein has two larger functional components, one called "glutarate sensor" (amino acids 692 – 704)[36] and the other one called "entrance lid" (amino acids 541 – 548)[40], see Figure 4. The glutarate sensor acts to firmly "grip" the glutamic acid moiety of the substrate in the active site because ligand-free GCPII (PDB entry 2OOT)[38] or GCPII with its substrate NAAG (PDB entry 3BXM)[16] or glutamate (PDB entry 2C6G)[36] bound in the active site features the glutarate sensor in the closed conformation (Figure 4A). On the other hand, the GCPII-phosphate complex (likely approximating how the protein might look like when the substrate is being attacked by the active site nucleophile $OH^-$, see also section 1.2.2.1.1) features the open conformation of the glutarate sensor (PDB entry 2C6P[36], Figure 4A). α-carbons of Tyr692 and Ser704 represent the „hinges“ of the glutarate sensor, i.e. sites where the translational movements of this loop are made possible through rotation of adjacent peptide planes. The entrance lid has been captured even in three conformations (Figure 4B) and its hinges are α-carbons of Asn540 and Tyr549. The closed conformation is observed when small substrates/ligands bind, e.g. NAAG (PDB ID 3BXM)[16], the open conformation when some larger molecule is bound, e.g. an unhydrolyzable analogue of $FolGlu_1$ (MPE[40], PDB entry 3BI1),

and the half-opened conformation when three urea-based inhibitors are bound (PDB entries 4NGM, 4NGP and 4NGS[44]), see Figure 4B. In addition, the entrance lid may also be disorderd like when phosphate or glutamate is bound in the active site (PDB entries 2C6P or 2C6G, respectively)[36].

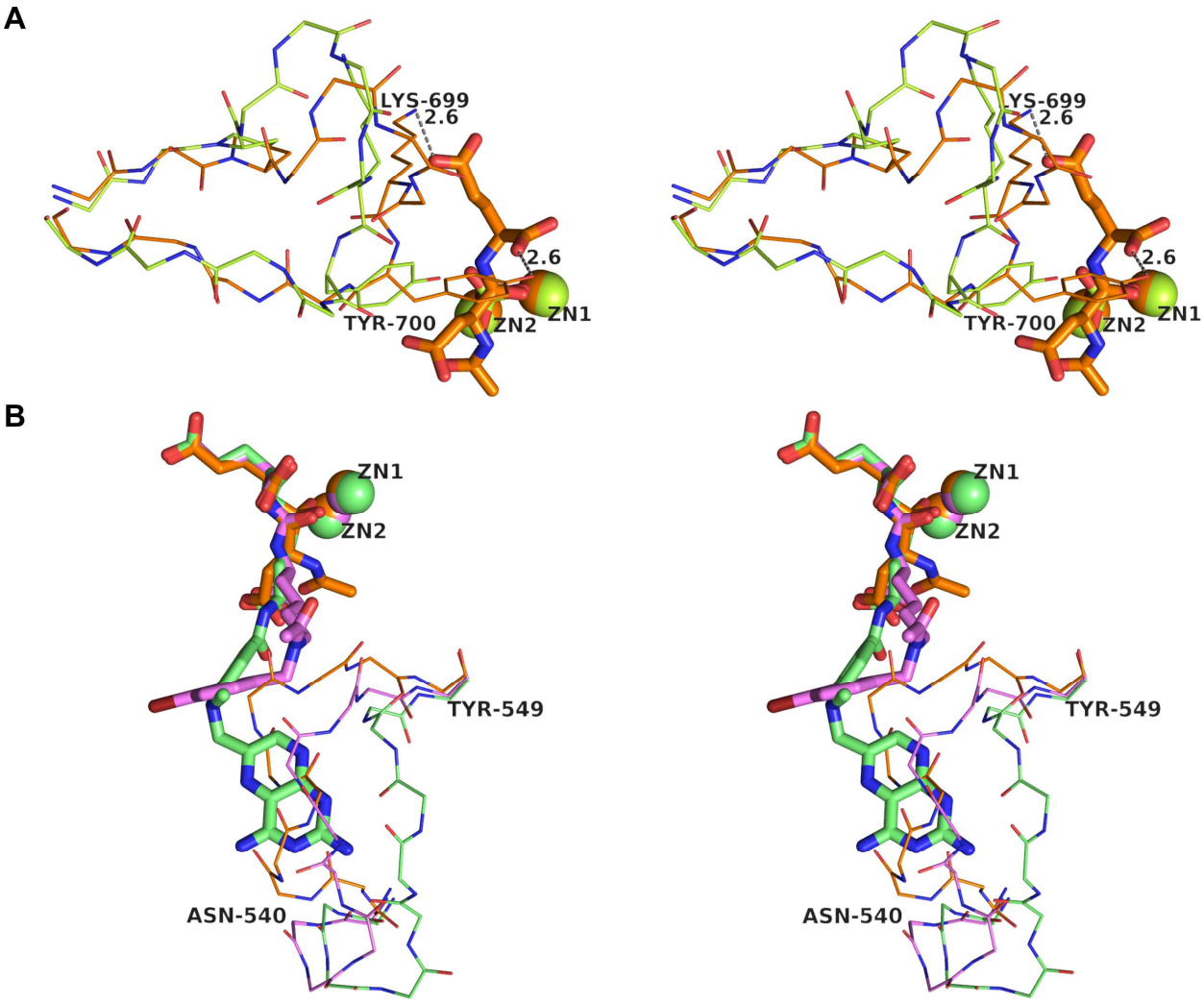


**Figure 4: Flexible parts of GCPII - the glutarate sensor and the entrance lid.** Images are rendered in cross-eye stereo representation. Active-site zinc atoms are depicted as spheres. Binding distances are indicated by gray dashed lines and a number in Å. Images were created using PyMol[46]. (A) Comparison of the open (GCPII-phosphate complex, colored orange, PDB entry 2C6P[36]) and closed conformation (GCPII-Glu424Ala-NAAG complex, colored light green, PDB entry 3BXM[16]) of the glutarate sensor. Substrate/phosphate anion is shown in stick representation, glutarate sensor as mainchain lines. Lys699 and Tyr700 are depicted as whole residues. (B) Overlay of the X-ray structures of the GCPII-Glu424Ala-NAAG complex (orange, PDB entry 3BXM), GCPII-urea inhibitor complex (pink, PDB entry 4NGM[44]), and GCPII-MPE (unydrolyzable analog of $FolGlu_1$, green, PDB entry 3BI1[40]), showing that the entrance lid (amino acids 540 - 549) can adopt three conformations, namely closed, half-open, and open, respectively. Note that the pteridine ring of MPE occupies space in which it would clash with both closed and half-open conformation of the entrance lid.

The active site is built of substrate-binding and zinc-chelating amino acids. The two active-site zinc atoms are coordinated in a tetrahedral fashion by His553, Asp387, Asp453, His377, Glu425[35,36,38] at approximately 2.0 Å distances (Figure 5A). In between the two zinc atoms, an $OH^-$ anion/$H_2O$ is

bridged (also at 2.0 Å distances)[16] so that it co-forms the tetrahedral zinc-coordination framework. The bridging $OH^-/H_2O$ serves to cleave the scissile petide bond[16] and represents thus a centre surrounded by the S1' and S1 site. The S1' site, binding usually the C-terminal glutamic acid moiety, is composed of Lys699, Tyr700, Phe209, Arg210, Asn257, Gly427, Leu428 and Gly518 (Figure 5B). The S1 site, binding either N-acetyl-L-aspartate moiety[16] or a glutamate moiety[40], is composed of Asn519, Arg534, Arg536, Tyr552 and Zn1 (Figure 5B).

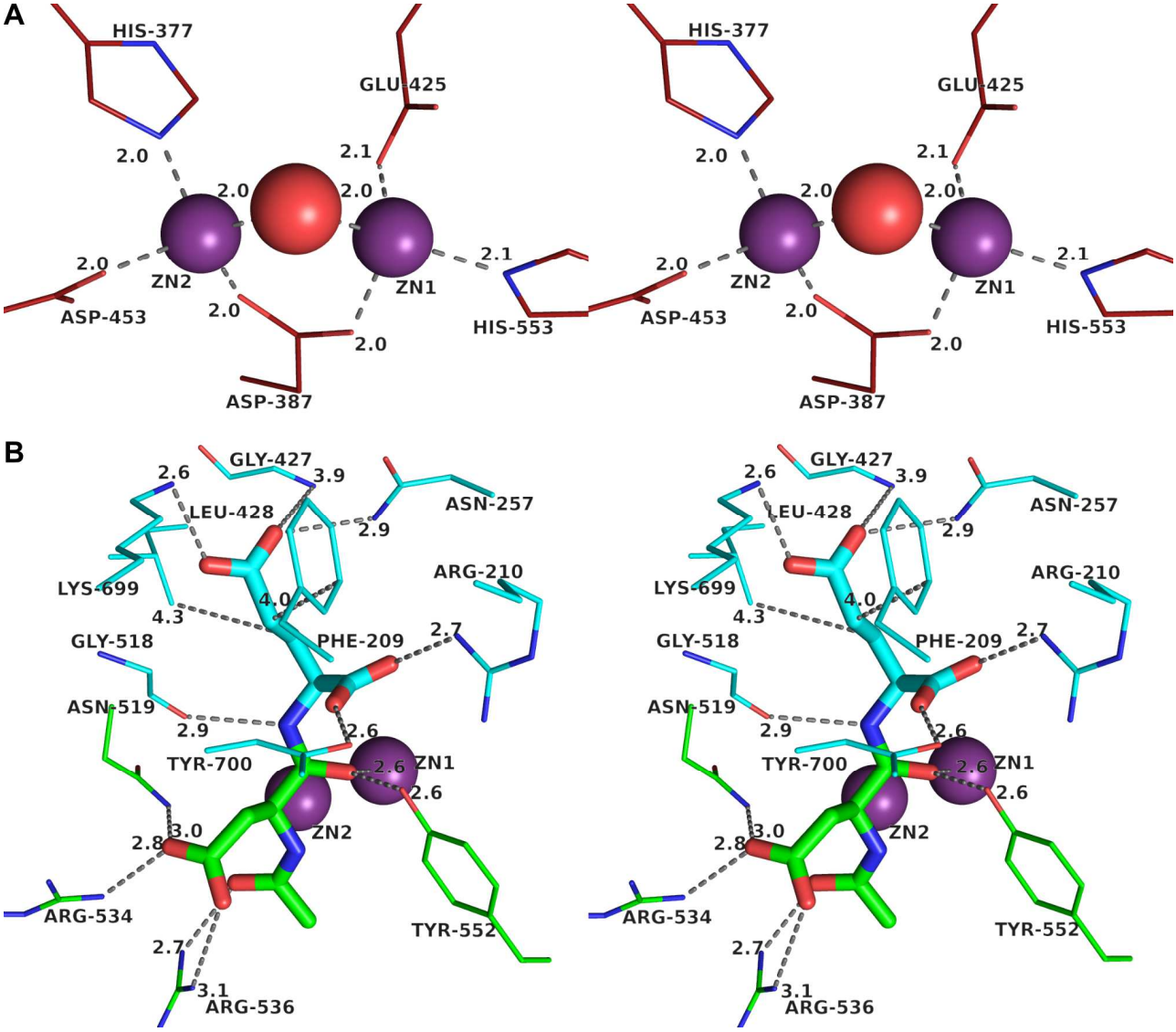


**Figure 5: Spatial arrangement of the active site residues, rendered in cross-eye stereo representation.** Active-site zinc atoms are depicted as purple spheres. Binding distances are indicated by gray dashed lines and a number in Å. Both panels are derived from the X-ray structure of the GCPII-Glu424Ala-NAAG complex (PDB entry 3BXM[16]). Images were created using PyMol[46]. (A) Zinc-coordinating residues, including active-site water. Active site water is shown only as its oxygen atom, in sphere representation. Zinc atoms are coordinated in a nearly perfect tetragonal manner and the active site water molecule is one of the ligands. (B) S1' (cyan) and S1 (green) sites of GCPII. NAAG is shown in stick representation. Tyr700 is truncated to provide a clearer view.

There are also two exosites in the GCPII structure. One of them is located near the surface of GCPII, formed by amino acids Arg463, Arg511 and Trp541[43] (see 1.2.2.3.2.4) whereby Trp541 is part of the entrance lid[40]. These three amino acids were shown to be able to bind dinitrophenyl moiety, as documented by a series of X-ray structures of GCPII in complex with a classic urea inhibitor linked to the dinitrophenyl moiety[43] (refer to section 1.2.2.3.2.4 for structural images). This exosite has thus been called arene-binding site (ABS)[43]. The other exosite, called hydrophobic accessory pocket, is located near the S1 site and is discussed in connection with X-ray structures of GCPII in complex with inhibitors (see section 1.2.2.3.2.5).

It is also noteworthy that many of the available structures of GCPII contain electron desity map for several N-glycosidically linked saccharide moieties.

## 1.2.2.3.1. Complex with the Substrate NAAG

After observing that the activity of GCPII can be completely abolished by the mutation Glu424Ala[16], it was possible to obtain a high resolution X-ray structure of GCPII complexed with its substrate NAAG (PDB ID 3BXM)[16]. QM/MM calculations based on this structure elucidated also the probable reaction mechanism[16] (see section 1.2.2.1.1). This 3D structure further reveals that the whole substrate is fixed by a number of interactions (Figure 5B) and that both the glutarate sensor and the entrance lid are in the closed conformation[16] (Figure 4A,B).

## 1.2.2.3.2. Complexes with Inhibitors

Because GCPII is under intensive investigation as a candidate drug target (see section 1.2.3.1), tens of X-ray structures with various inhibitors are already available (see following sections 1.2.2.3.2.1 - 1.2.2.3.2.5).

### 1.2.2.3.2.1. Transition State Analogues and Unhydrolyzable Peptide Bond Analogues

2-(phosphonomethyl)pentanedioic acid (2-PMPA), a transition state analogue and first potent inhbitor of GCPII, was synthesized and characterized already 1996[47]. X-ray structure of GCPII with 2-(phosphonomethyl)pentanedioic acid has been solved altogether three times at resolutions 2.2 Å (PDB entry 2JBJ[37]), 1.7 Å (PDB entry 2PVW[39]) and 1.6 Å (PDB entry 3RBU[18]). Although it might seem that the phosphoryl moiety could be the most important unit providing the high-affinity binding [$K_s$ of $Zn_3(PO_4)_2$ is $9 \cdot 10^{-33}$], it is probably not the case because 2-(phosphonomethyl)succinic acid, featuring not a glutamate but instead an aspartate analogue, possesses a potency lower by more than three orders of magnitude[47]. On the other hand, phosphate itself inhibits with $IC_{50}$ of 100 μM[1] to 10 μM[17] while L-glutamate with $IC_{50}$ of only 428 μM[39].

X-ray structures of GCPII with three unhydrolyzable transition state analogues of its natural substrates, 2-[(3-{4-[(2,4-diamino-pteridin-6-ylmethyl)-amino]-benzoylamino}-3-carboxy-propyl)-hydroxy-phosphinoylmethyl]-pentanedioic acid (abbreviated as MPE[40], analogue of $FolGlu_1$), (2S,3′S)-{[(3′-amino-3′-carboxy-propyl)-hydroxyphosphinoyl]methyl}-pentanedioic acid (EPE[40], analogue of a di-γ-L-glutamate moiety of $FolGlu_{>1}$ substrates), (2S)-2-{[(2-carboxy-ethyl)-hydroxy-phosphinoyl]methyl}-pentanedioic acid (SPE[40], analogue of NAAG) reveal that the mode of binding of the P1' moiety (pentanedioic acid) of all three inhibitors is virtually identical to the arrangement seen when NAAG is bound to inactive GCPII Glu424Ala (PDB entry 3BXM[16], Figure 6). Further, the comparison of complexes of GCPII with SPE and NAAG shows that NAAG and SPE bind in an almost identical way, and complexes of GCPII with MPE and EPE show how $FolGlu_1$ might probably bind to GCPII (Figure 6).

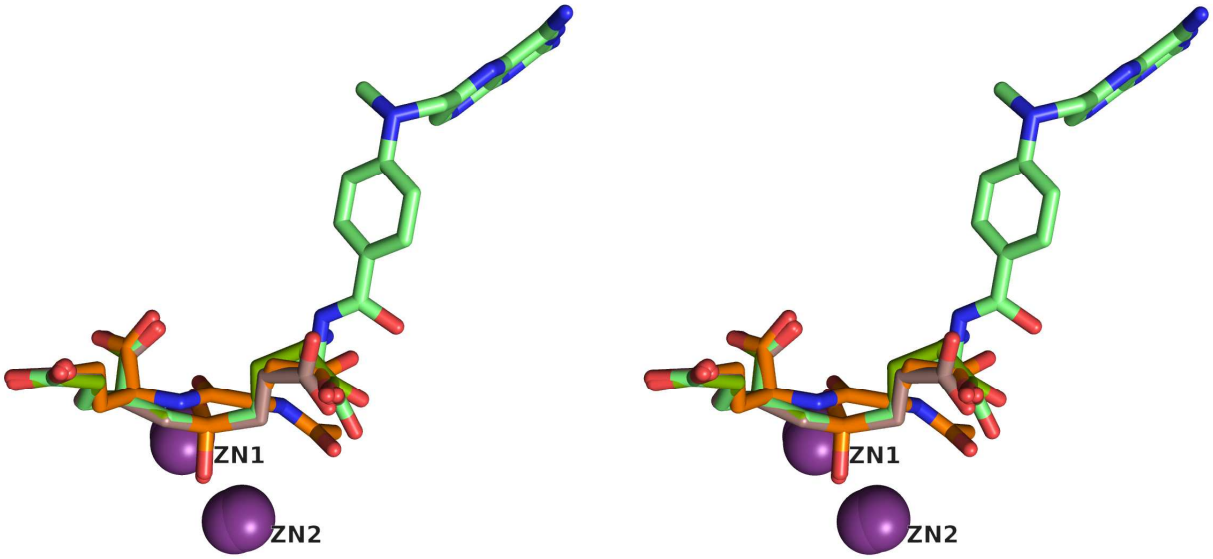


**Figure 6: Structural overlay of the GCPII-Glu424Ala-NAAG complex with unhydrolysable transition state analogs of NAAG and $FolGlu_1$.** The image is rendered in cross-eye stereo representation. Zinc atoms are depicted as purple spheres. NAAG (PDB entry 3BXM[16]) is colored orange, and the inhibitors MPE and EPE in hues of green and SPE light pink (see the maintext for exact description of the inhibitors). MPE and EPE bind in a so similar way that they are hardly distinguishable. Binding of both the P1' moieties (glutamate) and P1 moieties is very similar. Note that one oxygen of the phosphonate replaces the active-site water molecule. The structural image was created using PyMol[46].

Unhydrolyzable analogues of peptide bond which are the most frequently seen in structures of GCPII include urea. First four structures with inhibitors containing the urea moiety were published 2008[41]. In all these structures, urea and glutamic acid moiety is positioned always the same way.

### 1.2.2.3.2.2. Substrate Requirements of the S1' and S1 Sites

Although GCPII, as its name suggests, requires a glutamate in the P1' position, this requirement is not absolute. The S1' site can freely bind also other molecular patterns like 1-carboxycyclopropyl (PDB entry 4OC0[45], Figure 7A), (1S)-1-carboxy-2-[(2S)-oxiran-2-yl]ethyl (PDB entry 4OC1[45], Figure 7B), (1S)-1-carboxybut-3-yn-1-yl (PDB entry 4OC2[45], Figure 7C), (1S)-1-carboxy-2-(furan-2-yl)ethyl (PDB entry 4OC3[45], Figure 7D), (1S)-1-carboxy-2-(pyridin-4-yl)ethyl (PDB entry 4OC4[45], Figure 7E), (S)-carboxy(4-hydroxyphenyl)methyl (PDB entry 4OC5[45], Figure 7F) or 3,5-dioxo-[1,2,4]oxadiazolidin-2-yl (quisqualate, PDB ID 2JBK[37], Figure 7G). Most structures, however, feature a glutamate (PDB entry 2C6C, 2C6P[36], 3BI1[40], 2XEI, 2XEG, 2XEF, 2XEJ[43], 4NGM, 4NGR, 4NGN, 4NGP, 4NGQ, 4NGS, 4NGT[44]) or a glutamate-like moiety (structures with the inhibitor 2-PMPA, PDB entry 2JBJ[37], 2PVW[39] and 3RBU[18]) in the S1' site.

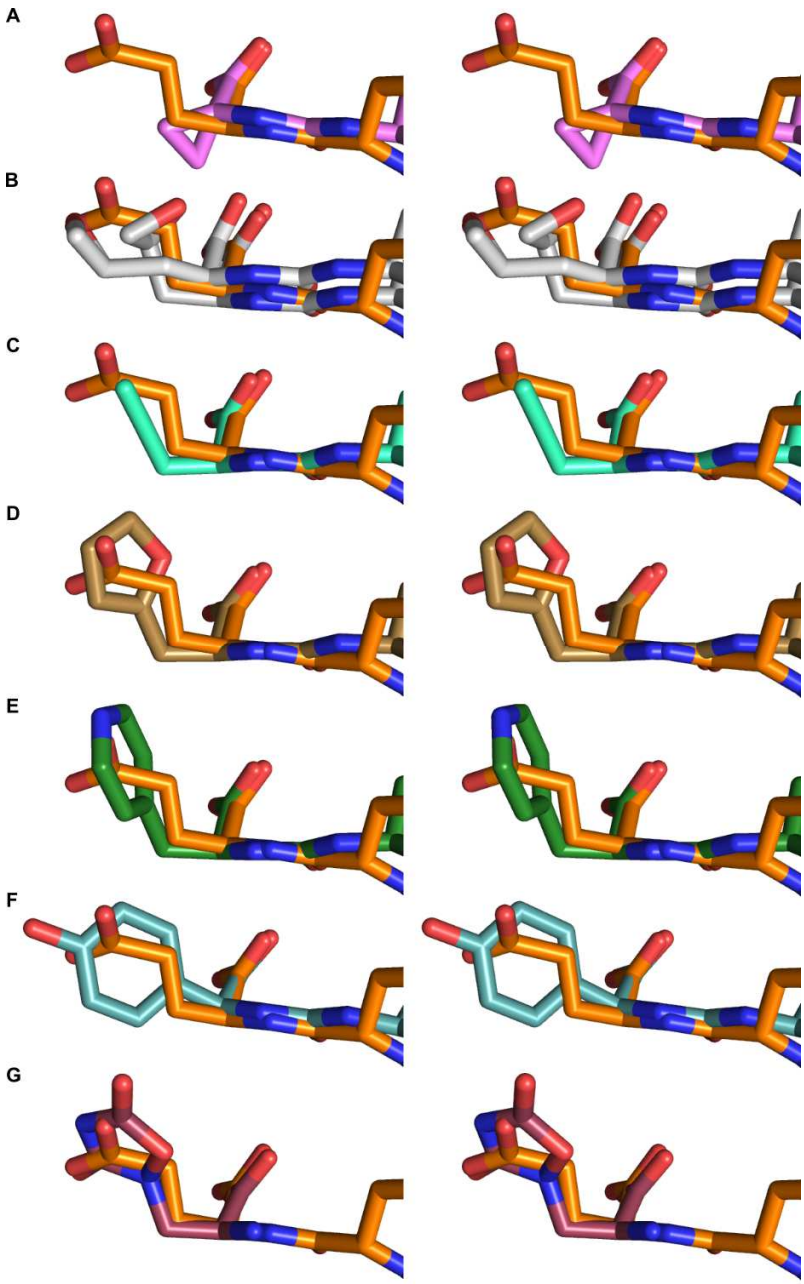


**Figure 7: Structural overlay of GCPII-inhibitor complexes featuring non-glutamate P1' moieties.** Only the P1' moiety is shown, always in overlay with glutamate moiety of NAAG (of the GCPII-Glu424Ala-NAAG complex, PDB entry 3BXM[16]). Structural images were created using PyMol[46]. Shown here are the P1' moieties of inhibitors in complex with GCPII, deposited as PDB entries 4OC0 (A), 4OC1 (B), 4OC2 (C), 4OC3 (D), 4OC4 (E), 4OC5 (F), and 2JBK (G).

This large variety of structures has been solved because all currently available GCPII inhibitors are negatively charged and thus not orally available[32,34] and unable to cross blood-brain barrier (see also section 1.2.3.1.3). Hence finding some uncharged moieties like the ones mentioned above and characterizing them structurally was a first step in rational drug design (which was a predecessor approach to the current effort of developing prodrug forms of already available inhibitors, see section 1.2.3.1.3).

The S1 site allows for a more substantial variability of the P1 moieties than the S1' site does[40] (see also section 1.2.2.2). One reason for this is thought to be the flexibility of Arg536[41]. Structures of GCPII with inhibitors thus contain moieties as diverse as 4-iodobenzyl (PDB entry 2C6C[36]), lysine (PDB entries 4OC0, 4OC1, 4OC2, 4OC3, 4OC4, 4OC5[45], 4NGM, 4NGR, 4NGN, 4NGP, 4NGQ, 4NGS, 4NGT[44] and 4OME[48]), (1H-1,2,3-triazol-1-yl)-1-carboxypentyl (PDB entries 2XEI, 2XEG, 2XEF, 2XEJ[43]) or analogue of γ-linked glutamate (PDB entry 3BI1[40]).

### 1.2.2.3.2.3. Potential S2 Site

Because of lacking structural data, the S2 site and its amino acid side chains cannot be conclusively defined yet. However, based on the above mentioned structures of GCPII with MPE (analogue of glutamylmethotrexate, PDB entry 3BI1[40], see above for section 1.2.2.3.2.1) and with a *closo*-carborane[48] inhibitor (PDB entry 4OME[48]), it can be at least speculated that the S2 site might be the space which is occupied by the phenyl ring of MPE or the carborane moiety, respectively, mainly because it is located right next to the S1 site, it is distinct from any other pocket (see sections 1.2.2.3.2.4 through 1.2.2.3.2.5) and represents a "bridge" between S1 and arene binding site which is at the surface. If true, then it would be delineated by the side chains of Arg463, Glu457, Tyr700 and Trp541 and the backbone carbonyl of Lys207.

### 1.2.2.3.2.4. Arene-binding Site Moieties

Binding of only one inhibitor moiety, dinitrophenyl[43] (PDB entries 2XEF, 2XEG, 2XEI), to the arene-binding site (ABS) (see section 1.2.2.3) has been characterized at the structural level (Figure 8). Although this distal moiety is attached to the urea-based inhibitor via a linker composed of different number of polyethylene glycol units, the dinitrophenyl moiety is always stacked between the ABS residues Trp541 and Arg511. Arg463 was claimed to be also part of the ABS[43], but its contribution to the overall binding seen in these three X-ray structures, as assessed by distances between the aromatic moiety and this amino acid being larger than 4.0 Å, is probably rather marginal.

Interestingly, X-ray structure of GCPII in complex with MPE (unhydrolyzable analogue of $FolGlu_1$, see also above, 1.2.2.3.2.1, PDB entry 3BI1)[40] shows that the inhibitor's aminopterine moiety, which is another aromatic moiety and would not surprise to be employing the ABS residues as well, is somewhat disordered, lies outsite the ABS, and rather marginally interacts with Trp541 only (Figure 8).

Non-canonical binding of a moiety into the ABS has been described in structural terms only recently[49]. In this X-ray structure (PDB entry 4X3R[49]), a moiety composed of linearly connected

pyridine, piperazine and benzene rings ("rigid arm"[49]) binds to Arg463 and Arg511 in a standard way, but to Trp541 only in way of T-shape stacking interaction[49] (Figure 8). This moiety confers extraordinarily high selectivity toward GCPII (over GCPIII), the highest reported so far[49] (for a quantitative information, see section 1.3.5).

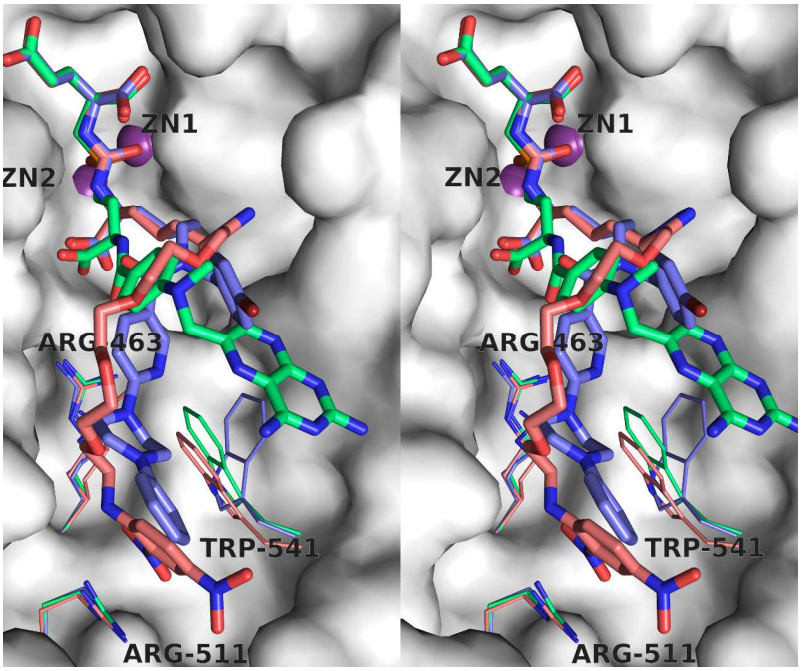


**Figure 8: The arene-binding site (ABS) of GCPII - structural overlay of three known moieties targeting the ABS.** The picture is rendered in cross-eye stereo representation. The arene binding site amino acid residues Arg463, Arg511 and Trp541 are shown as lines. Overlaid structures are derived from GCPII-inhibitor complexes deposited as PDB entries 3BI1[40] (inhibitor is shown as green sticks; its name is abbreviated as MPE and its structure is introduced in the section 1.2.2.3.2.1 with a stereo image), 4X3R[49] (inhibitor is shown as blue sticks; only one conformation of its electron-dense part is shown) and 2XEG[43] (inhibitor is shown as pink sticks; its name is abbreviated as ARM-P4 and its formula is introduced in the section 4.2.3). Arg463 forms the ABS only marginally. Please note that only the ARM-P4 inhibitor fits perfectly into the arene-binding site. MPE lies even outsite of it, but at least interacts with the Trp541 residue. The image was created using PyMol[46].

### 1.2.2.3.2.5. Hydrophobic Accessory Pocket

Hydrophobic accessory pocket has been described in early structural studies of GCPII[41]. It is the space which is reported to become available when Arg536 transits to the "binding" conformation[41] from flopping between two conformations as seen in the ligand-free structure of GCPII (the other one called "stacking", Figure 9A, PDB entry 2OOT)[38] on a concurrent shift of Arg463 from the "down" to the "up" conformation enforced onlyby binding of an adequate moiety into the hydrophobic accessory pocket, as seen e.g. in some structures with inhibitors[41] (and also PDB entry 4NGQ)[44] (Figure 9B). If, on the other hand, inadequate molecule binds, e.g. NAAG (PDB entry 3BXM[16]), then the hydrophobic accessory pocket does not open - it remains half-closed by Arg463 in the "down" position (Figure 9C).

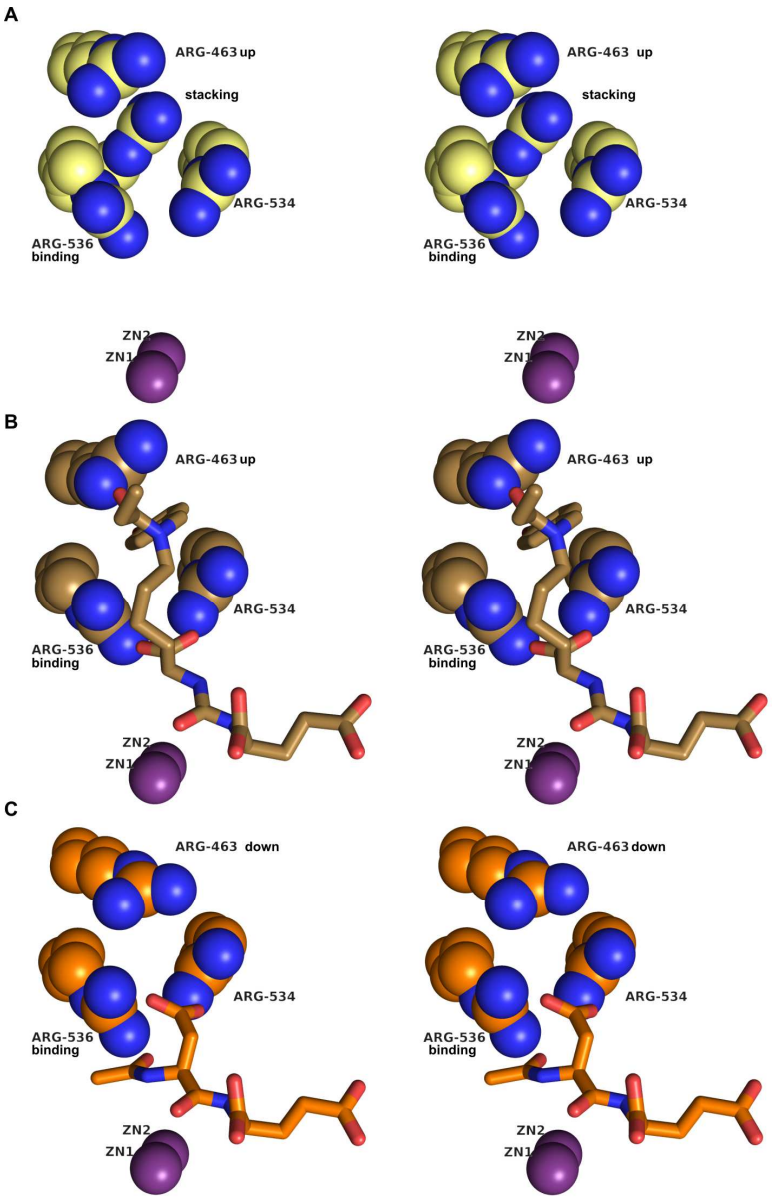


**Figure 9: The hydrophobic accessory pocket of GCPII.** All pictures are rendered in cross-eye stereo representation. The images were created using PyMol[46]. Active-site zinc atoms are depicted as purple spheres. Hydrophobic accessory pocket is formed by the residues Arg463 (conformations "up" and "down"), Arg534, and Arg536 (conformations "binding" and "stacking"). (A) In the ligand-free structure of GCPII (PDB entry 200T[38]), the hydrophobic accessory pocket is filled by Arg536 itself, as it flips between "binding" and "stacking" conformations. (B) If a proper moiety engages the hydrophobic pocket as seen with the here depicted inhibitor (PDB entry 4NGQ[44]), both Arg536 and Arg463 adopt the conformations to maximize the available space between them, i.e. "binding" and "up", respectively. (C) The hydrophobic accessory pocket remains half-closed by Arg463 in the "down" conformation if some moiety, like here the β-carboxylate of the N-acetyl aspartate moiety of NAAG (PDB entry 3BXM[16]), engages the Arg536 in the "binding" conformation, while no moiety stacks between the two arginines (Arg536 and Arg463).

## 1.2.3. Physiological Functions

GCPII has several enzymatic activities (see sections 1.2.2.1.1 – 1.2.2.1.3), which makes it a multifunctional protein[50] having several physiological functions. The already known ones include neuromodulation[51] through cleavage of the neuropeptide NAAG[4] and the participation in the intestinal absorption of dietary folic acid through deglutamylation of provitamin forms of folic acid (vitamin $B_9$)[6,52]. GCPII is additionally expressed in normal and cancerous prostate and tumour neovasculature. However, the physiological role of GCPII in these tissues still remains to be elucidated (see section 1.2.3.3).

### 1.2.3.1. Neuromodulatory Function

In the tissues of the central nervous system, GCPII is expressed predominantly on astrocytes[53–55] from white matter, presumably on fibrous astrocytes[54]. By hydrolyzing the most abundant mammalian peptide neurotransmitter, NAAG[51], into N-acetyl-L-aspartate and glutamate, it also

elicits a neuromodulatory response because NAAG has been shown to act as a selective agonist at metabotropic glutamate receptor 3 (mGluR3)[51,56–59] (see also section below). This agonism of NAAG at mGluR3 is thought to serve to presynaptically inhibit glutamate release[60–64] and thus, more generally, to down-modulate neuronal activity (see section below). Glutamate, if present at a too high concentration in the extraneuronal space, damages neurons through their overstimulation[65] in a process called excitotoxicity or oxidative glutamate toxicity (see also section 1.2.3.1.3.1). Expression of GCPII in the white matter[54] also colocalises with the site of maximal NAAG concentration as quantified by nuclear magnetic resonance (NMR). According to this approach, NAAG is 1.5 - 2.7 mM in white matter compared to 0.6 - 1.5 mM in gray matter[66].

For a certain period of time, it was believed that NAAG is a weak agonist (or even an antagonist) of the N-methlyl-D-aspartate receptor (NMDAR), but the latest view is that it was likely a mistake[67].

### 1.2.3.1.1. Structural and Molecular Basis of the Down-modulatory Function of NAAG and the Activating Function of GCPII

To understand the neuromodulatory role of NAAG and GCPII, it is primarily necessary to understand the role of glutamate. In the neuronal tissue, glutamate functions as the main excitatory neurotransmitter[68,69] and extracellular glutamate receptors are divided into two groups, based on the type of signal they elicit[68]. Namely, the slow metabotropic glutamate receptors (mGluRs) belonging to class C G-protein-coupled receptors[68–70] (signal transduction through enzymatic activity) and the fast glutamate-gated ion channels (ionotropic receptors transducing signals through changing ion-specific permeability of membranes)[68]. The former group is further subdivided into three classes, group I (includes mGluR1/5), group II (mGluR2/3) and group III (mGluR4/6/7/8)[71], the latter constitutes of NMDA (N-methlyl-D-aspartate), AMPA [(2S)-2-amino-3-(3,5-dioxo-1,2,4-oxadiazolidin-2-yl)propanoic acid)] and kainate receptors[68]. mGluRs can also form specific heterodimers which increases the overall complexity[70,72].

Excitatory pathways are functionally opposed, besides e.g. by the inhibitory γ-aminobutyric acid (GABA) recptors[73–75], also by the above mentioned agonism of NAAG at mGluR3[68] (see also below). This function correlates well with the localization of Group II mGluRs (mGluR2/3) which are located mostly presynaptically and their function is to inhibit neurotransmitter release [70,76] and to induce long-term depression (LTD)[70] of excitatory synaptic transmission (see also below).

The effect of NAAG agonism is a generally believed and experimentally supported phenomenon[58,61,67,77,78] that is considered neuroprotective (see section 1.2.3.1.3.1). However, there are two serious conceptual problems: (1) mGluR3, the target receptor of NAAG, is a glutamate

receptor with reported affinity for NAAG in the range 65 μM ($EC_{50}$) to > 1 mM ($K_I$)[57,79] and affinity for glutamate in the range 41 nM[79] ($K_I$) to 58 nM[80] ($EC_{50}$), whereby the extraneuronal glutamate concentration is maintained usually in the range 0.2–5 μmol/L[81]. (2) In rats, agonism of NAAG also at the mGluR2 has been reported, with a $K_I$ value of 134 μM[82], whereby binding at mGluR2 is 12-fold weaker than on mGluR3[59].

Moreover, one study even claims that NAAG is not an agonist of human and rat mGluR3 receptor[80] and concludes that the agonist effect observed in many studies is only the effect of glutamate impurity in the NAAG preparations containing usually around 0.4 –0.5 % glutamate (which means that a 68 μM NAAG concentration is in fact 0.27 μM glutamate, a concentration which is several orders of magnitude above the glutamate's $K_I$ value and accordingly high enough to elicit an agonistic effect, see above). This study, however, describes a weak effect of 1 mM NAAG at mGluR3 and does not dissect whether this is the effect of some residual glutamate, which is present even after a thorough purification, or the effect of NAAG itself. Taken together, affinity of NAAG to mGluR3 in the millimolar range still cannot be excluded and it may be the reason why there is still no structural information about this interaction.

In summary, the physiological role of NAAG's agonism at mGluR2/3 (group II) seems to be down-modulation of synaptic activity, hence GCPII is actually an activating protein. The idea of such a function is further supported by the localisation of mGluRs: mGluR2/3 (group II) are localised on the preterminal axon[65] or postsynaptically[69] (mGluR3 presynaptically, mGluR2's directly on the presynaptic membrane of the synaptic cleft[65]), mGluR1/5 (group I) perisynaptically on the postsynaptic membrane[65] and mGluR7/8 (group III) synaptically on the presynaptic membrane[65].This likely means that this localisation pattern of mGluRs may serve to make a presynatic neuron terminal to become less excitable via group II and III mGluRs and to make the postsynaptic membrane more excitable via group I mGluRs (see above). On top of that, NAAG is synthesized in neurons, astrocytes and microglia[55,83] from NAA and glutamate by recently identified ATP-dependent enzymes (see section 1.2.3.1.2). Moreover, the concentration of NAAG might reflect the function of mitochondria[84], at least for three reasons: (1) The rate of synthesis of NAA is tightly coupled with neuronal glucose metabolism[85], (2) NAAG is present at ~ 10 % of the NAA[55], and (3) the concentration of NAA in neurons is 10 - 20 mM[55,86] (second highest of all amino acids in CNS[87]). Also, high NAA concentration in Canavan diesease, a hereditary aspartoacylase deficiency, is connected with NAAG aciduria[55]. As already mentioned above, NAAG's affinity to mGluR3 is rather low (65 μM - > 1 mM), so its down-modulatory effect might become noticeable when the neuronal viability is at its high (concentrations of NAA and NAAG are

high) and may simply represent a mechanism of preventing neuronal overactivity[64]. Correspondingly, the concentration of NAA is directly related to neuronal function and viability[55,86–90] and inhibition of GCPII shows beneficial effects in various neurological conditions (see section 1.2.3.1.3).

mGluR3 receptors are expressed also on astrocytes[69] and activation of astrocytic group II mGluRs on glial cells increases the release of transforming growth factor β (TGF-β, cytokine involved in tissue repair[91]) which in turn exerts a neuroprotective effect[78,92–94]. Because, throughout the brain, the concentration of NAAG varies more than that of NAA (which is rather constant)[95] and increases caudally proceeding from cerebrum to spinal cord[95] (besides the above mentioned difference in white versus gray matter[66], see 1.2.3.1), the TGF-β pathway triggered by NAAG likely represents a functionally related requirement for highly neuroprotective conditions for the spinal cord and brain stem

### 1.2.3.1.2. NAAG is a Neurotransmitter

NAAG is distributed throughout neurons, including axons and synaptic terminals[66,96]. It is present also in synaptic vesicles and released from axon termini following initiation by an AP in a $Ca^{2+}$-dependent manner[51,86]. Transport of NAAG into synaptic vesicles is mediated by sialin[97]. NAAG is synthesized by NAAG synthetase I (NAAGS I)[98,99] and NAAG synthetase II (NAAGS II)[20] and synthesis is performed primarily by neurons[55], but also by oligodendrocytes and microglia[100].

After its release into the synaptic cleft, NAAG performs its neuromodulatory function (see sections 1.2.3.1 and 1.2.3.1.1) and is degraded by GCPII.

### 1.2.3.1.3. Inhibition of GCPII in Various Neurological Conditions

In the CNS, NAAG probably serves to down-modulate the neuronal activity (see sections 1.2.3.1 and 1.2.3.1.1), and this is why inhibition of GCPII shows beneficial effects in several acute and chronic conditions, e.g. traumatic brain injury[61], schizophrenia, addictive disorders, depression, epilepsy and pain[69]. Until recently, testing of GCPII inhibitors was limited to unpractical methods of administration (parenteral[34]) because there were no orally available ones. For example, 2-PMPA is a 0.275 nM inhibitor[47,49], but is not orally available[32]. However, esterification of polar groups of a drug may increase its oral availability[34,101] and diesterification of the GCPII inhibitor ZJ-43[102] warrants effective oral availability[103]. For now, the focus is thus to synthesize some orally available prodrugs of already known and potent GCPII inhibitors which would enable testing and possibly the use even in humans.

#### 1.2.3.1.3.1. Traumatic Brain Injury

In accordance with the down-modulatory function of NAAG and the up-modulatory function of GCPII, inhibition of GCPII by 2-PMPA, ZJ-43 or prodrugs of ZJ-43 robustly protects against ischemic brain injury[61,78,103–106].

The mechanism of action, by which neuroprotection (in traumatic brain injury) is achieved by inhibiting GCPII, is believed to be mediated by group II mGluRs[104,107], although tests in group II mGluRs knockout animals have not been done yet. The increased NAAG concentration then decreases glutamate release via mGluR3[78], counteracting the glutamate excitotoxicity seen in traumatic brain injury[108–110].

#### 1.2.3.1.3.2. Schizophrenia

Preliminary experiments with a non-genetic model of schizophrenia in mice came up with the evidence that inhibition of GCPII might be beneficial also in schizophrenia[111].

Genes related to schizophrenia have been known for almost a decade [112] and they encompass, inter alia, glutamergy-related genes, including the gene coding for mGluR3[62,112,113].

#### 1.2.3.1.3.3. Drug Addiction

It has been convincingly shown that NAAG and 2-PMPA inhibits intravenous cocaine self-administration in rats[114]. However, drug addiction seems to be a more complex phenomenon linked to a variety of receptors including not only mGluR3 but also mGluR2[115]. For example, an earlier study shows that mGluR2 knockout mice enhancedly respond to cocaine[69]. Finally, NAAG's affinity to mGluR2 has been quantified only in rats (see 1.2.3.1.1), and also other mGluRs are involved in drug seeking behaviour[69].

#### 1.2.3.1.3.4. Depression

One NMR study reports that in patients with treatment-resistant depression, an increase in NAA was detected in the left amygdalar region after successful treatment with electroconvulsive monotherapy[84]. This conclusion means that depression might be yet another neurological condition in which production or concentration of brain NAA/NAAG is decreased (see section 1.2.3.1.1) and that GCPII might be a drug target for this condition as well.

#### 1.2.3.1.3.5. Epilepsy

At the genetic level, epilepsy has been linked to ion channels[116] and excitatory amino-acid transporter 1 (EAAC1)[117]. Epilepsy can also occur after traumatic brain injury[118], during ageing[119,120] or as a consequence of a brain tumor or alcohol and drug abuse. Additionally, oxidative stress is increasingly accepted as an important factor in epilepsy[121] and knockout of EAAC1 in rats[117] produces epileptic phenotype which highlights the importance of maintaining proper glutamate level in the extracellular compartment of brain. In agreement with the down-modulatory function of NAAG, inhibition of GCPII protects mice against cocaine kindled seizures[122]. Epilepsy is therefore another neurological condition which might be ameliorated by inhibition of GCPII.

#### 1.2.3.1.3.6. Pain and Peripheral Neuropathy

Inhibitors of GCPII have also been successfully tested in animal models of pain[78,123] which is, moreover, in agreement with the observations that agonists at group II mGluRs can also be used to manage pain[69]. Inhibition of GCPII has already shown promising results also in treating peripheral neuropathy in animal models[34,124,125].

#### 1.2.3.1.3.7. Anxiety

Because group II mGluRs (mGluR2/3) are involved in anxiety[69,126], inhibition of GCPII might become therapeutically significant also for this condition.

### 1.2.3.1.4. NAAG Seems to be Important for Intelligence

Although the relationshiop of NAAG and intelligence has not been thouroughly studied yet, there might be some because it has been shown using NMR that there is a connection between NAA (precursor to NAAG) concentration in the brain and intelligence[89,127,128] and that both lower and higher concentration of NAA in specific brain regions can predict higher intelligence[89] (see also section 1.2.3.1.1). Furthermore, patients with multiple sclerosis exhibit lower level of NAAG in the hippocampus and cognitive impairment whereby the inhibition of GCPII is being investigated as a possible treatment for cognitive impairment[129,130].

### 1.2.3.1.5. Concerns about the Inhibiton of GCPII

Inhibition of NAAG has been considered a potential candidate for becoming one of the general procedures for the treatment of acute brain injury (see sections 1.2.3.1.3 and 1.2.3.1.3.1). As mentioned above (sections 1.2.3.1.3.2, 1.2.3.1.3.3 and 1.2.3.1.3.6), inhibition of GCPII might also be relevant for treating schizophrenia, drug addiction or pain.

However, the way of GCPII inhibitors to clinical practice may be longer than initially thought. For example, in individuals with genetically disrupted aspartoacylase (enzyme hydrolyzing NAA to aspartate and acetate, see section 1.2.3.1.1), there is an increase in NAA[55,83] (and likely also in NAAG[83] as evidenced by NAAG aciduria[55]) and a decrease in oligodendrocyte-mediated axon myelination[55,83] which indicates that inhibition of GCPII might reduce neuronal myelination. Similar indications arise from two cases of an unknown severe CNS disorder accompanied by increased NAAG concentration in cerebrospinal fluid (with intact GCPII) and by almost complete absence of cerebral myelination[131]. On the other hand, GCPII knockout mice showed mild phenotypes of decreased anxiety and increased food intake and increased mean arterial blood pressure and[77]. However, they exhibited reduced myelin sheaths and diameters of axons of periferal nerves[77] (whereby myelination of CNS was not investigated).

Should long-term administration of GCPII inhibitors not be possible for the above mentioned reasons, the desirable down-modulatory effect at mGluR3 (or perhaps on the whole group II mGluRs, see sections 1.2.3.1.1 and 1.2.3.1.3.3) might be better achieved by direct group II selective agonists[69], although differentiating between mGluR2 and 3 might be difficult or not possible[132].

## 1.2.3.2. Absorption of Provitamin Forms of Vitamin $B_9$ (Folic Acid)

Through its folyl-poly-γ-glutamate carboxypeptidase activity, GCPII releases free folic acid[5,6] which is then ready to be absorbed in the small intestine.

## 1.2.3.3. Unknown Function in Prostate Cancer, Tumor Neovasculature and Other Tissues

Many proteins have multiple functions and GCPII is no exception[50]. Besides its known funtions as NAAG and $FolGlu_n$ hydrolase, there are likely two more functions to be elucidated - in prostate (1.2.3.3.1) and in tumour neovasculature (1.2.3.3.2). Its function in other tissues remains unresolved (1.2.3.3.3).

### 1.2.3.3.1. Prostate Cancer

mRNA level of GCPII (PSMA) shows the highest relative expression in normal prostate (with approximately 10-fold lower expression also in liver, kidney and brain)[12,13]. Its expression increases manyfold in prostate cancer[12] and is down-regulated by dihydrotestosterone[3]. Further, its expression increases[3,12,133] during antiandrogen therapy, which is used for treatment of prostate cancer[134], and is the highest in androgen deprived states[3]. This led to the idea that GCPII could be a suitable

clinical marker for high-grade prostate carcinomas and a target for therapeutic molecular addressing[12]. Furthermore, prostate tumors, as they progress, tend to lose its tissue-specific antigens called prostate specific antigen (PSA) and prostatic acidic phosphatase (PAP), while GCPII is usually still expressed[12], so this allows for GCPII to be currently explored as a target for molecular probes exploiting a very recent technological advance - combined positron emission tomografy and magnetic resonance imaging scanners (PET/MRI)[135]. For example, it was easier to distinguish a prostate cancer metastase to bone using PET/MRI in comparison to the combined positron emission tomografy and computer tomography imaging (PET/CT)[135]. Imaging using probes for PET/CT is also being tested[136,137].

Finally, it has been reported that GCPII increases the adhesion of prostate cells on bone marrow matrix[138]. This was the first evidence providing a possible explanation why prostate cancer cells metastasise to bone.

#### 1.2.3.3.2. Tumor Neovasculature

Using the 7E11-C5.3 antibody (which binds the intracellular epitope MWNLLH[139]), it has been shown that GCPII is expressed also in tumor-associated neovasculature but not in normal tissue capillaries[140]. In accord with this finding, GCPII knockout mice show severely impaired angiogenesis[141]. The exact biochemical role of GCPII in tumor neovasculature and angiogenesis remains, however, elusive.

#### 1.2.3.3.3. Other Tissues

At the mRNA level, GCPII shows relatively high expression, besides the prostate, also in liver and kidney[13]. The function in these tissues has yet to be elucidated, too.

### 1.2.3.4. Controversial Physiological Effects of the GCPII His475Tyr Polymorphism

His475Tyr is a naturally occuring human polymorphism[142]. Originally, it was believed that this polymorphism is associated with impaired intestinal absorption of dietary folates[142], but a plethora of follow-up studies brought only contradictory data. For example, some studies were claiming that His475Tyr polymorphism is linked neither to folate nor to homocysteine concentration in blood[143–145] (600-1900 subjects per study), while another study (2700 subjects) concluded that His475Tyr is associated with higher folate and lower homocysteine blood levels[146]. Furthermore, one recent study claims that the His475Tyr polymorphism is associated with depressive symptoms[147].

## 1.2.4. Paralogs of GCPII - GCPIII, NAALADase L, PSMA-L

In humans, there are twelve paralogs of GCPII[12]. Among the most known are GCPIII, prostate specific membrane antigen like protein (PSMAL), N-acetylated α-linked acidic dipeptidase-like protein (NAALADase L), N-acetylated α-linked acidic dipeptidase-like protein 2 (NAALADase L2), plasma glutamate carboxypeptidase (PGCP), transferrin receptor protein 1 (TfR1) and transferrin receptor protein 2 (TfR2)[12].

Interestingly, structure and function of NAALADase L has been elucidated very recently. This dizinc metallopeptidase serves in the human ileum as an aminopeptidase[148]. NAALADase L2, in contrast to GCPII, is expressed not apically, but at the basal surface, where it enhances attachement to the extracellular matrix[149]. PGCP was recently shown not to cleave NAAG[150].

## 1.2.5. Orthologs of GCPII

Orthologs of GCPII are present in most of animal species, for example in mouse, rat and pig, but not in plants or yeast[14]. In these animals, GCPII shares >90 % sequence similarity with the human variant[14].

# 1.3. Glutamate Carboxypeptidase III

Glutamate carboxypeptidase III (GCPIII), similarly to GCPII, is also known under several names. These other names include N-acetylated α-linked acidic dipeptidase II (NAALADase II), citrylglutamate hydrolase and β-citrylglutamate hydrolase. However, the latter is the most relevant because β-citryl-L-glutamate (BCG) is the primary substrate for GCPIII[8].

## 1.3.1. GCPIII Gene

The coding DNA sequence of GCPIII is localised to the 11q14.3-q21 locus[12].

## 1.3.2. GCPIII mRNA

mRNA in different tissues has been quantified by reverse transcription polymerase chain reaction (RT-PCR) only in mouse, showing highest expression in testes, uterus, bladder and lung[8]. An earlier study based on northern blot analysis and RT-PCR found the highest level or mRNA in mouse testes and ovary[151]. In mouse brain, the level of mRNA of GCPIII in brain is approximately two fold higher in neurons than astrocytes[151] (which stands in contrast to GCPII found primarily on astrocytes, see section 1.2.3.1).

Northern blot analysis of human tissue samples showed highest expression in testes as well[152] and low expression also in ovary, spleen, prostate, heart and placenta[152].

## 1.3.3. GCPIII Protein

GCPIII shares 67 % sequence identity and 81 % sequence similarity to GCPII[152] and, as it is the case for GCPII, N-glycosylation is important for its enzymatic activity[26]. In analogy to GCPII, GCPIII is predicted to be a type II transmembrane protein. Amino acids 9-31 are predicted to be the transmembrane part[151], so the most of its part is likely exposed to the extracellular environment. Because enzymatic activities (see section 1.3.3.1) have only recently been characterized, there is no enzyme commision number assigned to it yet. Because of its similarity to GCPII, both at sequence[26] and structural[153] level, GCPIII might be also active only as a dimer (see section 1.2.2). The main characteristics of GCPIII, making it quite different from GCPII, is its loose binding of Zn2[153]. While GCPII binds both its zinc atoms so tightly that their occupancies are 100 %[36], occupancy of the co-catalytic Zn2 in GCPII is in the range 0.45 - 0.80[153] and it is speculated that this is the reason why GCPII cleaves its substrates independently of metals, while GCPIII in a metal-dependent manner[7,8] (see also section 1.3.3.1).

### 1.3.3.1. Enzymatic Activities

GCPIII was first shown to hydrolyze N-acetyl-L-aspartyl-L-glutamate (NAAG)[152] to N-acetyl-L-aspartate (NAA) and L-glutamate, and later β-citryl-L-glutamate (BCG)[7,8] to citrate and L-glutamate, whereby, somewhat paradoxically, BCG has been known since 1978[30]. Initially, it was incorrectly believed that GCPIII possesses also dipeptidylpeptidase IV-like activity[152], but this idea has been disproven several years later[26]. GCPIII hydrolyzes its substrates in a metal-dependent manner[7,8] and the proposed reason for this is a lower occupancy of the Zn2 atom of GCPIII (see 1.3.3)[8]. The proposed reason for this is the only difference of the active site of GCPIII in comparison to GCPII - GCPIII has a serine in the position 509, while GCPII has an asparagine at the corresponding position (519)[8]. Asn519 is able to stabilize the Zn2-binding Asp453 at a chelating distance, while Ser509 cannot, leaving the corresponding Asp443 in two conformations (PDB entry 3FF3)[153]. The translational freedom of Asp443 results also in a lower occupancy of the neighbouring chlorine ion (70 %)[153]. This represents a difference to GCPII where the chlorine atom and the dizinc cluster have a 100 % occupancy[35,36] .

### 1.3.3.1.1. BCG-hydrolyzing Activity

As mentioned in the section 1.1, β-citryl-L-glutamate (BCG) hydrolyzing enzyme has been discovered already three decades ago, but it could be ascribed to a particular protein sequence only recently[8]. What is interesting and unique about the BCG hydrolyzing activity is the fact that it is metal-dependent (as shown using mouse GCPIII)[7,8]. In contrast to NAAG hydrolyzing activity (see below, section 1.3.3.1.2), BCG hydrolysis is most effective when GCPIII is saturated with calcium and it is also approximately two fold lower when GCPIII is saturated with manganese(II) ions[8] (see previous section 1.3.3.1).

The calcium-dependent hydrolysis could be physiologically relevant , because GCPII likely acts at the cell surface (see section 1.3.3) or inside some organelle, where calcium concentration is around 2.5 mM, and also because this activity the highest $k_{cat}$ value[8]. However, it is only a working hypothesis as it is still not known where GCPIII is present at the protein level (see also section 1.3.4).

### 1.3.3.1.2. NAAG-hydrolyzing Activity

GCPIII hydrolyzes N-acetyl-L-aspartyl-L-glutamate (NAAG)[26,152]. This activity might compensate for the missing activity of GCPII and account for the mild phenotype of GCPII knockout mice[77,154] because the overall catalytic efficiency is approximately three fold lower[26] (these mice have only significantly increased blood pressure, see section 1.2.3.1.5). pH optimum of this activity lies around 8.5[26].

Similarly to BCG-hydrolyzing activity, also NAAG hydrolysis is metal-dependent. There is, however, a difference in the preferred metals. $k_{cat}$ of NAAG hydrolysis is enhanced in the presence of manganese(II) cations so that it reaches a value of approximately 0.8 $s^{-1}$ [8], while, in contrast, it is reported to reach an approximately hundred times lower value in the presence of calcium[8]. In comparison to BCG, NAAG-dependent preference for calcium is thus the opposite (see above, section 1.3.3.1.1).

### 1.3.3.1.3. $FolGlu_n$-hydrolyzing Activity

So far, nothing has been found out about a possible $FolGlu_n$ hydrolyzing activity of GCPIII.

### 1.3.3.1.4. NAAG2-hydrolyzing Activity

NAAG2 hydrolyzing activity has been investigated only for mouse GCPII and III. It has been only found out that mouse GCPIII may be able to hydrolyze NAAG2[29], but no kinetic parameters are available yet.

## 1.3.3.2. X-ray Structure

There are only four X-ray structures of GCPIII[153]. The structures of GCPII and III are very similar. Importantly, the active site residues and zinc chelating amino acids His367, Asp377, Glu415, Asp443 and His543 of GCPIII correspond to GCPII exactly both in terms of identity and structure (for GCPII, the zinc chelating amino acids are His377, Asp387, Glu425, Asp453 and His553). The main functionally related structural difference between GCPIII and II (mentioned already in the section 1.3.3.1) is GCPIII's flexible Asp443 and consequentially lower occupancy of the active-site zinc atom Zn2 (approx. 0.45–0.80 instead of 1.00 seen in GCPII)[153]. GCPII, in contrast, features a rigid Asp453 firmly chelating Zn2[35]. The flexibility of GCPIII's Asp443 is made possible by a Ser509 instead of GCPII's Asn519 which abolishes a hydrogen bond between Asp453 and Asn519 and makes the Asp443 free to adopt two conformations (see 1.3.3.1). This view is also supported by site-directed mutagenesis transforming GCPIII into "GCPII" (Ser509Asn) and vice versa GCPII into "GCPIII" (Asn519Ser)[8].

As opposed to GCPII for which the X-ray structure of the complex with its substrate NAAG is available, such a structural information about GCPIII is not available yet.

# 1.3.4. Physiological Function

Physiological function of GCPIII is not known. Limited information is available also on the tissue distribution of the protein. This is given by GCPIII's high sequence identity and similarity to GCPII[152] which complicates the production of any GCPIII-specific antibody. The only method how to detect GCPIII at the protein level is to investigate tissues lacking GCPII using an antibody against GCPII which is cross-reactive to GCPIII[155]. Other approaches include investigating the tissue distribution of GCPIII using a GCPII antibody in a GCPII knockout animal (see below) or determining the BCG-hydrolyzing activity[8] (see below, 1.3.4.1).

## 1.3.4.1. Tissue Distribution of GCPIII in Animal Models

Before it became generally known that BCG is the specific substrate of GCPIII[8], the tissue distribution of GCPIII at the protein level could be investigated only in GCPII knockout mice using

NAAG hydrolyzing activity assay. This pioneering approach revealed that the expression of GCPIII was the highest in brain, spinal cord, kidney and liver[154] (other tissues were not examined). Although GCPII knockout in mouse does not alter the expression level of GCPIII in brain as measured by mRNA[151], the above mentioned tissue distribution of GCPIII in GCPII knockout mouse might be of limited relevance because the knockout itself might change the expression profile of GCPIII in all other tissues (whereby this question has not been rigorously addressed yet).

Using the specific substrate of GCPIII, β-citrylglutamate hydrolyzing (BCG,), it has been discovered that the distribution of BCG-hydrolyzing activity in lysates of mouse tissues[8] overlaps with the previously published tissue distribution measured by Northern blot analysis[151] and also with the mRNA profile of GCPIII[8], showing the highest expression/activity in testes, uterus and bladder[8].

In 1982, the tissue distribution of a citrylglutamate hydrolyzing enzyme in rats has been published[7]. According to this study, the expression of the citrylglutamate hydrolyzing enzyme was highest in testes[7]. However, it is has not been published until now whether this enzyme was the rat orthologue of GCPIII.

## 1.3.5. Inhibitors

Specific inhibitors of GCPIII are not available because GCPII and III differ so slightly (see section 1.3.3.1) that they show a very similar inhibitory profile[14,26,47,49]. However, there are already GCPII-selective inhibitors[49]. The selectivity of one of them (6600 times more selective to GCPII[49]) makes it possible to inhibit GCPII while preserving the putative activity of GCPIII.

# 2. AIMS OF THE STUDY

- Design and analyse novel inhibitors of GCPII potentially crossing blood-brain barrier.
- Structurally and biochemically characterize the folyl-poly-γ-L-glutamate carboxypeptidase activity of GCPII.
- Compare folyl-poly-γ-L-glutamate carboxypeptidase activity of GCPII and GCPIII.
- Find and characterize a specific substrate of GCPIII and analyze its distribution in human tissues.
- Find structural explanation for the distinct specificites of GCPII and GCPIII and for the metal-dependent hydrolytic activity of GCPIII (but not GCPII).

# 3. MATERIALS AND METHODS

## 3.1. Chemicals, Other Materials, Instrumentation and Software

### 3.1.1. Chemicals

**Affymetrix**
octaethylene glycol monododecyl ether
**Bio-Rad**
AG 1-X8 resin, Protein Assay Kit cat # 5000006, Precision Plus Protein™ All Blue Prestained Protein Standards
**Biotica**
Ampicillin
**Biotium Inc.**
nucleic acid gel stain GelRed™
**Chemapol**
potassium chloride
**Combi-Blocks**
D-biotin
**Duchefa Biochemie**
4-morpholinopropanesulfonic acid
**Exbio**
antibody GCPII 04
**Finnzymes**
Phusion High-Fidelty DNA Polymerase
**Fisher Chemical**
Acetonitrile
**Fluka**
N,N'-Methylenebisacrylamide
**Generi Biotech**
oligonucleotides
**Hampton Research**
Izit Dye, 50 % v/v Pentaerythritol propoxylate
**Invitrogen**
agarose, Hygromycin B
**Laboratory of Radioisotopes at IOCB**
[$^{3}$H]β-citryl-L-glutamate, [$^{3}$H]N-acetyl-L-aspartyl-L-glutamic acid
**Lab-Scan**
Methanol
**Lachner**
silver nitrate, sodium phosphate dibasic, sucrose
**New England Biolabs**
restriction endonucleases, T4 ligase
**Penta**
acetic acid, chloroform, ethanol, formaldehyde, formic acid, glucose, isopropanol, hydrochloric acid, phosphoric acid, potassium hydroxide, potassium phosphate monobasic, sodium acetate, sodium chloride, sodium hydroxide
**Pharmacia**

0.20 M sodium borate buffer pH 10.0
**Promega**
Pfu DNA polymerase, Tris Base
**Roche**
Protease Inhibitor Cocktail Tablets cOmplete EDTA-free
**Roth**
scintillator Rotiszint® eco plus
**Schircks Laboratories**
pteroyldi-γ-L-glutamic acid, pteroylhepta-γ-L-glutamic acid (ammonium salt), pteroylhexa-γ-L-glutamic acid (ammonium salt), pteroylpenta-γ-L-glutamic acid, pteroyltetra-γ-L-glutamic acid, pteroyltri-γ-L-glutamic acid
**SDT**
Cassein Buffer
**Serva**
agarose, ammonium persulfate
**Sigma-Aldrich**
acetonitrile, ammonium iron(II) sulfate, ammonium persulfate, L-aspartic acid, BIS-TRIS propane, bovine serum albumin, calcium chloride, citric acid, cobalt(II) chloride, copper(II) chloride, copper(II) sulfate, dimethyl sulfoxide, ethylenediaminetetraacetic acid, folic acid, L-glutamic acid, HEPES (4-(2-hydroxyethyl)-1-piperazineethanesulfonic acid), Kit for Molecular Weights 14,000-500,000 Non-denaturing, LB Agar, lithium chloride, magnesium chloride hexahydrate, manganese(II) chloride, 2-mercaptoethanol, methanol, 3-mercaptopropionic acid, N-acetyl-L-aspartyl-L-glutamic acid, oligonucleotides, orthophtalaldehyde, PEG 3350, PEG 8000, phenol solution cat # P4557, potassium acetate, potassium chloride, pteroic acid, RNAse A, sodium azide, sodium carbonate, sodium dodecyl sulfate, Sypro Orange Protein Gel Stain, trisodium citrate, Triton X-100, Trizma® base, Trypan Blue, zinc chloride
**Thermo Scientific**
Albumine Standard cat # 23210, anti mouse antibody horseradish peroxidase conjugate cat # 31436, Casein Blocker cat # 37532, SuperSignal® West Dura Extended Duration Substrate cat # 34076, NeutrAvidin-HRP conjugate
**Top Bio**
dNTP
**USB**
Tween 20
**VWR**
Acetonitrile

## 3.1.2. Other Materials

0.22 μm column pre-filter, 2.1 mm (Waters)
0.22 μm nitrocellulose and PVDF membranes for filtering (Merck Millipore)
12-channel pipette 2 - 20 μl neo (Gilson)
12-channel pipette 20 - 200 μl C200-12 (Capp)
12-channel pipette 20 - 200 μl neo (Gilson)
15-Well Plates EasyXtal (Qiagen)
35 mm culture dishes (Nunc)
96 U-shape well plates (P-lab)
96 well crystallization plate for sitting drop vapor diffusion MRC 2 Well Swissci UVP (Hampton Research)
affinity tag AviTag™ (Avidity)

Amicon® Ultra 0.5 mL (Merck Millipore)
Calcium Phoshpate Trasfection Kit (Invitrogen)
chromatography paper (Whatman)
column Acquity UPLC HSS T3 1.8 µm, 2.1 x 100 mm (Waters Corporation)
column HiLoad™ Superdex™ 200 10/300 GL (GE Healthcare)
column HiLoad™ Superdex™ 200 16/600 prep grade (GE Healthcare)
competent cells E. coli DH5α (Novagen)
competent cells E. coli TOP 10 (Invitrogen)
cryogenic vials 1 ml (Corning)
CrystalSupports EasyXtal (Qiagen)
crystallization plates EasyXtal 15-Well (Qiagen)
crystallization screens JCSG+ Suite, PACT Suite (Qiagen)
dialysis devices Slide-A-Lyzer™ MINI (Thermo Scientific)
disposable gravity-flow columns (Thermo Scientific)
DNA electrophoresis Owl™ EasyCast™ B2 Mini Gel Electrophoresis System (Thermo Scientific)
Drosophila Schneider's S2 cells (Invitrogen)
eppendorf tubes 1.5/2.0 ml (Sarstedt)
falcon tubes 15/50 ml (Sarstedt)
fetal calf serum (Sigma-Aldrich)
hemacytometer Bright-Line® (Reichert)
Human MTC Panel I and II (Takara Bio)
LabScale TFF (Merck Millipore)
LightCycler® 480 Sealing Foil (Roche)
medium Sf-900 II (Gibco)
MilliQ deionized water (Merck Millipore)
motorized repetitive dispenser Repetman® (Gilson)
nitrocellulose membrane (Merck Millipore)
pCoHYGRO vector (Invitrogen)
PCR 12-strips (BIOplastics BV)
PCR tubes Axygen® (Corning)
pH indicator paper strips (Lachner)
pMT/BiP/V5-HisA vectors (Invitrogen)
QIAprep® Spin Miniprep Kit (Qiagen)
QIAquick Gel Extraction Kit (Qiagen)
Repetman® tips (Gilson)
scintillation vials Macro 20 mL (Karell)
sealing tape HDCLEAR (Shur Tech Brands, LLC)
spinner flasks (Corning or Bellco Glass Inc.)
Stratagene QuickChange™ Site-Directed Mutagenesis Kit cat #200518
Streptavidin Mutein Matrix (Roche)
ultrafiltration module Pellicon XL Biomax 100 (Merck Millipore)
VanGuard™ HSS T3 1.8 µm pre-column for Acquity UPLC columns, 2.1 x 50 mm (Waters)
western blotting detection reagent Luminata™ Crescendo Western HRP Substrate (Merck Millipore)

## 3.1.3. Instrumentation

adjustable angle rotating shaker LD79250112 (Kisker Biotech)
centrifuge Beckman Allegra X-15R (Beckman Coulter)
centrifuge Eppendorf 5415 R (Eppendorf)

centrifuge Heraeus Biofuge Pico (Heraeus Instruments GmbH)
centrifuge Heraeus Megafuge 2.0R 8106H (Heraeus Instruments GmbH)
centrifuge Heraeus Multifuge 3SR (Heraeus Instruments GmbH)
centrifuge IEC CL10 (Thermo Scientific)
ChemiDoc-It™ Imaging System (UVP)
$CO_2$ incubator MCO-17AI (Sanyo)
crystallization robot Model 620-1000-10 (Art Robbins Instruments)
electrophoresis unit for polyacrylamide gels Mighty Smalll II (GE Healthcare)
Environmental Shaker Model 10X 400 (Sanyo Gallenkamp PLC)
HPLC Äkta Purifier™ 10 (GE Healthcare)
incubator IPP400 (Memmert)
Labo Autoclave (Sanyo)
LAS-3000 Imaging System (Fuji)
LightCycler®480 II (Roche)
liquid chromatograph Agilent 1200 and Agilent 1260 (Agilent Technologies)
magnetic stirrer KMO 2 basic (IKA)
magnetic stirrer RCT basic (IKA)
magnetic stirrer RCT standard (IKA)
mass spectrometer Agilent 6224 TOF LC/MS (Agilent Technologies)
microscope Eclipse TS100 (Nikon)
mixing block MB-102 (Bioer)
mixing block Thermomixer Comfort (Eppendorf)
orbital shaker Innova44 (New Brunswick)
orbital shaker KS 260 basic (IKA)
pH meter pH 50 (XS instruments)
plate reader Infinite M1000 (Tecan)
rocker Sky Line DRS-12 (Elmi)
sonication bath Kraintek 12 (Kraintek)
sonication bath S 30 Elmasonic (Elma)
spectrophotometer NanoDrop ND-1000 ( Thermo Scientific)
spectrophotometer UNICAM UV 500 (Thermo Electron Corporation)
thermal cycler TGradient (Biometra)
tissue lyser TissueLyser II (Qiagen)
Tri-Carb 2900TR (Perkin Elmer)
vacuum freeze dryer Labconco catalog number 7753511 (Labconco Instruments)
vacuum freeze dryer LD plus (Christ)
vortex LTM2 (Vývojové dílny ČSAV)
vortex MX-S (Dragonlab)
water bath (Grant Instruments)
water bath TW8 (Julabo)
wet blotting unit Mini PROTEAN® Tetra Cell (Bio-Rad)

## 3.1.4. Software

AMBER 8.0
CASTp online tool for analysis of protein cavities (http://cast.engr.uic.edu)[156]
Caver plugin for PyMol[157]
CCP4[158–160]
ChemDraw 13 (Perkin Elmer)
ComQum[161]

Corel Draw (Corel Corporation)
GraFit 5 (Erithacus Software Ltd)
Image J (National Institute of Health, USA)
ImageQuant TL 2003.02 (Amersham Biosciences)
Mapmask[160]
Microsoft Office 2003/2010 (Microsoft)
Molrep[158,159,162]
Phaser[163]
Phenix[164]
PyMol[46]
Refmac[165,166]
TurboMole 6.6 suite[167]
Vector NTI 11 (Invitrogen)
Wincoot[168]
XDS[169,170]

# 3.2. Methods

This section describes common methods and modified commom methods in brief and methods developed in our laboratory, being a basis for the findings introduced in this thesis, in detail.

## 3.2.1. Preparation of Recombinant DNA

**Agarose Gel Electrophoresis**

For analytical and preparative purposes, DNA of interest was subjected to common Tris-Acetate-EDTA buffered (TAE) 1 % agarose gels pre-mixed with GelRed according to manufacturer's instructions. The electrophoresed DNA gel was then visualized using ultraviolet light.

**Treatment of DNA with Restriction Endonucleases**

For verfying whether a specific mutation was introduced into a vector, acquiring a specific stretch of DNA coding for a protein („insert") or demethylation of DNA, restriction endonucleases were used. DNA was treated with them according to manufacturer's instructions.

**Gel Extraction**

To purify an insert for re-ligation into a vector of interest, a vector or a PCR product, the vector cleaved by two restriction endonucleases was DNA-electrophoresed and the corresponding band cut out under UV light. Afterwards, the gel or the PCR product was treated using the QIAquick Gel Extraction Kit according to manufacturer's instructions to obtain the pure insert or vector or PCR product. Its concentration was assessed using nanodrop spectrophotometer.

**Ligation**

Purified inserts were ligated into the vector of interest using the T4 ligase overnight at 16.0 °C. Typical volume was 20 µl and the ratio insert to vector varied from 0.64 to 1.6.

**Transformation of Competent Cells**

The competent cells *E. coli* DH5α or TOP 10 (50 µl) were mixed with the purified or unpurified vector (0.10 - 10 µl), kept 30 min on ice, subjected to a 90-second 42.0 °C heat shock, incubated in LB medium for 60 minutes and plated on ampicillin (100 µg/ml) LB agar plates for an overnight incubation at 37.0 °C. A single colony was picked with a plastic pipetting tip.

**Small Scale Preparation of Plasmid DNA**

Small scale preparation of plasmid DNA (on a 20 µg scale) was carried out using the QIAprep® Spin Miniprep Kit. Starting material was always a culture of *E. coli* cells grown in 12 ml of LB medium supplemented with ampicillin (100 µg/ml), shaken overnight at 220 RPM at 37.0 °C.

**Site-directed Mutagenesis**

For introducing an engineered amino acid mutation into GCPII or GCPIII, we proceeded as instructed by the QuickChange™ Site-Directed Mutagenesis Kit

**Large Scale Preparation of Plasmid DNA**

Large scale preparation of plasmid DNA (on a 0.5 mg to 2.0 mg scale) were done using the classic phenol chloroform extraction[171].

**DNA Sequencing**

Protein coding sequences of all engineered vectors were checked by dideoxynucletide-terminated sequencing[172].

## 3.2.2. Sodium Dodecylsulfate Polyacrylamide Gel Electrophoresis (SDS-PAGE)

Protein mixtures were separated for the purpose of analysis using the SDS-PAGE pioneered by Laemmli[173]. GCPII or GCPIII, as a complex mixture or as a purified sample, were analyzed using a 11 % acrylamide gel. Visualization was achieved by a modified silver staining protocol (see below).

**Silver Staining of Protein Polyacrylamide Gels**

The separation patterns of protein mixtures on polyacrylamide gels (see above, section 0) were visualized by the common silver staining procedure, with only slightly modified times of incubation in the individual solutions. Specifically, incubation in 12 % (v/v) acetic acid, 50 % (v/v) methanol

and 0.05 % 100% formalin (v/v) was 7 minutes, washing by 50 % (v/v) methanol 3 x 3 minutes, washing by deionised water 3 x 5 seconds, soaking with $AgNO_3$ (2 g/l) 7 minutes, and washing with 12 % (v/v) acetic acid and 50 % (v/v) methanol prior to scanning 4 minutes.

## 3.2.3. Work with S2 Cell Cultures

**Stable Transfection of S2 Cells Using Calcium Phosphate**

Stable transfection of S2 cells using calcium phosphate was performed essentially the same as described previously[15].

**Trypan Blue Exclusion Assay**

Viable cells in a conditioned S2 cell culture medium were counted using a microscope, hemacytometer and the Trypan Blue exclusion assay as summarized elsewhere[15].

## 3.2.4. Protein Production

**Large Scale Production of AviTag™-GCPII and GCPIII**

Production of AviTag™-GCPII and GCPIII at liter scales using S2 cells was achieved the same way as reported earlier[15] and was extended also to all mutants of GCPII and GCPIII.

**Affinity Purification of AviTag™-GCPII and GCPIII**

This study employed the previously published procedure of purifying AviTag™-GCPII[18] using Streptavidin Mutein Matrix.

**Gel Permeation Chromatography**

Following the affinity purification of AviTag™-GCPII and GCPIII, a gel permeation chromatography step was included to maximize the purity. Usual procedure made use of a 30 cm long Superdex 200 column (1 cm in diameter), with 10 mM Tris, 0.15 M NaCl pH 7.4 as a mobile phase. Typical flow rate was 0.50 ml/min. The separation process was monitored online by measuring the absorbance at 280 nm post-column.

## 3.2.5. qPCR Estimation of Tissue Distribution of GCPII and GCPIII

The distribution of mRNA in human tissues was estimated using qPCR and the Human MTC Panel I and II. The employed protocol was a standard procedure described elsewhere (manuscript under revision).

## 3.2.6. Hanging Drop Vapor Diffusion Method of Protein Crystallization

Herein reported crystal structures were obtained from protein crystals which were grown using the hanging drop vapor diffusion method in an identical way reported previously[38], with minor modifications[174]. The 1.00 μl of protein were mixed not with 1.00 μl of precipitant, but with 1.00 μl of precipitant diluted 9:1 (v/v) with 10 mM water solution of $FolGlu_n$ substrates. $FolGlu_{1-4}$ were dissolved in their acid form, $FolGlu_{5,6}$ as their ammonium salts..

## 3.2.7. 96 Well Plate Bio-Rad Protein Assay

For quantifying total protein in a sample, the Bio-Rad Protein Assay Kit was employed, with minor modifications 160 μl 97 mM HEPES and 0.15 M NaCl pH 7.5 (NaOH) was used as a buffer. As a calibrant, 2 mg/ml BSA standard was used. Samples, including the calibrant, were typically added in 0.500 - 1.900 μl volumes, whereby their volume was neglected. Finally, 40 μl of the protein assay reagent was added. Content of each well was mixed by taking 100 μl in and out by a 12-channel pipette. Absorbance was then recorded using a plate reader at the 595 nm wavelength.

## 3.2.8. Western Blotting as an Analytical and Quantitative Tool

To assess the quantity of GCPII or GCPIII in complex mixtures, such as conditioned S2 cell culture medium, standard Western blotting procedure using a wet blotting apparatus was employed. The final blots were developed using a common chemiluminescent HRP detection reagent. If quantification was needed, the bands of a calibration curve and samples were processed using the software Image J.

## 3.2.9. Radiometric Assay of NAAG- and BCG-hydrolyzing Activity

NAAG-hydrolyzing activity of GCPII and GCPIII was quantified, in selected cases, using the established radiometric assay[1]. Additionaly, BCG-hydrolyzing activity could be assayed in the same way whereby glutamate of BCG was labeled the same way as described for NAAG. Only minor modifications to this radiometric method were introduced (for both NAAG and BCG). For example: (1) The elution volume was reoptimized to find out that 2.4 ml elution volume of 1.0 M formic acid gave better results than originally published 2.0 ml. (2) Bed volume could be reduced from 1.0 ml of AG 1-X8 resin to 0.50 ml (elution volume became accordingly two times lower). (3) 0.20 M potassium phosphate pH 7.4 as a stopping buffer was replaced by a buffer of the same composition except for addition of 2.0 mM 2-mercaptoethanol, because, in our hands, 2-mercaptoethanol

exchibited superior efficiency in terminating the enzymatic activity of GCPII. (4) The amount of scintillator for each reaction was reduced to just 6 or 3 ml (for 1.0 or 0.50 ml bed volumes, respectively). (5)The enzymatic reactions themselves were adapted to a 96-well-plate format.

### 3.2.10. Preparation of Human Tissue Lysates

Tissue lysates were prepared using a tissue lyser instrument in a lysis buffer composed of 50 mM Tris-HCl and 0.15 M NaCl pH 7.4 supplemented with protease inhibitors without EDTA. Approximately 30 mg of a human tissue sample was cut on dry ice in a flow box and transfered into a 2 ml eppendorf tube. 10 µl of the lysis buffer per 1 mg of tissue, a corresponding volume of protease inhibitors, and a 5 mm steel ball was added. Using a pre-chilled block (-20 °C), samples were lysed for 180 seconds at maximum speed. Lysates were then spined down at maximum speed for 1 minute at 4 °C, diluted if necessary, and supplemented with Tween 20 to a final 1 % concentration. Finally, samples were sonicated in a sonication water bath with ice for 4 x 15 seconds and centrifuged at maximum speed for 15 minutes at 4 °C. The supernatants were flash-frozen in liquid nitrogen and stored at -80°C until further use.

### 3.2.11. Differential Scanning Fluorimetry

To assess thermal stability of GCPII and GCPIII, its various mutants and the influence of various metals on stability of GCPIII, standard protocol for differential scanning fluorimetry using Sypro Orange dye[175,176] was employed, with only minor modifications - protein amount per well was 3.9 µg, total volume was 50 µl, and Sypro Orange was diluted only 3125 x (instead of 5000 x recommended by the manufacturer).

### 3.2.12. Novel UHPLC Assay for Non-radioactive Quantification of Glutamate

Enzymatic reactions were performed in a buffer without a primary amine or in a buffer with ≤ 25 mM of it. Reactions in 25 mM Bis-Tris Propane pH 7.5 or in 25 mM Tris pH 7.5 were quenched by the addtition of 10.0 µl of 0.37 M phosphoric acid with 22 µM 2-(phosphonomethyl)-pentanedioic acid or 2.99 µl of 0.41 M phosphoric acid, 72 µM 2-(phosphonomethyl)-pentanedioic acid and 7.2 µM 2-mercaptoethanol, respectively. 250 µl of reactions in 25 mM Tris pH 7.5 were lyophilised and re-dissolved in 25.0 µl of ultrapure water to provide a 10-fold pre-concentration. Then, a fully automatic procedure of derivatization by an orthophtalaldehyde (OPA) solution was done on a liquid chromatograph, mounted with the Acquity UPLC HSS T3 1.8 µm column (2.1 x 100 mm) in

line posterior a 0.22 µm pre-filter (2.1 mm) and the VanGuard™ HSS T3 1.8 µm pre-column (2.1 x 50 mm), and with its column tepmerature conditioning set to 40.0 (25 mM Bis-Tris Propane pH 7.5) or 70.0 °C (25 mM Tris-HCl pH 7.5). Sample temperature was kept at 4.0 °C. Autosampler of the liquid chromatograph derivatized primary amines by adding 11.0 or 99.0 µl of OPA solution (0.94 M Bis-Tris Propane pH 9.6, 0.10 M OPA, 0.30 M 3-mercaptopropionic acid and 4.0 % acetonitrile for 25 mM Bis-Tris Propane pH 7.5 or 40.6 mM 2-mercaptopropionic acid and 33.0 mM OPA in 200 mM sodium borate pH 10.0 for 0.25 M Tris pH 7.5, respectively). This procedure took approximately 7 minutes and injection volumes were usually 100.0 µl. The analyses themselves consisted of 13.80 min at 0.7% B, 0.05 min change to 80.0% B, 1.00 min at 80.0% B, 0.05 min change back to 0.70% B, 0.60 min at 0.7% B, injection of 20.0 ul of 16-fold diluted 85% phosphoric acid pH 2.5 (NaOH) to dissolve precipitate of metalhydroxides, and 10.50 min re-equilibration at 0.7% B (25 mM Bis-Tris Propane pH 7.5) or 2.70 min at 4.0% B, 0.10 min change to 80.0% B, 4.70 min at 80.0% B, 0.10 min change back to 4.0% B and 8.40 min of re-equilibration (25 mM Tris-HCl pH 7.5). The analytes were detected using fluorescence (excitation at 340 nm, emission at 450 nm). The limit of quantification was estimated as average of the blank measurement plus 10 x SD of the blank. For both methods, mobile phase A was 25 mM sodium phosphate pH 6.0 supplemented with 0.02 % $NaN_3$ and mobile phase B was acetonitrile.

### 3.2.13. Novel UHPLC Assay for Quantifying $FolGlu_n$ Substrates (Non-radioactive)

Enzymatic reactions were performed in 25 mM Bis-Tris Propane pH 7.5 or in 25 mM Tris pH 7.5 and were quenched by the addtition of 10.00 µl of 0.37 M phosphoric acid with 22 µM 2-(phosphonomethyl)-pentanedioic acid or 2.99 µl of 0.41 M phosphoric acid, 72 µM 2-(phosphonomethyl)-pentanedioic acid and 7.2 µM 2-metcaptoethanol, respectively. Injection volumes could, again, be up to 100.0 µl. Column temperature was 50.0 °C, flow rate 0.400 ml/min. Elution was performed in the isocratic fashion. Mobile phases were the same as for the glutamate quantification method (see above, 3.2.12). Analytical runs consisted of 1.80 minutes at 2.1 or 2.0 /1.5/1.1/0.4/0.2 % B, 0.10 minute change to 20.0% B, 1.10 minutes at 20.0% B, 0.10 minute change back to 2.1 or 2.0 /1.5/1.1/0.4/0.2 % B and 7.40 minute re-equilibration when cleavage of the $FolGlu_{1/2/3/4/5}$ substrates was analyzed. For $FolGlu_6$, the analytical run consisted of 2.10 minutes at 0.0 % B, 0.05 minute change to 20.0% B, 0.85 minutes at 20.0% B, 0.10 minute change back to 0.0 % B and 7.40 minute re-equilibration. $FolGlu_1$ hydrolyzis was also analyzed by a re-optimized method featuring column temperature of 40.0 °C. The analytical runs consisted of 2.50 minutes at

2.7 % B, 0.10 minute change to 50.0% B, 1.10 minutes at 50.0% B, 0.10 minute change back to 2.7 and 10.20 minute re-equilibration.

# 4. RESULTS

## 4.1. Cloning GCPII and GCPIII and Various Mutants into AviTag™ Vectors for the Expression in *Drosophila* S2 Cells

After introducing the facile protein purification method for AviTag™-proteins by Tykvart *et al.*[18], all studied proteins were succesfully cloned into the AviTag™ vector[18] and produced using *Drosophila* S2 cells. GCPII and GCPIII was produced typically at around 20 and 4 mg per liter of medium, respectively. The purifications yields were usually around 20 %. Purity of the AviTag™-proteins was around 90 % and could be further increased by gel permeation chromatography.

## 4.2. Biochemical Characterization of Distinct Substrate Specificities of Human GCPII and GCPIII and Various Mutants

In this section, the discovery of a novel specific, physiologically relevant, substrate of GCPIII will be covered, revealing thus distinct substrate specificities of GCPII and GCPIII. Further, we also provide thorough biochemical and computational evidence on the molecular basis of the different substrate specificities of these two paralogous enzymes.

### 4.2.1. Novel UHPLC Assays of NAAG- and Folyl-poly-γ-L-glutamate-hydrolyzing Activity

The traditional radiometric method of assaying NAAG-hydrolyzing activity, based on the chromatographic separation of radiolabeled products of NAAG, is very tedious and expensive[1], which was a good motivation for an attempt to improve it.

Initially, as published in 2014[174] by us, the assay was similar to classic amino acid analysis, i.e. derivatization of secondary amines by orthophtalaldehyde. However, this variant required laborious and precision-limiting lyophilization a re-dissolution of the samples, so it was superseded by a much more convenient method, employing a novel derivatization formulation and a technologically advanced T3 stationary phase which is a $C_{18}$ phase tolerating even 100 % water (see section 3.2.12).

Using the same instrumentation, column and mobile phases (see section 3.2.13), we also developed a new method for quantifying $FolGlu_n$. This was very practical because all enzymatic activities of GCPII and GCPIII could be assessed in a single sequence, which could be 2 x 96 samples using standard autosampler. The only major difference was the absence of the need for derivatizing the

analyte, since the $FolGlu_n$ substrates possess an intrinsic fluorophore (the pteroid acid). The $FolGlu_n$ substrates were hydrolysed by GCPII/III in an appropriate buffer and the products separated by reversed-phase UHPLC C18 column. The products of hydrolysis were detected and quantified using absorbance at 281 and 357 nm and the analytic methods were around 16 minutes long overall. The absorbance at 281 nm provided a comfortable means of quantification, whereas the absorbance at 357 nm was rather weak but specific, so it could be exploited for deciding whether there is some interfering compound.

### 4.2.1.1. NAAG-hydrolyzing Activity

Our novel UHPLC assay is suitable for quantifying as low as 20 - 30 nM glutamate. Together with transferring the assay to a 96-well-plate format, it became a higher-throughput and fully automated method. Each analysis run featured peaks of aspartate and glutamate separated by around 7.5 minutes (Figure 10).

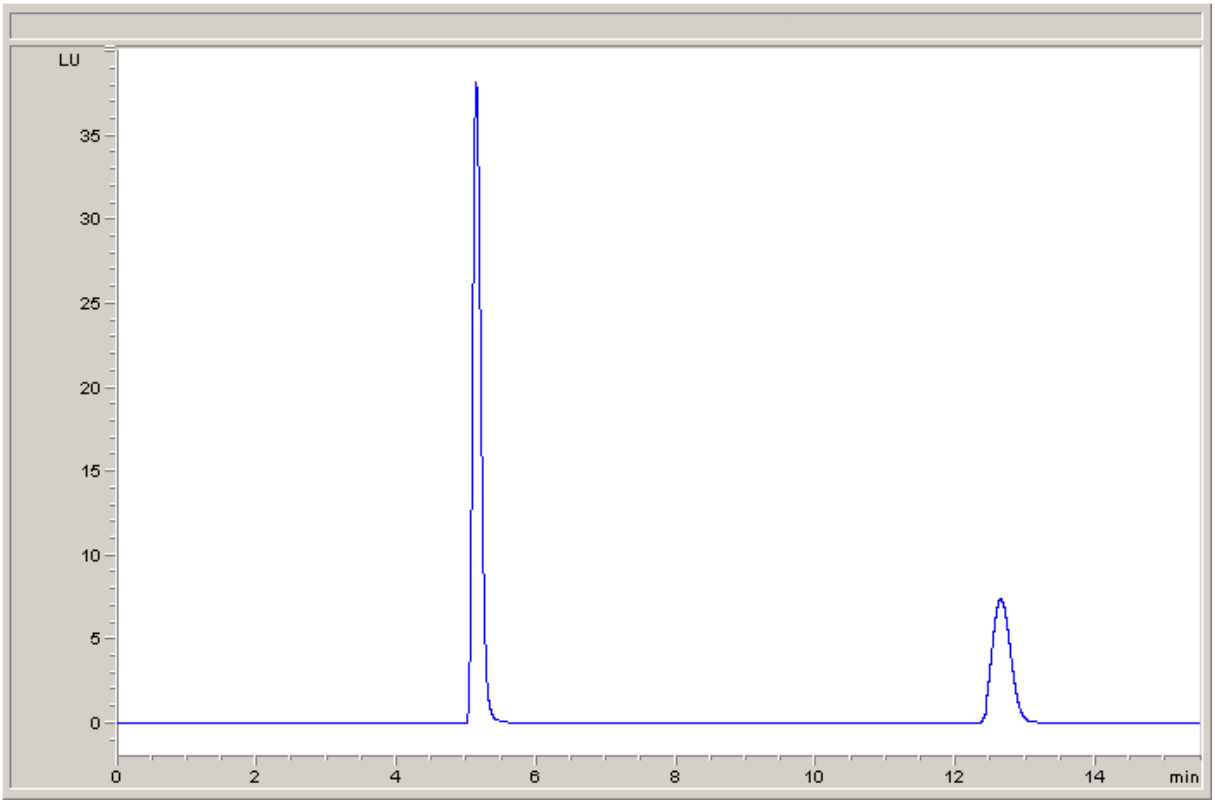


**Figure 10: A typical glutamate quantification chromatogram of our UHPLC method.** The product of hydrosis of NAAG, BCG or NAAG2 (glutamate) is analyzed on a C18 column (2.1 x 100 mm) in 25 mM Tris or bistrispropane, pH 7.5. The peaks are orthophtalaldehyde derivatized aspartate (left) or glutamate (right). Elution occured isocratically at 99.3 % A (25 mM phosphate, pH 6.0; see section 3.2.12 for more details) and 0.7 % B (acetonitrile), with flow rate 0.400 ml/min at around 500 bar. One run took approximately 34 minutes. Analytes were monitored online at 450 nm (emission, excitation was done with 340 nm vawelength). Axes are described on the bottom right (x, time in minutes) or upper left (y, fluorescence units).

## 4.2.1.2. Folyl-poly-γ-L-glutamate-hydrolyzing Activity

Besides our novel NAAG-hydrolyzing assay, we succeeded in developing a cheap and fast method for quantifying folyl-poly-γ-L-glutamic acids, which enabled us to characterize the folyl-poly-γ-L-glutamate hydrolyzing activity of human GCPII and GCPIII (see below, section 4.2.2).

Peaks of $FolGlu_n$ and $FolGlu_{n-1}$ were sufficiently separated by a time window of around two minutes (Figure 11) and their shape resulted in the limit of quantification being usually in the range 3 nM - 0.03 μM, which was enough for most $K_M$ values to be measured with an acceptable precision.

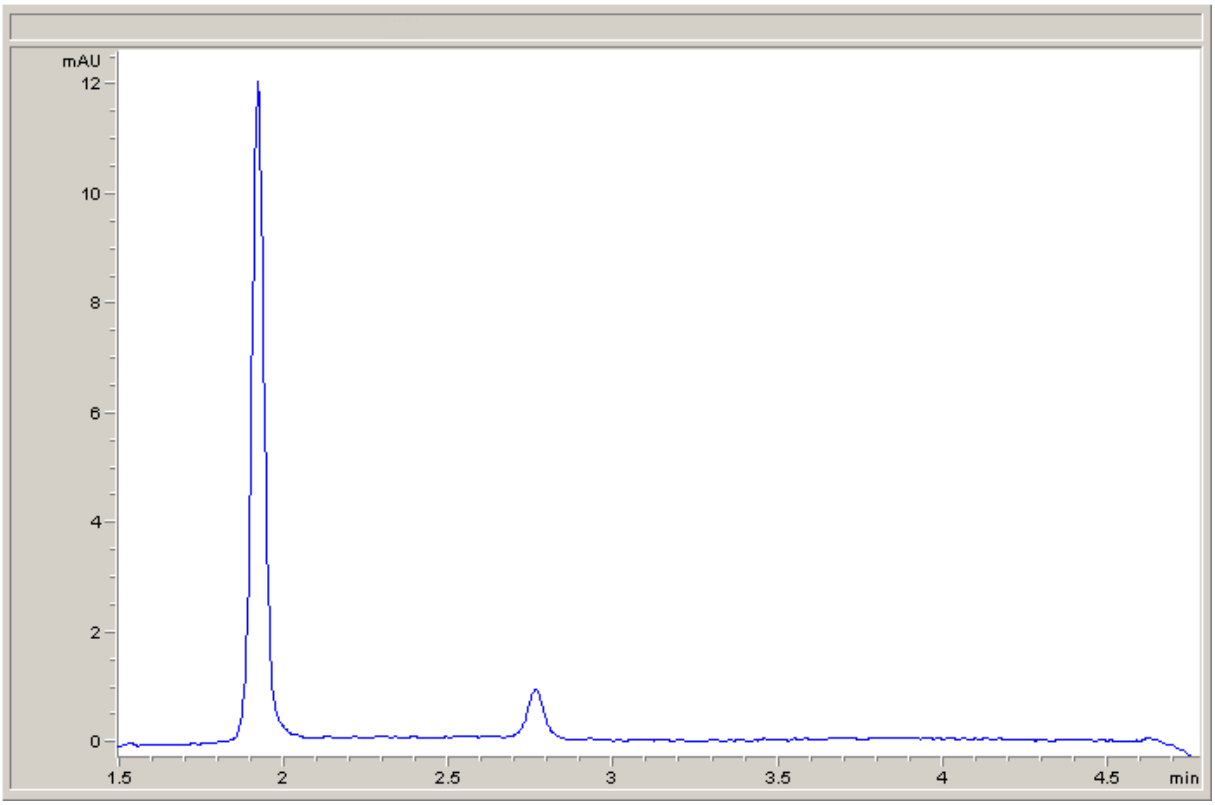


**Figure 11: A typical $FolGlu_n$/$FolGlu_{n-1}$ quantification chromatogram of our UHPLC method.** The products of hydrosis of $FolGlu_1$ ($FolGlu_1$ and $FolGlu_0$) are analyzed on a C18 column (2.1 x 100 mm) in 25 mM Tris or bistrispropane pH 7.5, with or without sodium chloride or detergent. The peak on the left is $FolGlu_1$, the peak on the right is $FolGlu_0$. Elution occured isocratically at 100.0 - 97.3 % A (25 mM phosphate, pH 6.0; see section 3.2.13 for more details) and 0.0 - 2.7 % B (acetonitrile), with flow rate 0.400 ml/min at around 500 bar. One run took approximately 17 minutes. Analytes were monitored online at 281 nm. Axes are described on the bottom right (x, time in minutes) or upper left (y, absorbance units).

## 4.2.2. Characterization of Folyl-poly-γ-L-glutamate-hydrolyzing Activity of GCPII, GCPII His475Tyr and GCPIII

Using our novel UHPLC method for quantifying folyl-poly-γ-L-glutamate hydrolyzing activity, we showed that human GCPII cleaves $FolGlu_n$ substrates at the efficiency comparable to that known for NAAG (Figure 12A).

As discussed in the Introduction, one of the important polymorphisms previously associated with altered folate metabolism is His475Tyr. Therefore, it was of interest to analyze the ability of this mutant protein to hydrolyse $FolGlu_n$ substrates. To this end, we prepared recombinant GCPII mutant bearing the corresponding mutation by expression in Drosophila Schneider's cells (see Materials and Methods, sections 3.2.3 and 3.2.4) and analyzed its enzymatic activities using novel assays described above.

We found that the mutation likely cannot influence folate levels through altered enzymatic activity, because, in our hands, both mutated and wild-type enzymes hydrolyzed $FolGlu_n$ substrates with almost identical effectivity (Figure 12A,B,C). Surprisingly, GCPII His475Tyr showed slightly different kinetic parameters for the the hydrolysis of NAAG whereby it was a $k_{cat}$ effect (Figure 12B,C) (see Discussion).

Finally, we determined the kinetic parameters for the hydrolysis of $FolGlu_n$ substrates by GCPIII to find out that this enzyme cleaves NAAG and $FolGlu_1$ with comparable catalytic efficiencies as GCPII does, while the remaining $FolGlu_{2\text{-}6}$ are cleaved approximately by one order of magnitude less efficiently (Figure 12A). This difference was mainly a consequence of $K_M$ being approximately one order of magnitude higher for $FolGlu_{2\text{-}6}$ (Figure 12B,C), although $k_{cat}$ values were lower as well. In further investigations, the reason for lower $K_M$ values has been attributed to modifications of the arene-binding site in GCPIII (see 1.2.2.3.2.4 and 4.2.3). The hydrolysis of NAAG by GCPIII was the opposite - in comparison to GCPII, it was slower due to a lower $k_{cat}$ (Figure 12A,B,C).

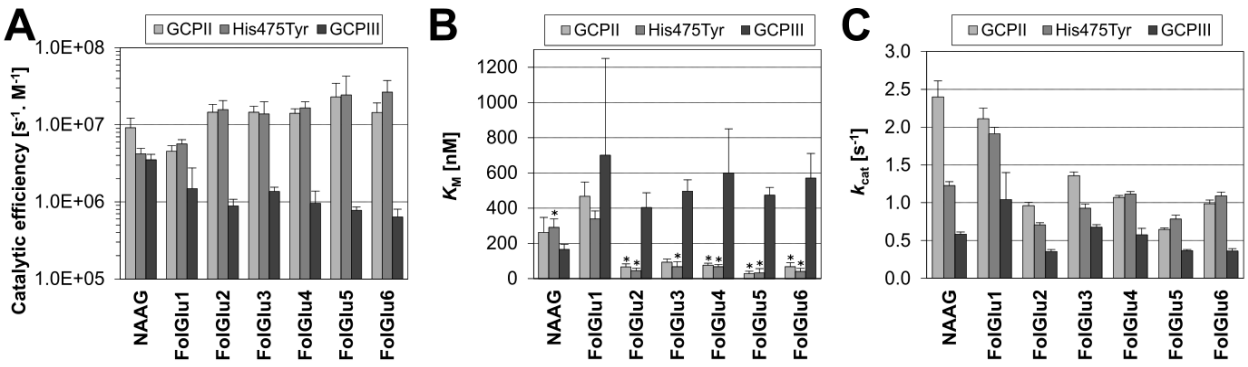

**Figure 12: Comparison of folyl-poly-γ-L-glutamate hydrolyzing activities of recombinant human GCPII, GCPII His475Tyr and GCPIII.** Graphical representation of the kinetic constants of $FolGlu_n$ hydrolysis by GCPII, GCPIII and His475Tyr mutant of GCPII. Error bars represent standard deviation. The reaction buffer was 25 mM Tris pH 7.5. * indicates that $K_M$ value was lower than the lowest substrate concentration. (A) Catalytic efficiencies. (B) $K_M$ values. (C) $k_{cat}$ values.

## 4.2.3. Arene-Binding Site and its Relevance to Folyl-poly-γ-L-glutamate-hydrolyzing Activity of GCPII

After the arene-binding site (ABS) was described in 2010[43] (see 1.2.2.3.2.4), we were able to show that it is this exosite which interacts with the pteroic acid moiety of $FolGlu_n$ substrates, both at the structural (see 4.3.1) and the biochemical level (see below).

In order to assess the significance of the ABS at the biochemical level, two approaches were taken - mutagenesis of the ABS of GCPII combined either with kinetic studies using natural $FolGlu_n$ substrates or with inhibition studies.

To find out how significant is the near-surface exosite, the ABS, for the hydrolysis of $FolGlu_n$ substrates, we performed site-directed mutagenesis of the putative ABS. The single mutations Trp541Ala, Arg511Leu and Arg463Leu had almost no effect on the hydrolysis of $FolGlu_n$ substrates, while they imposed quite a substantial deterioration of NAAG-hydrolyzing activity (Figure 13).

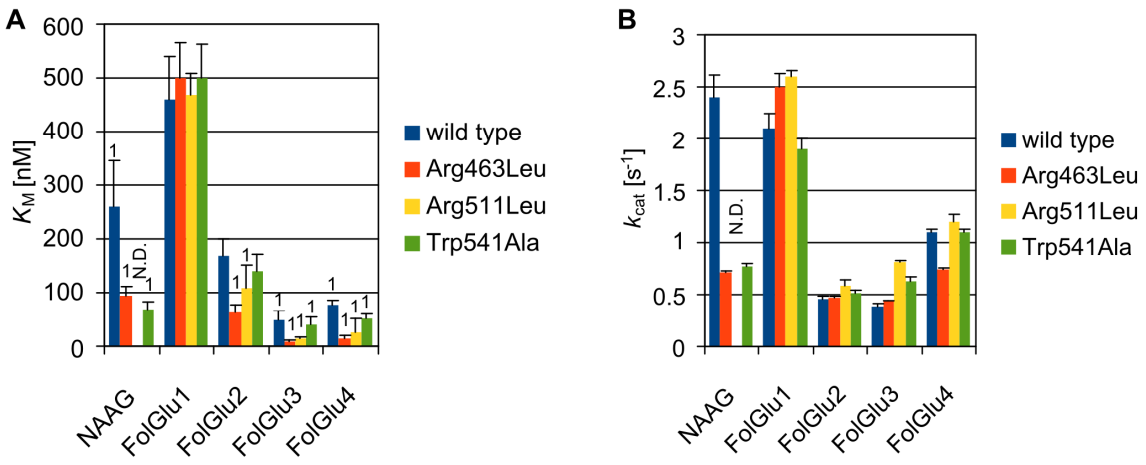


**Figure 13: Kinetic parameters for the hydrolysis of $FolGlu_n$ substrates and NAAG by GCPII and its arene-binding site (ABS) mutants.** This figure shows that the mild single mutations Trp541Ala, Arg511Leu, Arg463Leu of GCPII do not alter the $FolGlu_n$-hydrolyzing activity, and that these mutations change only the NAAG-hydrolyzing activity. The reaction buffer was 25 mM Tris pH 7.5. N.D., not determined. Error bars represent standard deviation. 1 indicates that the $K_M$ value was lower than the lowest substrate concentration. (A) $K_M$ values. (B) $k_{cat}$ values.

The rather marginal importance of the ABS for the hydrolysis of $FolGlu_n$ substrates [evident also from a comparison of the kinetic data contained in Figure 12 (wild-type GCPIII) and Figure 13 (wild-type GCPII and ABS mutants)] is in agreement with the marginal difference between the ABS residues of GCPII and its counterparts in GCPIII. They are the same except for Trp541 of GCPII, which is a lysine residue in GCPIII (Lys531), and this subtle difference confers only higher $K_M$ values of individual $FolGlu_{2-6}$ substrates for GCPIII (in comparison to GCPII, Figure 12). This increase in $K_M$ values is thus likely not a consequence of a "disruption" of the ABS of GCPIII but instead a consequence of infavourable interaction of Lys531 with the aromatic pteridine ring of $FolGlu_n$ substrates.

To further analyze the ABS, we determined how specific GCPII inhibitors, ARM-P2,4,8 (shown to interact with this exosite)[43] (Figure 14A), inhibit the hydrolysis of $FolGlu_1$ by GCPII wild type and Trp541Ala[174] (Figure 14B). In agreement with previously published data[43], the ARM-P2 compound inhibited wild-type GCPII with the lowest $K_I$ value (Figure 14B) and there was the most notable difference between wild type and Trp541Ala for the ARM-P4/8 inhibitors[174] (Figure 14B). Therefore, we investigated the inhibitory potency of ARM-P4 also toward other mutants - Arg511Leu and Arg463Leu (Figure 14B). A trend of decreased binding affinitiy was observed, although, somewhat unexpectedly, the mutant Arg511Leu bound the ARM-P4 inhibitor with the same affinity as wild-type, and the mutation Arg463Leu lead to a decreased binding affinity in comparison to Arg511Leu.

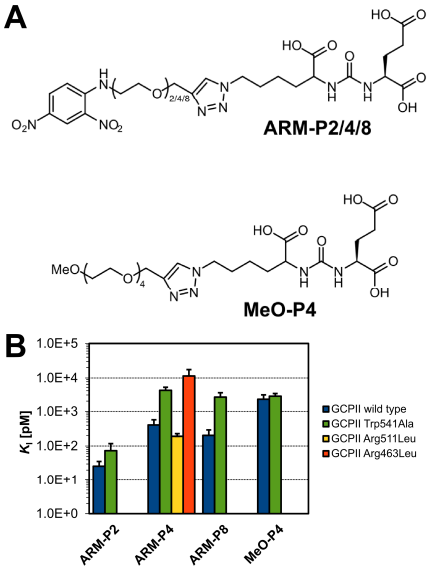


**Figure 14: ABS-targeted inhibitors and ABS mutants of GCPII.** (A) Structure of ARM-P2,4,8[43] inhibitors and the control compound MeO-P4. (B) Comparison of Trp541Ala (green) mutant to wild-type GCPII (blue) in terms of affinity for ARM-P2,4,8 and MeO-P4 inhibitors, determined as $K_I$ values. The inhibitor ARM-P4 was additionally tested also with mutants Arg463Leu (red) and Arg511Leu (yellow).

## 4.2.4. The First Specific Substrate of GCPIII - β-citryl-L-glutamate

Independently of the pioneering work by Collard *et al.*[8], we were able to identify the decades-long known non-standard dipeptide β-citryl-L-glutamate (BCG) as a hot candidate for a substrate of GCPII or GCPIII. BCG was successfully synthesized by Jiří Schimer at our institute (manuscript under revision).

### 4.2.4.1. Metal-dependent Hydrolysis of BCG by GCPIII and its Superior Specificity over GCPII

In contrast to the pioneering work by Collard *et al.*[8], which studied the mouse homolog of GCPIII, we studied recombinant human GCPIII expressed in *Drosophila* S2 cells as a fusion protein with the AviTag™ (see 4.1). Additionally, we also tested all conceivable, physiologically relevant metals - $Ca^{2+}$, $Mn^{2+}$, $Zn^{2+}$, $Fe^{2+}$, $Cu^{2+}$, $Co^{2+}$ and $Mg^{2+}$, which lead us to the observation that the NAAG- and BCG-hydrolyzing activity of GCPIII is dependent also on cobalt(II) ions, while $Fe^{2+}$, $Cu^{2+}$ and $Mg^{2+}$ ions had no effect. We also found out that even the hydrolysis of $FolGlu_1$ is activated by $Mn^{2+}$, $Zn^{2+}$ and $Co^{2+}$ ions.

All other biochemical parameters were similar to those published for recombinant mouse GCPIII[8]. For example, the hydrolysis of BCG is performed by GCPIII with a $k_{cat}$ value of 14.00 $s^{-1}$ ± 0.50 and 4.26 ± 0.22 $s^{-1}$ in the presence of 2.5 mM $Ca^{2+}$ and 0.25 mM $Mn^{2+}$, respectively (compare to the values 6 and 3 $s^{-1}$ for the recombinant mouse GCPIII[8]). $Zn^{2+}$ activated the hydrolysis of $FolGlu_1$ so that the $k_{cat}$ value increased by more than one order of magnitude to 0.846 $s^{-1}$, whereby $K_M$ value remained comparable. A comprehensive comparison of $Ca^{2+}$, $Mn^{2+}$ and $Zn^{2+}$ dependent kinetic parameters for the hydrolysis of BCG, NAAG and $FolGlu_1$ is shown in the Figure 15. Overall, we can conclude that metals cations tend to increase only $k_{cat}$ values (Figure 15B), up to by 4 orders of magnitude in case of the hydrolysis of BCG by GCPIII, and that $K_M$ values remain largely unchanged or change only up to by 1 order of magnitude (Figure 15C).

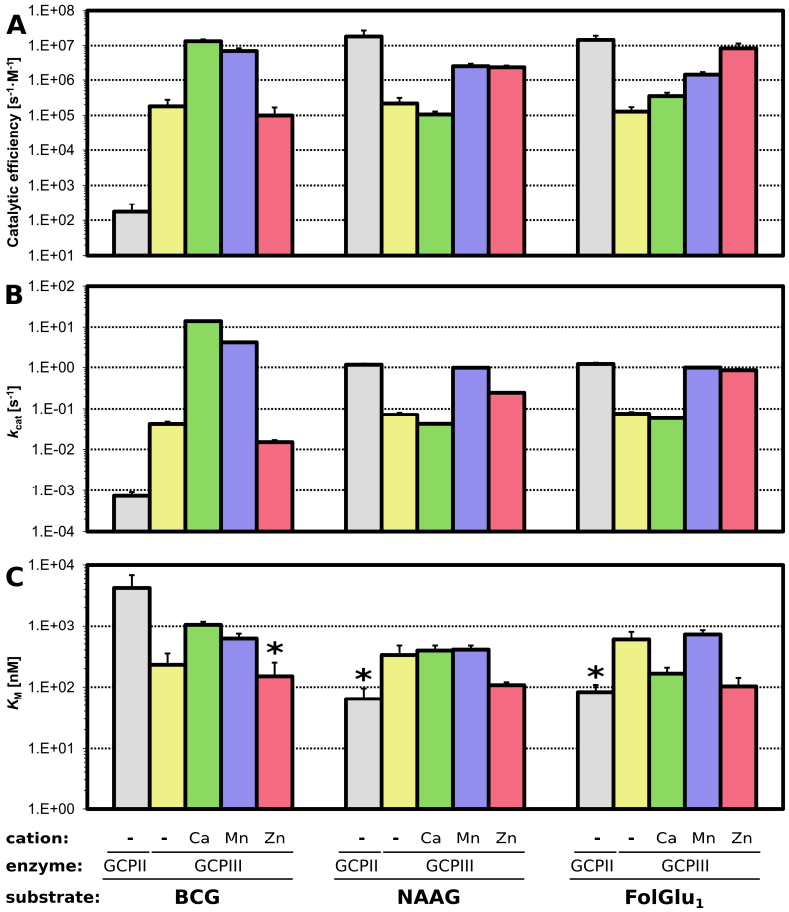


**Figure 15: BCG is a highly selective substrate of GCPIII.** This comparison highlights the ability of GCPIII to hydrolyze BCG in a $Ca^{2+}$ and $Mn^{2+}$ dependent manner and NAAG and $FolGlu_1$ in a $Mn^{2+}$ and $Zn^{2+}$ dependent manner. The reaction buffer was 25 mM bistrispropane, pH 7.5 (prepared from ultrapure water). Error bars stand for the standard deviation. * indicates, that the $K_M$ values were lower than the lowest substrate concentrations. (A) Catalytic efficiencies. (B) $K_M$ values. (C) $k_{cat}$ values.

As shown in the Figure 15, human GCPII is capable of hydrolyzing BCG as well, although, compared to GCPIII, with a several-orders-of-magnitude lower catalytic efficiency and $k_{cat}$ value and a higher $K_M$ value (Figure 15A,B,C).

## 4.2.4.2. Occupancy of the Zinc Atoms in GCPIII

As reported previously by our group[153], the occupancy of Zn1 and Zn2 atoms in the active site of GCPIII X-ray structures varies in the range 0.80-0.95 and 0.45-0.80, respectively. To further confirm these findings, we conducted an AAS analysis of the zinc content of GCPII and GCPIII (manuscript under revision).

We found out that the ratio of zinc to protein molecule is 1.40 for GCPII and 1.13 for GCPIII. Together with the structural data[153], this was the second clue that the Zn2 atom might be bound so

loosely that it might be replaced by some other metal, as proposed by Collard *et al.*[8]. We addressed this issue experimentally and computationally (see below for section 4.2.4.3).

## 4.2.4.3. Indirect Evidence That GCPIII Might Feature an Active-site Heterometallic Cluster

To provide more reliable data than published[8] or QM/MM data (see 4.3.2.2, manuscript in submisstion), we performed several experiments providing indirect evidence, that the metals like $Ca^{2+}$ or $Mn^{2+}$ might indeed bind to the active site. These included determining the $K_I$ of $Ca^{2+}$ (see below, 4.2.4.3.1), inhibition studies with BCG and citrate in the presence of various metals (see 4.2.4.3.2) and differential scanning fluorimetry with GCPIII and GCPIII Glu414Ala in the presence of BCG and various metals (see 4.2.4.3.3).

### 4.2.4.3.1. Dissociation Constant of $Ca^{2+}$

To analyze the hypothesis that Zn2 could be replaced by another metal (see 4.2.4.1 and 4.2.4.2), we studied the inhibition of $FolGlu_1$ hydrolyzing acitivity of GCPIII by increasing amounts of $Ca^{2+}$ in the presence of moderate concentration of $Zn^{2+}$ (0.10 mM). $Ca^{2+}$ confers a roughly 15 times lower $k_{cat}$ value for the hydrolysis of $FolGlu_1$ than that confered by $Zn^{2+}$ (see Figure 15). Adding $Ca^{2+}$ into a $FolGlu_1$ hydrolysis reaction was thus almost the same as adding an inhibitor and this data could be fitted with a sigmoid to yield an $IC_{50}$ value of 20.3 ± 1.3 mM and ultimately a $K_I$ value of 17.9 ± 2.3 mM.

### 4.2.4.3.2. Inhibition Studies Suggesting that BCG Could Participate in Binding the Metal 2 Atom in the Active Site of GCPIII

We analyzed competitive inhibition of $FolGlu_1$ hydrolyzing activity by BCG, citrate and glutamate in the presence of selected metal ions (Figure 16). We found that while inhibition by glutamate is identical regardless the metal cation used, the inhibition by citrate or BCG is slightly improved in the presence of $Ca^{2+}$ or $Mn^{2+}$ (Figure 16), suggesting that BCG might participate in binding these metals to possibly replace Zn2.

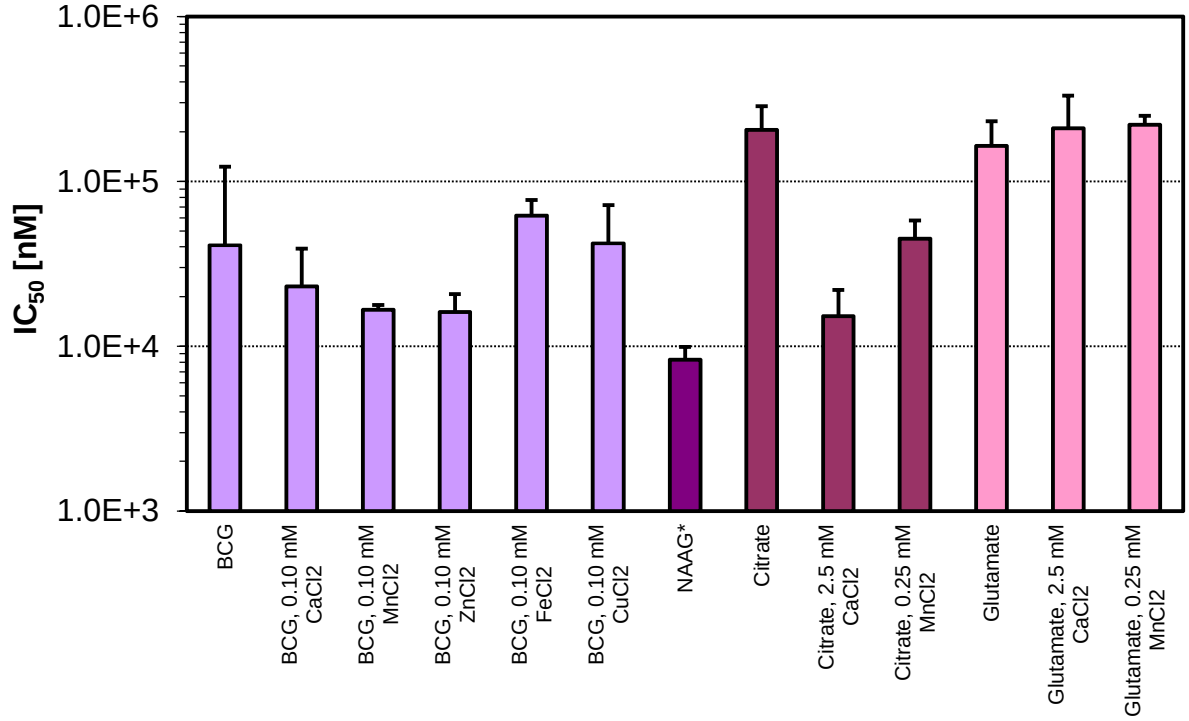


**Figure 16: Inhibition assay of GCPIII with BCG, citrate and glutamate in combination with various divalent metals.** BCG and Citrate (violet and red, respectively) inhibit slightly more effectively in the presence of $Ca^{2+}$ and $Mn^{2+}$, while glutamate (pink) inhibits the same no matter which divalent metal is present. As a control, inhibition by NAAG (purple) is also shown. The reaction buffer was 25 mM bistrispropane, pH 7.5, 0.15 M NaCl, 0.0010 % C12E8 (* indicates, that the buffer was by mistake slightly different - 25 mM bistrispropane, pH 7.5, 0.14 M NaCl, 0.00090 % C12E8). Substrate was 0.40 μM $FolGlu_1$. As a source of $Fe^{2+}$ cations, $Fe(NH_4)_2(SO_4)_2 \cdot 6H_2O$ (Mohr's salt) has been used. Error bars represent standard deviation. Please note that BCG and NAAG are cleavable.

## 4.2.4.3.3. Differential Scanning Fluorimetry

Using differential scanning fluorimetry, we were able to show that $Ca^{2+}$ ions confer an increase in thermal stability of GCPIII, as assessed by the temperature midpoint for the unfolding transition, $T_m$, by approximately 3.5 °C (5.0 mM, pH 7.5), $Zn^{2+}$ by 11 °C (0.10 mM, pH 7.4) and $Mn^{2+}$ by 15 °C (5.0 mM, pH 7.5). For $Ca^{2+}$ ions, this effect was pH dependent - $T_m$ was lower in the absence of 5.0 mM $Ca^{2+}$ from 3 °C (pH 7.5) through 13 °C (pH 8.4) to 18 °C (pH 9.4), whereby the absolute value of $T_m$ in the presence of 5.0 mM $Ca^{2+}$ remained either constant or was lower by 2.9 °C for pH 9.4. A similar trend was observed also for the inactive mutant of GCPIII, Glu414Ala, for which $T_m$ was lower in the absence of 5.0 mM $Ca^{2+}$ from 6.8 °C (pH 7.5) through 17 °C (pH 8.4) to 19 °C (pH 9.4). BCG increased $T_m$ of GCPIII Glu414Ala only by 1.9 °C (pH 7.5), whereby the inactivating mutation itself incresed the $T_m$ by 3.1 °C (pH 7.5) (for GCPII, the mutation Glu424Ala incresed $T_m$ by 2.9 °C at pH 7.5). On the other hand, $Mg^{2+}$ (5.0 mM, pH 8.4) or $Cu^{2+}$ and $Fe^{2+}$ (0.10

mM, pH 8.4) failed to show any stabilization. Taken together, these results are yet another piece of indirect evidence that metals like $Ca^{2+}$, $Mn^{2+}$ or $Zn^{2+}$ bind specifically to GCPIII.

### 4.2.4.4. pH Optimum of BCG-hydrolyzing Activity of GCPIII

Because GCPIII cleaves NAAG in a pH-dependent manner, with pH optimum shifted by approximately 0.5 to basic conditions in comparison to GCPII[26] (to 8.5 in absolute value), we naturally determined the pH optimum also for the hydrolysis of BCG in the presence of physiologically relevant 2.5 mM $Ca^{2+}$ ions (using substrate concentration of 10 μM), buffering the whole pH range by 25 mM bistrispropane (Figure 17). As a result, the pH optimum has been determined to lie around the value 8.4 (Figure 17). At the pH optimum, the $k_{cat}$ value is approximately 2.6 times higher than at pH 7.4.

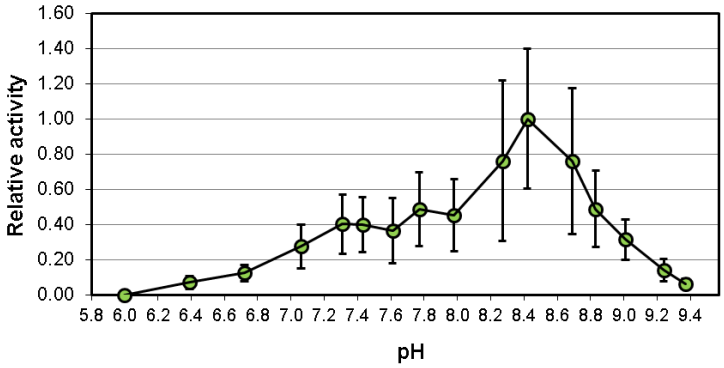


**Figure 17: The pH optimum of the hydrolysis of BCG by GCPIII in the presence of 2.5 mM $Ca^{2+}$ ions for near-saturation condtions (10 μM substrate).** The reaction buffer was 25 mM bistrispropane. Glutamate was assayed using our novel UHPLC assay (for more information, see 3.2.12). Error bars represent the standard deviation. 10 μM substrate means that it was present at the saturation level.

## 4.3. Structural Characterization of Distinct Substrate Specificities of GCPII and GCPIII

We were succesful at obtaining X-ray structures of GCPII Glu424Ala in complex with substrates as diverse as $FolGlu_{1\text{-}3}$ or BCG. Additionaly, we also computed a QM/MM model of how BCG might bind into GCPIII. All these results let us make relevant conclusion (see below) about what might be the structural basis for the distinct substrate specificities of GCPII and GCPIII.

## 4.3.1. Folyl-poly-γ-L-glutamic Acids and the Discovery of the S2 Site

Although the ability of GCPII to cleave folyl-poly-γ-L-glutamic acids has been decribed decades ago, there was no structural data describing the enzyme-substrate binding mode. Therefore, we set to analyze the structure of the complex using the inactive mutant GCPII Glu424Ala and $FolGlu_{1-6}$ substrates. Using the crystallization condition for GCPII previously published by Bařinka *et al.*[38], we also tried setting up hanging drops of GCPII Glu424Ala with $FolGlu_{1-6}$ substrates. The crystals diffracted to resolutions 1.70 Å ($FolGlu_0$), 1.65 Å ($FolGlu_1$), 2.00 Å ($FolGlu_2$), 1.65 Å ($FolGlu_3$), 1.54 Å ($FolGlu_4$) 1.61 Å ($FolGlu_5$) and 1.71 Å ($FolGlu_6$).

We only published the $FolGlu_{1-3}$ complexes[174], because these substrates were well defined by the electron density map (except for $FolGlu_3$ complex, where the benzoic acid and one N-terminal γ-L-glutamic acid moiety is less electron-dense). The $FolGlu_4$ complex had a good electron density for C-terminal tri-γ-L-glutamic acid moiety and a weak one between Trp541 and Arg511 (indicating that the pteroic acid of $FolGlu_4$ might be bound here in a similar manner as $FolGlu_3$, see Figure 18A). The $FolGlu_0$ and $FolGlu_{5-6}$ complexes were rather a puzzle, because in all of them, only the C-terminal tri-γ-L-glutamic acid moiety bound to the active site - almost the same way as in other $FolGlu_{>1}$ complexes - could be unambiguously identified (see also Discussion).

The exact mode of binding of $FolGlu_{1-3}$ is depicted in the Figure 18. The panel A, showing also electron density maps contoured at 1.0σ, makes it obvious that the residue Trp541 is inherently flexible and serves to interact with aromatic moieties of $FolGlu_{1-3}$ substrates in a μ-μ ($FolGlu_{1-3}$) or T-shape stacking ($FolGlu_{2-3}$) manner.

We also found out that the interactions described previously in the GCPII Glu424Ala-NAAG complex[16] for the S1' and S1 site are very similar in the case of $FolGlu_{1-3}$ complexes. Moreover, as illustrated by the structural overlay of $FolGlu_{1-3}$ shown in the Figure 18B, the spatial arrangement of the substrate moieties occupying S1' and S1 sites is almost invariant, whereas more distally, substrate moieties sneak with more positional freedom through GCPII in a tightly limited space. More specifically, our results newly define an S2 site (data not shown) with the residues Tyr700, Asn698, Arg463, backbone carbonyl of Lys207, Glu457 (marginally), and also Ser547 (this residue only for $FolGlu_1$) which is likely the reason why all $FolGlu_{1-6}$ complexes feature, in structural terms, a practically invariant C-terminal tri-γ-L-glutamic acid moiety. Futhermore, it is interesting to note that Asn698 is part of the glutarate sensor (see 1.2.2.3), so catching the substrate does not occur only at the S1' site as initially thought, but also here. Furthermore, our another structure - the GCPII Glu424Ala BCG complex (see below, 4.3.2.1) - captured the glutarate sensor in two conformations (4.3.2.1), whereby the sidechain of Asn698 was defined by the electron density map

only for the closed conformation (data not shown). Our result is also the conclusion, that there is nothing like S3 site, because it is not defined at all, and the glutamic acid moiety occupying this space in the $FolGlu_3$ complex has almost no electron density map.

Further, our results additionaly show that the aromatic interactions seen in the ABS take place at distances favorable for a relativly significant binding - 3.2 to 3.7 Å (Figure 18C). For example, Tyr700 or Arg463 and Trp541 bind the para-aminobenzoic acid of $FolGlu_1$ or $FolGlu_2$, respectively, and the pteridine ring of $FolGlu_{2-3}$ is wedged between Arg511 and Trp 541 (Figure 18C). These interactions are likely responsible for a very similar mode of binding into the ABS seen with $FolGlu_2$ and $FolGlu_3$, namely that the P3 moiety (glutamic acid) of $FolGlu_3$ only slightly bulges out of GCPII in comparison to $FolGlu_2$ (Figure 18A).

When we compare the mode of binding of $FolGlu_{1-3}$ substrates and the complex of GCPII with the best ABS-binding inhibitor ARM-P4[43] (structure shown in Figure 14A), and if the faint electron density between Trp541 and Arg511 in the $FolGlu_4$ complex is taken into account (mentioned above), we can conclude that from the structural point of view, the strongest binding of aromatic moieties is conferred by Trp541 and Arg511. This conlusion is also in a good agreement with kinetic data obtained for the hydrolysis of $FolGlu_n$ substrates by wild-type GCPII (see 4.2.2 and Figure 12), according to which $FolGlu_1$ (being too short to reach between these two residues, as shown by our structures - see Figure 18A) has almost one-order-of-magnitude higher $K_M$ than the other $FolGlu_{2-6}$ substrates, which are long enough to engage Trp541 and Arg511 (Figure 18A).

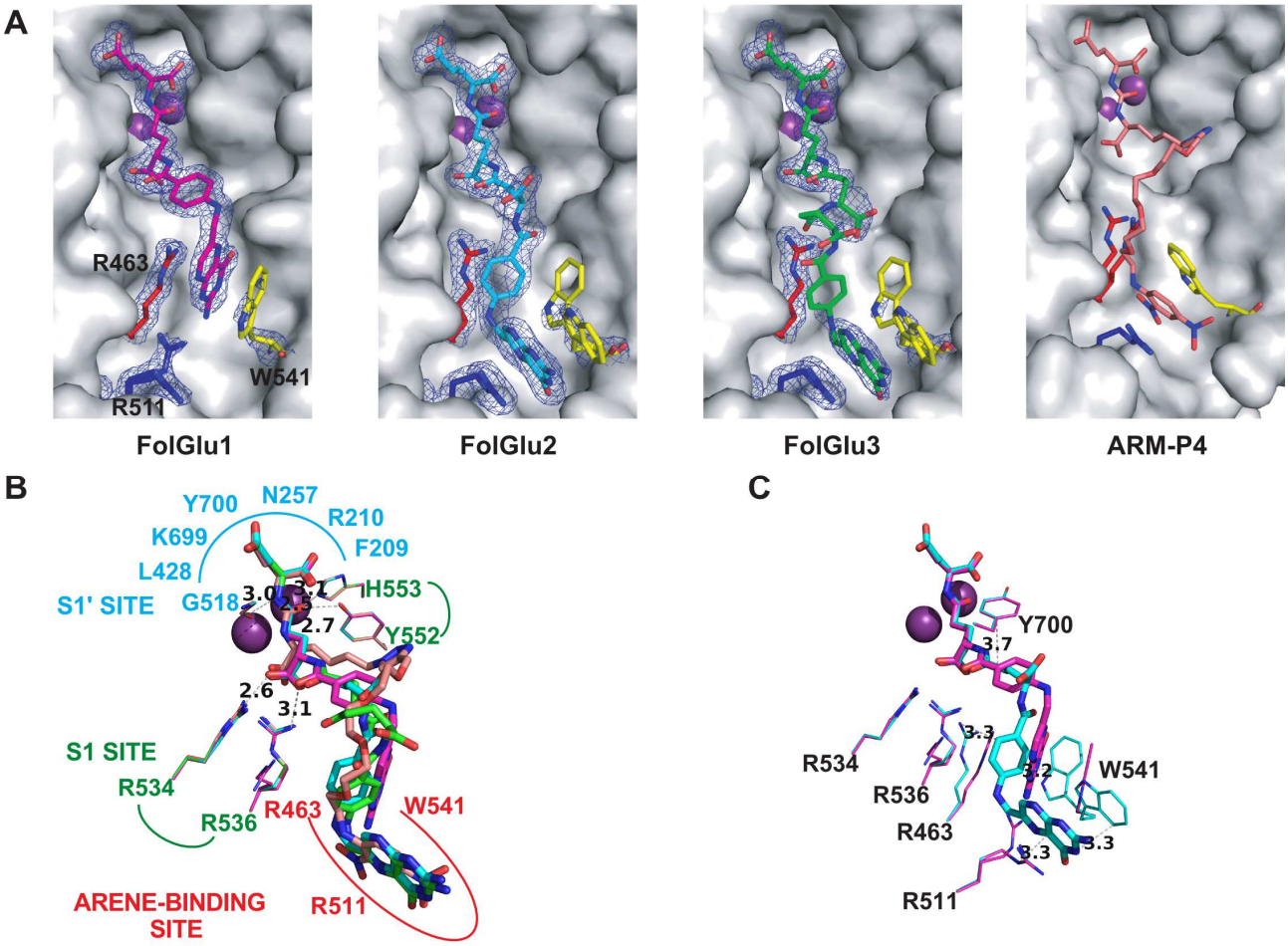


**Figure 18: The mode of binding of FolGlu$_{1\text{-}3}$ into human GCPII and its arene-binding site (ABS), and a comparison to the first ABS-binding inhibitor, ARM-P4[43].** Substrates are depicted in stick representation. FolGlu$_1$ (PDB entry 4MCP) is shown in magenta, FolGlu$_2$ (PDB entry 4MCQ) in cyan, FolGlu$_3$ (PDB entry 4MCR) in green and ARM-P4 (PDB entry 2XEG[43]) in pink. Active-site zinc atoms are colored purple and shown as spheres. Binding interactions are indicated by gray dashed lines and a number in Å. The structural images were created using PyMol[46]. (A) Detailed view of the ABS, with its residues Trp541, Arg511 and Arg463 shown in stick representation. Electron density maps ($2F_o$-$F_c$) are contoured at 1.0σ. ABS is oriented the same way as in the Figure 8. (B) Schematic representation of residues forming the S1', S1 and arene-binding sites, with FolGlu$_{1\text{-}3}$ shown in superposition. Indicated distances highlight how the peptide bond or the α carboxylate of the P1 glutamate is bound by His553, Tyr552, Zn1 (upper shpere) and Gly518 or Arg534 and Arg536, respectively. (C) Superposition of the FolGlu$_1$ and FolGlu$_2$ structures showing the hydrophobic interactions in the ABS and also between the para-aminobenzoic acid moiety of FolGlu$_1$ and Tyr700.

Another important finding derived from the complexes FolGlu$_{0\text{-}6}$ is that the entrance lid, defined by the residues 541 - 548, takes up the open conformation (see 1.2.2.3), which has typically been seen with bulkier molecules bound to GCPII.

Further, it has been previously reported that in the hydrophobic pocket of GCPII[41], Arg536 is present either in one or two conformations, with Arg463 present only in one of its two conformations. This holds true also for the GCPII-Glu424Ala-FolGlu$_{0\text{-}3}$ complexes. However, for the unpublished structures FolGlu$_{4\text{-}6}$, the opposite is true - Arg536 is always present in one

conformation (the binding conformation; for more information, see Figure 9 in the section 1.2.2.3.2.5), while Arg463 takes up both of its two possible conformations simultaneously.

## 4.3.2. The X-ray Structure of GCPII in Complex with BCG and the QM/MM Model of GCPIII in Complex with BCG

The following two sections, 4.3.2.1 and 4.3.2.2, describe the structural basis for the differences between GCPII and GCPIII.

### 4.3.2.1. X-ray Structure of the GCPII Glu424Ala β-citryl-L-glutamate complex

Because we were unable to obtain an X-ray structure of GCPIII Glu414Ala (the inactive mutant of GCPIII) in complex with β-citryl-L-glutamate (BCG), we set out to obtain and solve the structure of the complex of GCPII Glu424Ala with BCG. However, GCPII did not crystallize in the presence of BCG. Nonetheless, we were successfull in crystallizing free GCPII Glu424Ala and then soaking the crystals with BCG. The result is depicted in Figure 19 (diffraction data for 1.85 Å resolution, PDB entry 4F09, manuscript under revision). The occupancy of BCG was refined to only 70 %, which is likely the result of BCG's low affinity for GCPII ($K_M$ value of 4.2 μM, manuscript under revision). This lower occupancy gave rise to a relatively weak electron density map (Figure 19A). The overall mode of binding of BCG to GCPII is nearly the same as in the structure of GCPII Glu424Ala in complex with NAAG (Figure 19B, PDB entry 3BXM[16]). The GCPII Glu424Ala BCG complex, when compared to GCPII Glu424Ala in complex with NAAG (Figure 19B), is unique by the absence of the 4.0 Å hydrophobic interaction between the γ-methylene of glutamic acid moiety and the Phe209 and the 2.7 Å bond between Arg536 and the N-acetyl moiety of NAAG and by the presence of the 3.5 Å bond between Asn519 and the hydroxyl moiety of BCG.

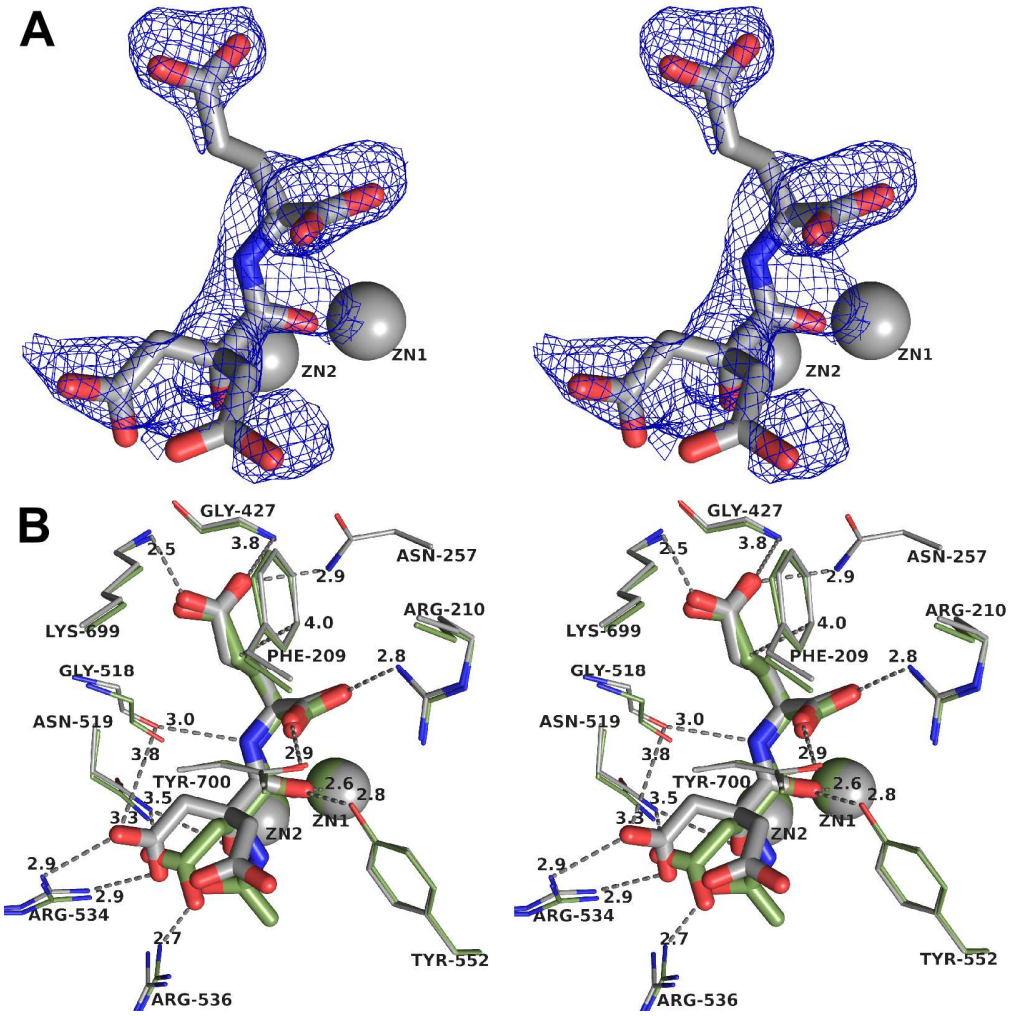


**Figure 19: X-ray structure of GCPII Glu424Ala in complex with BCG (GCPII-Glu424Ala-BCG), rendered in cross-eye stereo representation.** Zinc atoms are shown as spheres. BCG and NAAG are depicted in stick representation. The GCPII-Glu424Ala-BCG complex (PDB entry 5F09, manuscript under revision) is colored light gray and GCPII-Glu424Ala-NAAG (PDB entry 3BXM[16]) green. Binding interactions are indicated by gray dashed lines and a number in Å. Please note that Tyr700 is trimmed to provide a better view. The images were created using PyMol[46]. (A) Electron density map of BCG ($2F_o$-$F_c$), contoured at 1.0σ. (B) Overlay of the BCG structure with that of NAAG. Only side chains of substrate-binding residues are shown. The two interactions between Phe209 and the γ-methylene of glutamate moiety of NAAG (4.0 Å) and Arg536 and the carbonyl oxygen of the N-acetyl moiety of NAAG (2.7 Å) are found only in the GCPII-Glu424Ala-NAAG complex.

One striking feature of the GCPII Glu424Ala BCG complex was the presence of the glutarate sensor (see 1.2.2.3) in two equally populated conformations (Figure 20). This might be the consequence of the low affinity of BCG for GCPII ($K_M$ value of 4.2 μM, manuscript under revision). The previously reported structure of GCPII in complex with phosphate, which binds to GCPII with a similar affinity ($IC_{50}$ 10 μM[17]), features the glutarate sensor in the open conformation, almost identically as reported herein. However, the electron density map for the glutarate sensor of our structure of GCPII in complex with BCG was weak, and Lys699 and Tyr700 of the open conformation could be modeled only as stubs.

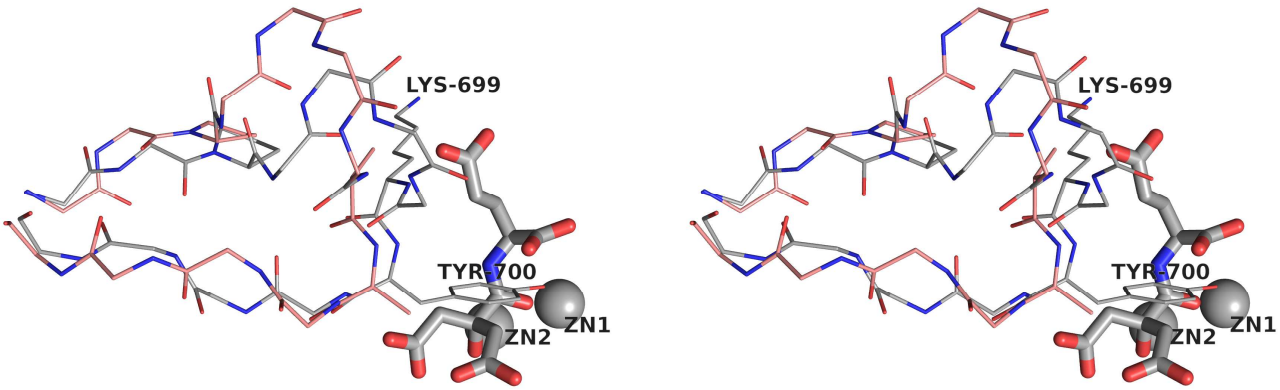


**Figure 20: The glutarate sensor of the GCPII-Glu424Ala-BCG X-ray structure, rendered in cross-eye stereo representation.** The open conformation is colored pink, the closed light gray. The glutarate sensor is shown only as mainchain, with the exception of Lys699 and Tyr700, where these two residues are shown with their complete side chains (closed) or as stubs (open). Zinc atoms are shown as spheres. BCG is depicted in stick representation and colored the same as the closed conformation. The image was created using PyMol[46].

## 4.3.2.2. The QM/MM Model of GCPIII in Complex with BCG, Featuring either a Homometallic Zinc-Zinc or a Heterometallic Calcium-Zinc Cluster in the Active Site

The availability of the X-ray structure of GCPII Glu424Ala in complex with BCG enabled us to attempt to model the structure of the homologous GCPIII in complex with the same compound using QM/MM approach (in collaboration with the group of Dr. Rulíšek at the IOCB). As a result, we obtained a QM/MM model of the GCPIII BCG complex. Its comparison to the X-ray structure of the GCPII Glu424Ala BCG complex suggests that it might well represent the most probable conformation of BCG bound to GCPIII (Figure 21).

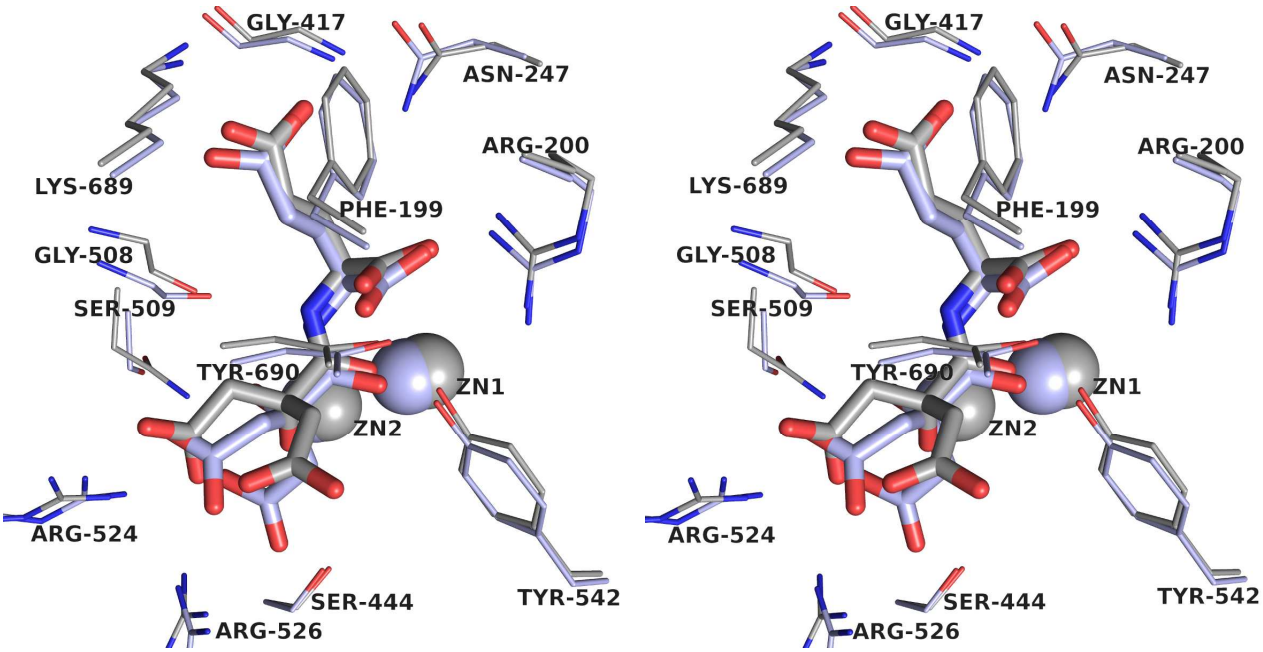


**Figure 21: Structural overlay of the X-ray structure of the GCPII Glu424Ala BCG complex and the QM/MM model of GCPIII BCG complex, rendered in cross-eye stereo representation.** The GCPII Glu424Ala BCG complex is colored light gray, the GCPIII BCG complex light blue. BCG is shown in stick representation. Residue labels correspond to that of GCPIII (their numbers are lower by 10 in comparison to GCPII). The acitve site looks very similar and the most notable difference is the orientation of the citrate moiety of BCG in the GCPIII BCG complex (rotated by approximately 90°). The image was created using PyMol[46].

This comparison additionaly shows that the most notable difference in binding of BCG into GCPIII (in comparison to GCPII) is the orientation of its citrate moiety (Figure 21). To be more specific, the citrate moiety of BCG is oriented in GCPII in such a way that its only interaction with the protein is hydrogen bonding to the Arg534 and Asn519 (Figure 22A). In GCPIII, on the other hand, it is rotated by approximately 90° (Figure 22B), which opens up the possibility of more interactions with the residues present in the active site - hydrogen bonding with Arg526 (the structural equivalent of Arg536 of GCPII) and Ser444 (Ser454 in GCPII), and also marginally with Ser509 in place of Asn519 in GCPII. Most importantly, the unfavourable orientation of the citrate moiety in the GCPII Glu424Ala BCG complex is likely stabilized by the presence of Asn519, which, in contrast to Ser509 of GCPIII, sterically hampers rotation of the citrate moiety into the more bonded conformation predicted by QM/MM for the GCPIII BCG complex (Figure 22).

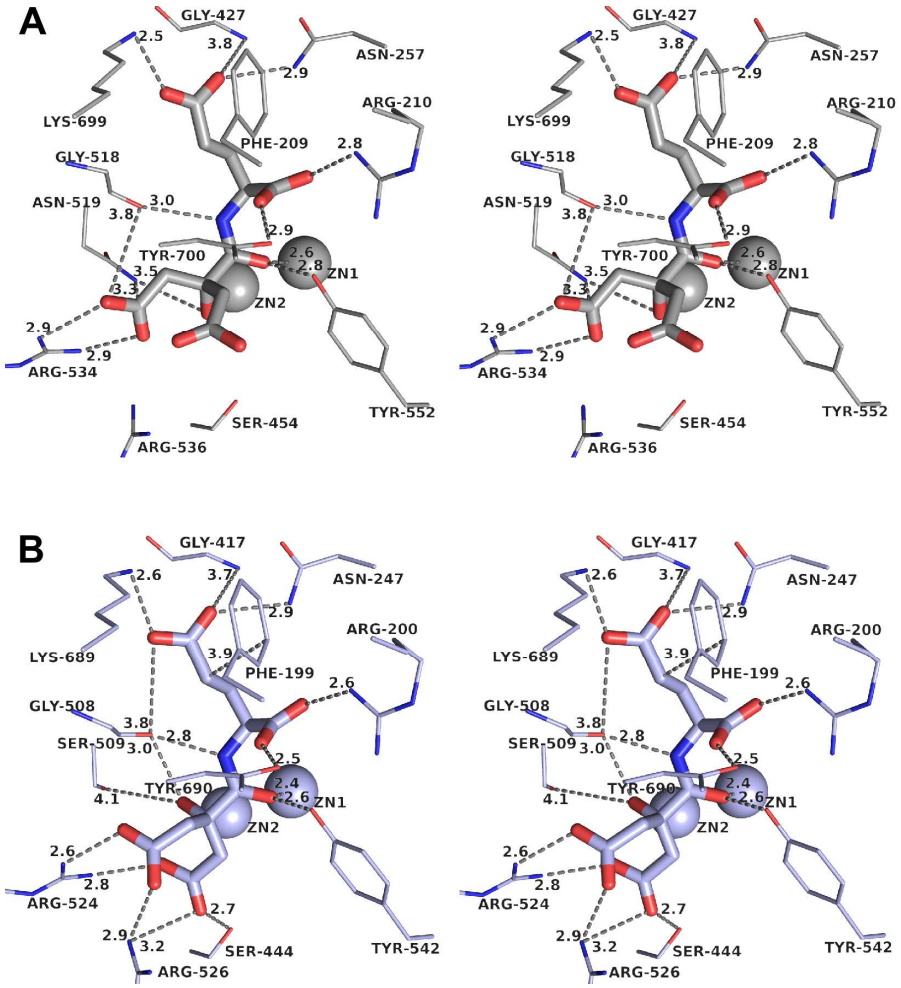


**Figure 22: Comparison of the interactome of BCG with active-site residues of GCPII and GCPIII, demonstrated in cross-eye stereo representation.** Zinc atoms are shown as spheres. BCG is depicted in stick representation and colored the same as the protein (see below). Binding interactions are represented by gray dashed lines and a number in Å. The images were created using PyMol[46]. (A) The GCPII-Glu424Ala-BCG X-ray structure (PDB entry 5F09, manuscript under revision), colored light gray. The citrate moiety interacts only with Arg534 and Asn519. (B) QM/MM model of the GCPIII BCG complex, colored light blue. The citrate moiety interacts with Arg524, Arg526, Ser444 and Ser509 (which substitutes Asn519 of GCPII). Please note that the citrate moiety is rotated in such a way which would not sterically be possible in GCPII because of the presence of Asn519.

The information on the metal dependence of GCPIII activity lead to to explore whether divalent cations could be directly responsible for the mechanism of catalysis of BCG by GCPIII. Therefore, our collaborators analyzed a whole panel of twelve QM/MM geometry optimizations: four groups of GCPII or GCPIII with NAAG or BCG, with the presence of Zn1-Zn2, Ca1-Zn2 and Zn1-Ca2 bimetallic clusters in the active site. It turned out that the QM/MM model of the GCPIII Ca2 BCG complex (further GCPIII-Ca2-BCG) not only features the BCG in a plausible conformation, but it also features the Ca2 atom coordinated in a typical, almost perfect, pentagonal bipyramidal manner, whereby the the axial ligands are His367 and the hydroxyl group of BCG, which is partially ionized by a nearby carboxylate of the BCG citrate moiety (Figure 23A,B). This partial ionization likely

contributes to the ability of BCG and the residues His367, Asp377, Glu414 and Asp443 to coordinate the Ca2 atom. Moreover, a comparison of GCPIII-Ca2-BCG and the X-ray structure of the GCPII Glu424Ala BCG complex (further GCPII-BCG) (Figure 23C,D) show, that the citrate moiety of BCG in the GCPIII-Ca2-BCG complex is rotated by approximately 90° in the same direction as in the QM/MM model of GCPIII-BCG complex (compare with Figure 22 and Figure 21). Further, the Zn1-Ca2 heterometallic cluster is slightly rotated in comparison to the Zn1-Zn2 cluster of GCPII-BCG (Figure 23C,D). It is interesting to note, that the active site water molecule is a part of the pentagonal plane formed by Asp377, Glu414 and Asp443 (Figure 23).

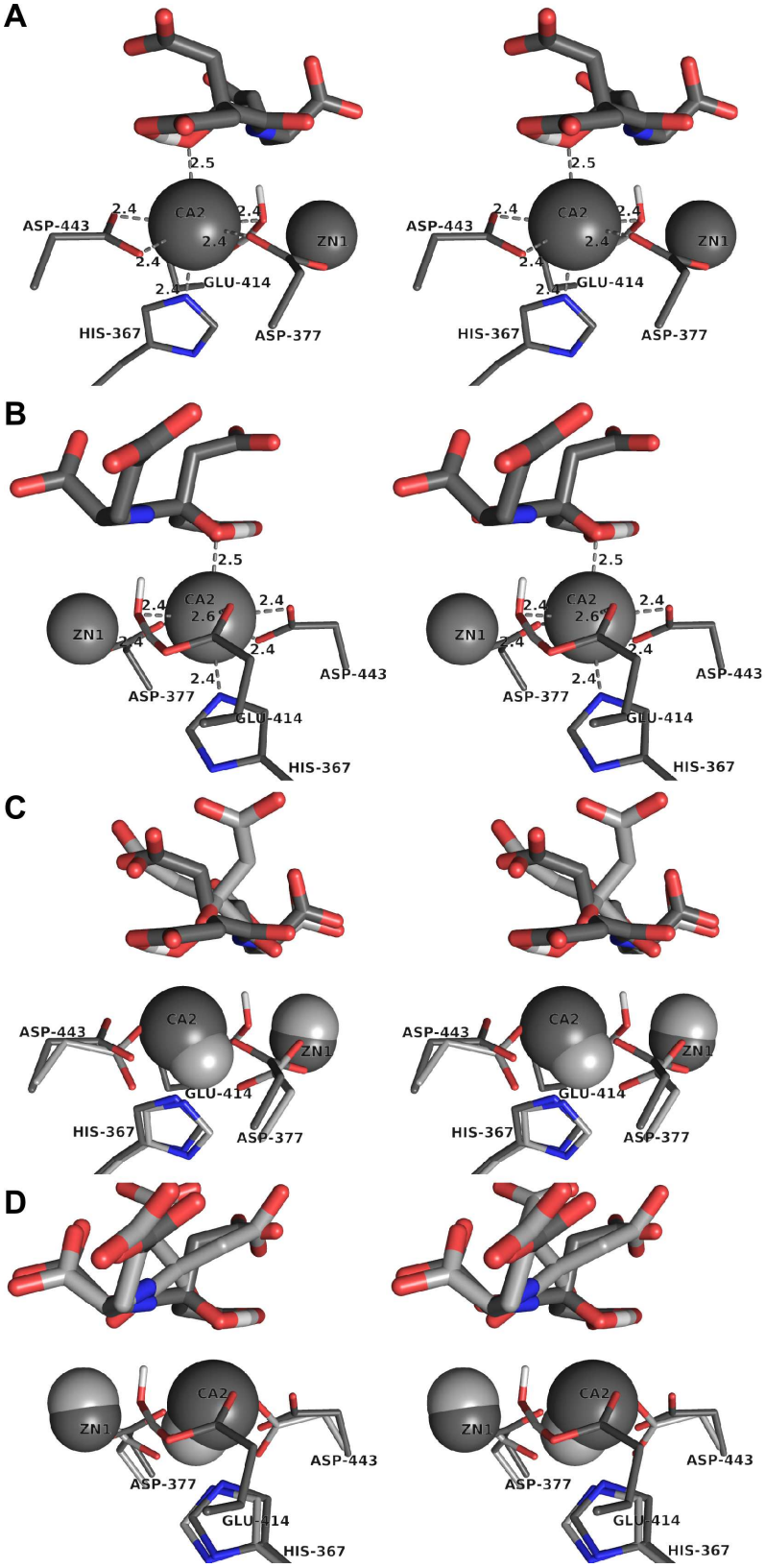


**Figure 23: QM/MM model of the GCPIII BCG complex, where active-site Zn2 is replaced by Ca2 (GCPIII-Ca2-BCG) and its comparison to the X-eay structure of the GCPII Glu424Ala BCG complex (GCPII-BCG, PDB entry 5F09 manuscript under revision).** All images are rendered in cross-eye stereo representation. Amino acid numbers refer to GCPIII (for GCPII, the numbers would be higher by 10). GCPIII-Ca2-BCG is colored steel gray, GCPII-BCG light gray. Metal atoms are shown as spheres, BCG in stick representation. Coordination distances of Ca2 are indicated by gray dashed lines and a number in Å. The images were created using PyMol[46]. (A,B) QM/MM model of GCPIII-Ca2-BCG detailing how the Ca2 atom of the proposed Zn1-Ca2 cluster might be coordinated. Please note that the hydroxyl group of BCG citrate moiety is likely partially ionized by the nearby carboxylate, which makes the almost perfect pentagonal bipyramidal coordination pattern characteristic for calcium possible. The hydrogen atom of the hydroxyl is shown bridged to the carboxylate. It is also interesting to note that the water molecule, forming one ligand in the pentagonal plane coordinating Ca2, is concurrently the activated nuclephile attacking the peptide bond. (B) differs from (A) by 180° rotation along the y axis. (C,D) GCPIII-Ca2-BCG is shown in overlay with GCPII-BCG. This superposition makes it obvious that the Zn1-Ca2 is slightly rotated in comparison to the Zn1-Zn2 cluster of GCPII-BCG. The activated water molecule, bridged between Zn1 and Zn2, is not depicted here, because it occupies almost the same space as that of the Zn1-Ca2 cluster. Another important feature of the GCPIII-Ca-BCG model is the orientation of the citrate moiety, which is, similarly to the GCPIII-BCG QM/MM model, rotated by approximately 90° in comparison to the citrate moiety of the GCPII-BCG structure. (D) differs from (C) by 180° rotation along the y axis.

Finally, we tried to assess computationally, whether the replacement of Ca2 is energetically favored in GCPIII. However. we were merely able to show that the cluster Zn1-Ca2 should be, in all cases, energetically more favored by a difference of approximately 10-15 kcal·mol$^{-1}$ in comparison to the Ca1-Zn2 cluster (manuscript under revision).

# 4.4. Tissue Distribution of Human GCPIII

We investigated the tissue distribution of GCPIII in human tissues both at the protein and mRNA level.

## 4.4.1. Tissue Distribution of Human GCPIII Determined by Enzymatic Assay

Because we identified a significant difference in substrate specificities of human GCPII and GCPIII (Figure 15 in the section 4.2.4.1), we could use NAAG and BCG to quantify them in human tissue lysates, respectively. In our reaction buffer, a molar concentration of GCPIII 60 times higher than that of GCPII caused only a 50 % interference, and GCPII did not interfer with the quantification of GCPIII at all even if it was 180 times more concentrated (Figure 24).

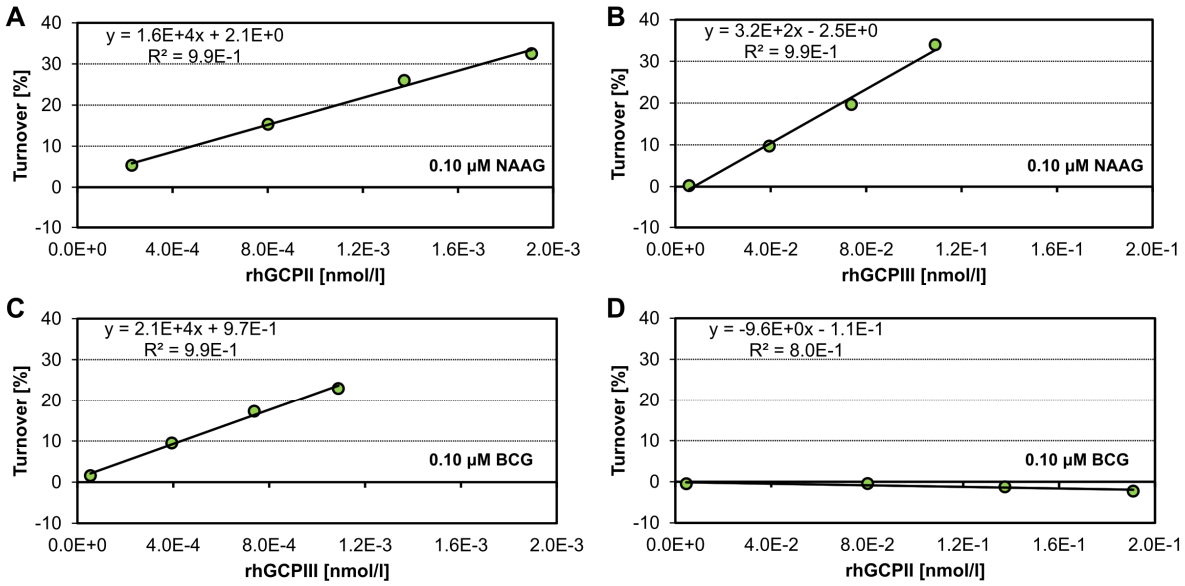


**Figure 24: Typical calibration curves for quantification of human GCPII and GCPIII in tissue lysates.** The reaction buffer was 20 mM Tris, 0.15 M NaCl, 2.5 mM $CaCl_2$, 0.1 % (v/v) Tween 20, pH 7.4. Final concentrations of BCG and NAAG in the analytical reactions are shown in the lower right part of each plot.

Our activity assay yielded a distribution pattern of GCPII similar to previously published mRNA data[13] (Figure 25), which was also similar to our own mRNA data (Figure 26, section 4.4.2). For

GCPII, three highest levels were found in brain, kidney and prostate, while for GCPIII, these were found in testes, prostate and ovary (Figure 25).

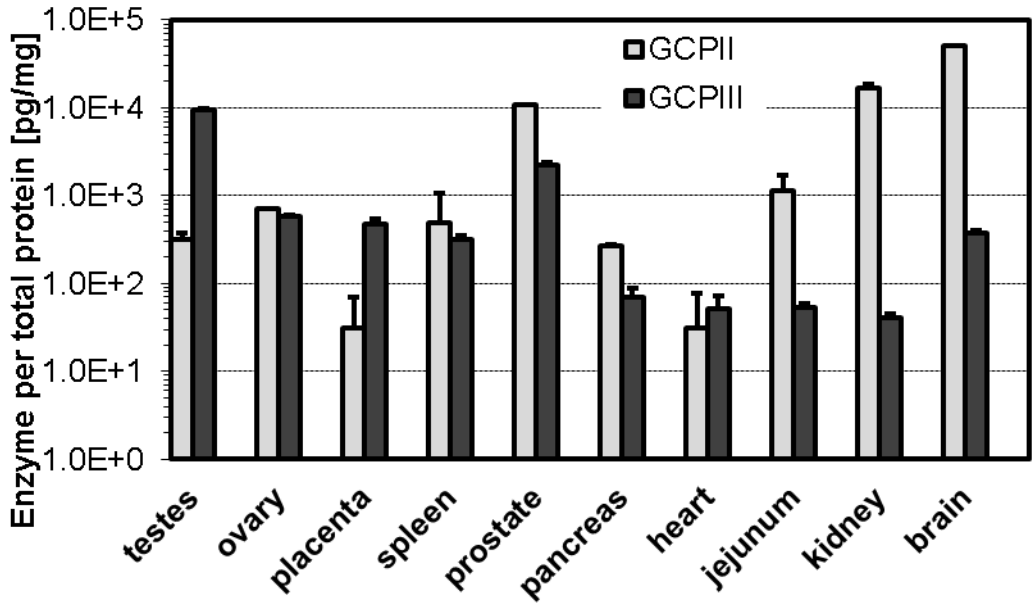


**Figure 25: Content of GCPII and GCPIII protein in human tissue lysates as assessed by the radiometric assay.** The reaction buffer was 20 mM Tris, 0.15 M NaCl, 2.5 mM $CaCl_2$, 0.1 % (v/v) Tween 20, pH 7.4. Error bars represent standard deviation from experiments carried out in duplicate. Please note that tissues are ordered the same as in Figure 26.

## 4.4.2. Tissue Distribution of Human GCPIII Determined by qPCR

We complemented the activity data by our own independent analysis of GCPII/GCPIII in human tissues on the mRNA level. For this aim, we used human Clontech tissue cDNA libraries (Human MTC Panel I and II, see 3.1.2 in Materials and Methods). The results were similar, except for that the GCPII prostate content was only two times higher that in the liver (tissue with the second highest content) (Figure 26). The third highest content was found in kidney. For GCPIII, the tissues with three highest levels were testes, ovary and placenta (Figure 26).

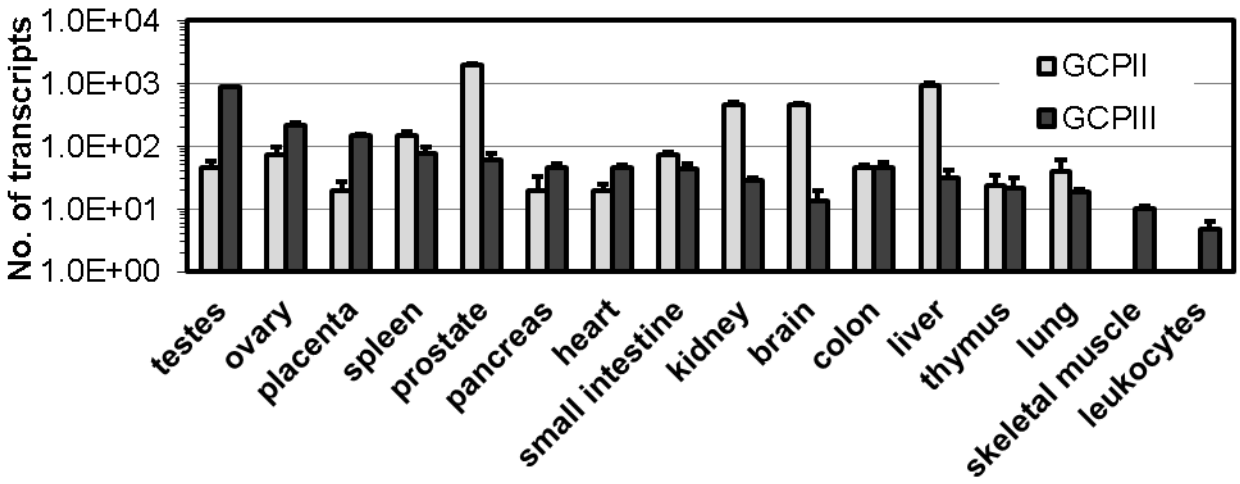


**Figure 26: mRNA levels of GCPII and GCPIII in human Clontech tissue cDNA libraries, as determined by qPCR.** The "No. of transcripts" refers to number of transcripts found in 1.0 µl of 10-fold diluted cDNA library. Error bars represent standard deviation from experiments carried out in triplicate. Tissues are ordered from higher to lower content of GCPIII mRNA, whereby the tissues, for which we do not have enzymatic data, are tethered at the end (colon to leukocytes). Please note that the first 10 tissues are ordered the same as in Figure 25.

## 4.5. X-ray Structure of GCPII His475Tyr

Because we wanted to shed light on the controversy about the influence of GCPII His475Tyr on the folate levels (see 1.2.3.4), we also crystallized this protein (besides the biochemical characterization of its $FolGlu_n$-hydrolyzing activity, see 4.2.2).

The structure revealed no significant differences between the wild-type and mutated enzymes - residue Tyr475 occupies the same space as His475 and has no apparent influence on the active site or any exosite of the enzyme.

## 4.6. More Lipohilic Inhibitors of GCPII

GCPII is active and physiologically relevant in the CNS and its inhibitors are neuroprotective as discussed in the Introduction (see 1.2.3.1.1, 1.2.3.1.3.1). Therefore, it is important to search for potent lipophilic compound capable of crossing the blood-brain barrier. For this task, we first searched for more lipophilic substrates that could serve as a basis for inhibitor design. We found out that the S1' site can bind even moieties as surprising as methionine and aminooctanoic or aminononanoic acid[177]. Structures of GCPII Glu424Ala with N-acetyl-L-aspartyl-L-methionine (PDB entry 3SJX), N-acetyl-L-aspartyl-L-2-aminooctanoic acid (PDB entry 3SJG), N-acetyl-L-aspartyl-L-2-aminononanonic acid (PDB entry 3SJE), and with (S)-2-(3-((L)-methionyl)ureido)-6-(4-iodobenzamido)hexanoic acid (PDB entry 3SJF)[177] show a structural overlap with the P1'

glutamate seen in the structure of GCPII with NAAG (PDB entry 3BXM[16]). For the two moieties longer than glutamate or methionine (PDB entry 3SJG, 3SJE), the extra atoms protrude into a nearby small pocket formed by residues Leu261, Gly263, Gly265, Gly427, Leu428, Ser431, Thr432, Asp520, Glu522, Val523, Gln526 und Arg527 (e.g. PDB entry 3SJE).

## 4.7. Selective Inhibitor of GCPIII

Because the main difference between GCPII and GCPIII is likely its wobble Zn2 that might be potentially replaced by other physiologically relevant cations like $Ca^{2+}$, $Mn^{2+}$ or $Zn^{2+}$, we hypothesized that a transition state analogue, which would have low affinity to zinc, but a high one to calcium, could perhaps be the basis for a GCPIII-selective inhibitor. To analyze this idea, we designed BCG analogs glutamyl sulfamide and urea derivatives (Figure 27) as potential specific inhibitors of GCPIII. In order to test them, we used our inhibition assay employing $FolGlu_1$ as a substrate in the presence of 0.10 mM $Zn^{2+}$ and 20 mM $Ca^{2+}$. We found out that the activity of glutamyl sulfamide [2-(sulfamoylamino)pentanedioic acid] is rather weak ($IC_{50}$ value of 7.39 ± 0.67 μM), but it is 3.8 times tighter than that for GCPII (28.2 ± 6.3 μM). Design of the urea analogs of BCG (Figure 27B,C) lead to weak inhibitors with no selectivity to GCPIII.

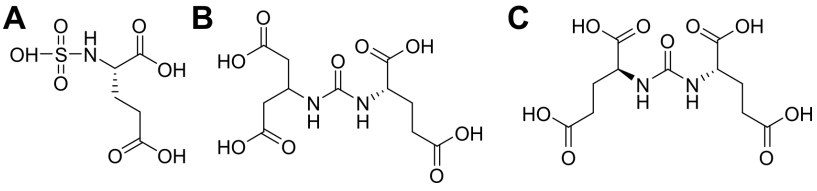


**Figure 27: Glutamyl sulfamide and urea inhibitors as a starting compounds for designing a GCPIII-selective inhibitor.** (A) Glutamyl sulfamide [2-(sulfamoylamino)pentanedioic acid]. (B) (S)-2-(3-(1,3-dicarboxypropan-2-yl)ureido)pentanedioic acid, the urea analog of BCG. (C) (2S,2'S)-2,2'-(carbonylbis(azanediyl))dipentanedioic acid, a control inhibitor.

## 4.8. Biochemical Characterization of N-acetyl-L-aspartyl-L-glutamyl-L-glutamate-hydrolyzing Activity of Human GCPII and GCPIII

Since N-acetyl-L-aspartyl-L-glutamyl-L-glutamate (NAAG2) was shown to be hydrolyzed by mouse GCPII[20] and GCPIII[29] (for structure of NAAG2, see Figure 1), we set out to investigate whether also human GCPII and GCPIII hydrolyze NAAG2. Taking into the metal-dependent hydrolysis by GCPIII (see section 4.2.4.1), we determined the NAAG2- and NAAG-hydrolyzing activities of GCPIII in the presence of 0.10 mM $Zn^{2+}$. As shown in the Figure 28, NAAG2 is a a

more favourable substrate for GCPIII than GCPII, namely by one order of magnitude in terms of catalytic efficiency (Figure 28A), and also in terms of both $K_M$ and $k_{cat}$ (Figure 28B,C). Furthermore, the largest difference consists in the observation that NAAG2 is a much less favourable substrate than NAAG for both GCPII and GCPIII (Figure 28A,B,C).

It is also worth mentioning that the kinetic parameters for hydrolysis of NAAG2 by GCPII were almost the same both in the presence and absence of 0.10 mM $Zn^{2+}$ (data not shown).

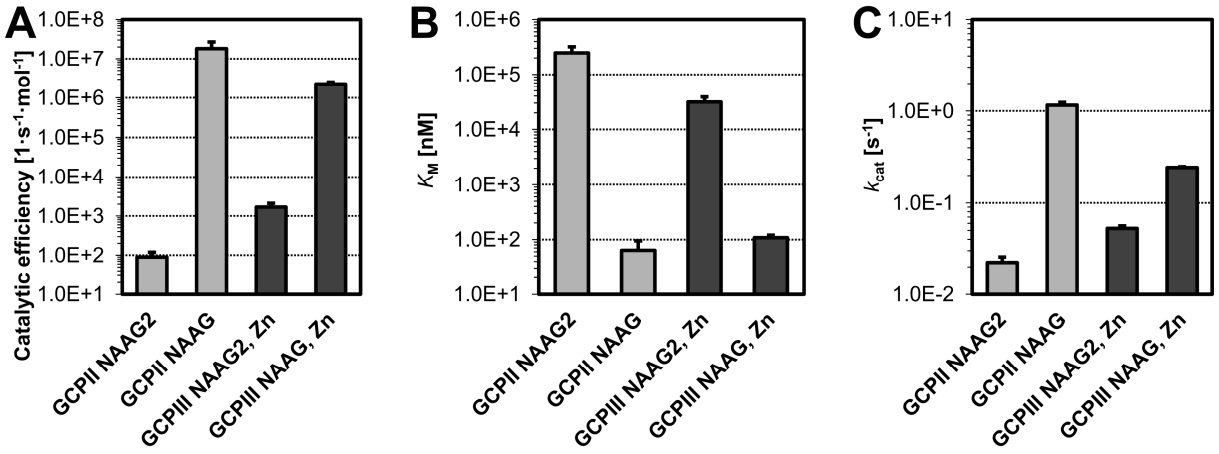


**Figure 28: NAAG2- and NAAG- hydrolyzing acitivty of human GCPII and GCPIII.** NAAG2- and NAAG-hydrolyzing activities of GCPIII have been assayed in the presence of 0.10 mM $Zn^{2+}$. The reaction buffer was 25 mM bisrispropane pH 7.5. Error bars represent standard deviation. (A) Catalytic efficiencies. (B) $K_M$ values. (C) $k_{cat}$ values.

# 5. DISCUSSION

Our first main achievement was the characterization of how GCPII binds $FolGlu_n$ substrates (provitamins $B_9$) by X-ray crystallography. We complemented these findings also with kinetic data, which were previously unknown. This structural investigation was the second study to characterize the arene-binding site (ABS), and the first to characterize the hydrolysis of $FolGlu_n$ substrates by human GCPII. Additionaly, we also characterized the S2 site and showed that GCPII does not contain any S3 site.

Our second main achievement was the identification of the decades-long known dipeptide β-citryl-L-glutamate (BCG) as the most specific substrate of GCPIII (independently to the work by Collard *et al.*[8]). In addition, we also found the probable structural basis of the fundamental difference in substrate specificities of GCPII and GCPIII, which possess active sites differing only by one amino acid (see 1.3.3.2).

There are, however, still issues, which require at least attention. For example, as it is obvious from the Figure 13 and Figure 15, our kinetic assays were sometimes near or even beyond the limit of quantification. This caused the $K_M$ value to be sometimes extrapolated. A further consequence is a higher experimental error. This approach was derived from the intital effort to keep the protein concentratin as low as possible, because it was not known, how much protein would the reversed-phase column tolerate. We could, of course, e.g. have affected the $K_M$ to achieve higher values by using a buffer containing some phosphate, but we decided not to go in this direction. However, for routine testing, where the true $K_M$ is not needed, such a change of reaction conditions by phosphate would be acceptable.

During processing of large amounts of $FolGlu_n$-hydrolysis data, we noticed that $FolGlu_n$ substrates are likely hydrolyzed in a distributive manner, because there were always only proportional peaks of $FolGlu_{n-1}$ or $FolGlu_{n-2}$ - for example, we never observed a peak of $FolGlu_n$ and $FolGlu_{n-3}$, while $FolGlu_{n-1}$ and $FolGlu_{n-2}$ would be missing. This conclusion is in agreement with the obtained $FolGlu_n$ $K_M$ values (which in the specific case of GCPII roughly correspond to its affinity to the substrates): the last link in the $FolGlu_n$ processing chain, $FolGlu_1$, has the highest $K_M$ (lowest affinity), so no accumulation of any intermediate is conceivable. Moreover, the affinity of GCPII for folic acit itself ($FolGlu_0$, vitamin $B_9$) is around 0.1 mM (unpublished observation), so even $FolGlu_1$ cannot accumulate (and, in practice, it did not).

For our $FolGlu_n$ assay, we used oxidized forms of $FolGlu_n$ substrates, because they are stable and readily available. Moreover, the affinity of GCPII for reduced forms of folates, which are

the forms found in living organisms, might be comparable, because the contribuition of the ABS to binding aromatic moieties is not that high as one would expect (see Figure 13 and Figure 14).

As shown in the Results section, we performed site-directed mutagenesis of the ABS exosite (Figure 14 in section 4.2.3). The ABS mutants appeared not to influence the $FolGlu_n$-hydrolyzing activity significantly (Figure 13 in section 4.2.3). If we analyze whether there are some other surface residues that could be responsible for the difference between GCPII and GCPIII, we find, for example, that near the ABS, there is a positive charge groove delineated by Lys610, Lys606, Arg605, Val602 and Arg598 (enumareted in increasing distance from the entrance channel), which could, hypothetically, serve as point of a first capture of the negatively charged $FolGlu_n$ substrates. The residues of this groove are replaced by Ser600, Asn596, Lys605, Glu592 and Gln588, respectively, in GCPIII, which are substitutions either disrupting the positive charge or even introducing a negative one. This stands in contrast to the differences in the flexible entrance lid of these two enzymes, namely Trp541 (GCPII) versus Lys531 (GCPIII), Glu542 v. Lys532, Phe546 v. Tyr536 and Gly548 v. Ser538, which represent rather neutral changes or introduce a weak positive charge. A possible thorough dissection of the differences between GCPII and GCPIII should thus investigate these above mentioned differences in the positive charge groove.

Nonetheless, the relevance of the ABS for the specificity of GCPII should not be underestimated. A good example is the recent observation by *Tykvart and Schimer et al.*[49] who showed that a proper ABS-targeting moiety can increase the selectivity to GCPII over GCPIII by more than three orders of magnitude. Moreover, this finding is also suported by an X-ray structure of this inhibitor in complex with GCPII (PDB entry 4X3R)[49].

GCPII differed in the $FolGlu_n$-hydrolyzing activity from GCPIII both in $K_M$ and $k_{cat}$ (Figure 12). However, $FolGlu_1$-hydrolyzing activity by GCPIII could be activated by 0.10 mM $Zn^{2+}$ to reach the activity of GCPII (in terms of $k_{cat}$, Figure 15). We chose this particular concentration of zinc, first, because pancreas releases zinc in its secretions at the amount of approximately 1 - 2 mg/day[178]. Second, GCPIII is expressed in jejunum at a level similar to GCPII (less by one order of magnitude, see Figure 25). Third, zinc concentation in the CNS is proposed to represent a signal (similarly to calcium) (see below). Fourth, the $Zn^{2+}$-activated hydrolysis of $FolGlu_1$ is half-saturated at approximately 6 μM $Zn^{2+}$ (unpublished observation, but preliminarily indicated by Collard *et al.*[8]), so its $FolGlu_n$ activity might well be relevant in GCPII knockout organisms and account for their relatively mild phenotype (see 1.2.3.1.5). It might be interesting to find out whether GCPII knockout mice are hypersensitive to zinc deficiency through decreased absorbtion of folic acid, whether they are more or less prone to carcinogenesis and whether some less glutamylated folates

can rescue their mild phenotype like increased blood pressure (see 1.2.3.1.5). However, it should be noted that the normal extracellular concentration of free zinc is very low[179], in contrast to total plasma concentration, whis is at the order of 10 μM[180]

The analysis of the structure-activity relationship of GCPII has important clinical implications. As described earlier in the thesis, a common polymorphism in GCPII gene leads to GCPII His475Tyr mutation that has been connected to altered folate levels (see 1.2.3.4). To analyze the hypothetical possiblity of altered $FolGlu_n$-hydrolyzing activity, we decided to solve the molecular structure of this particular mutant and study its enzymologic activity. We found that its structure is identical to to the wild-type GCPII and also experimentally proved the intuitive notion that it possesses unaltered $FolGlu_n$-hydrolyzing activity. We also found out that even the mutant's thermal stability is unaltered when compared to the wild-type enzyme - temperature midpoint for the unfolding transition ($T_m$) was only 2.0 °C higher[174]. Somewhat surprisingly, the His475Tyr mutation conferred less efficient hydrolysis of NAAG. We thus conclude that this mutation does not influence the proteolytic activity of the enzyme in terms of the hydrolysis of $FolGlu_n$; its influence on the folate metabolism in polymorphis organism, if any, must have other, more complex reasons[174].

To clarify the structural basis of how GCPII binds $FolGlu_n$ substrates, we crystallized GCPII in complex with $FolGlu_{0-6}$ (section 4.3.1) and solved their structures by X-ray crystallography. Out of these seven structures, only three - $FolGlu_{1-3}$ - yielded electron density maps complete enough for the models to be published. In the case of the other four GCPII Glu424Ala-$FolGlu_{0,4,5,6}$ complexes, only C-terminal tri-γ-L-glutamic acid moiety could be modeled into the active site of GCPII, whereby for $FolGlu_4$, there was additionally a faint electron density map indicating that its pteridine ring might be still partially wedged between Arg511 and Trp541. This could mean, that the $FolGlu_{4,5,6}$ substrates might be simply too long to engage the ABS. For $FolGlu_0$, which binds with approximately 0.1 mM affinity ($IC_{50}$, see above), the surprising density of a tri-γ-L-glutamic acid moiety might be the result of a possibility that the cultivation medium might contain some higher $FolGlu_{>4}$ molecules which might have remained bound throughout the purification of GCPII.

Very important feature of the substrate specificity of GCPIII is its ability to cleave the newly identified substrate, BCG. One of the aims of this project was to analyze the specificity of GCPIII for this substrate by structural analysis. All our efforts to obtain directly the structure of the complex of inactive mutant of GCPIII (Glu414Ala) with this substrate were unsuccessfull. The co-crystallization trials with GCPIII and calcium yielded either no, small or poorly diffracting crystals (2.7 Å at the best). In order to obatain a structural base for the later computational models of how BCG binds to both homologous enzymes, we decided to co-crystallize the inactive mutant of GCPII

(Glu424Ala) with BCG This was challenging as well. We were unable to get the crystals of the complex. Fortunately, it was possible to soak a ligand-free crystal of GCPII Glu424Ala with BCG and obtain a 1.85 Å resolution structure. We could then use this structure as a basis for the QM/MM models of GCPIII in complex with BCG (prepared in collaboration with Dr. Rulíšek and his collaborators at the IOCB in Prague). The results of this structural and computational study, in combination with our enzymological data (see Figure 15, section 4.2.4.1), could be summarized as follows: First, we corrected the wrong notion suggested by Collard *et al.*[8] that GCPII does not cleave BCG (see Figure 15, section 4.2.4.1). Second, we revealed the selectivity ratios for the GCPII- and GCPIII-catalyzed hydrolyses of NAAG and BCG, respectively (see Figure 24, section 4.4.1), and quantified GCPII and GCPIII in human tissue lysates. Third, we also determined the pH optimum of the BCG-hydrolyzing activity (see Figure 17 in section 4.2.4.4). Fourth, we quantified the influence of all physiologically relevant metals ($Ca^{2+}$, $Mn^{2+}$, $Zn^{2+}$) on the hydrolysis of all natural substrates and additionally discovered that $Co^{2+}$ enhances $FolGlu_1$ hydrolysis. Fifth, we showed GCPIII mRNA distribution in human tissues. Further, our structural, kinetic, biochemical, physico-chemical and computational data on GCPIII indicate, that the wobble Zn2 atom might be replaced e.g. by $Ca^{2+}$ or $Mn^{2+}$, and that this susbstitution can increase the $k_{cat}$ value to up to a tenfold of what is the $k_{cat}$ of GCPII. This suggests that the second zinc atom, Zn2, is not really essential for the formation of the active-site nucleophile. We can even speculate that the second zinc atom may serve as a certain „moderator“ which decreases the saturation speed of catalysis. This idea can, for example, be substantiated by drawing a comparison to glutaminyl cyclase, which has identical zinc-binding active site residues but only has one zinc atom whereby the $k_{cat}$ value is approximately 10 $s^{-1}$ (see 1.3.3.1). However, this hypothesis need to be further analyzed and experimentally verified.

We complemented the enzymologic data on GCPIII by the description of the tissue distribution of GCPIII, using both quantification of mRNA and β-citrylglutamate hydrolyzing activity. This is the first report on the human protein level in the literature. Due to the limited number of human postmortem samples available, we assayed only one tissue in all cases, so the interindividual variance is not included. Further, even though we used specific substrates for each homolog, the values are still influenced by inherent error coming from overlapping specificities of both enzymes to NAAG.

Regarding the physiological function of GCPIII, we can speculate that GCPIII might be somehow related to iron management[181,182]. We have the following reasons for such a hypothesis: (1) at pH 7.0, only $10^{-12}$ % of BCG-iron complex is dissociated[181], (2) free iron causes cellular damage through Fenton chemistry[181,183], and (3) BCG is able to prevent iron-dependent degradation

of plasmid DNA by ROS[181]. Additionally, (1) the highest levels of both GCPIII and BCG are found in adult rat testes[7,184] whereby the concentration of BCG is 0.7 mM BCG[184], (2) BCG is around 0.4 - 0.5 mM in newborn rat brains[184,185] and approximately ten times less concentrated in adult brains[184,185], and (3) the concentration of BCG is the highest in newborn rat organs and is markedly decreased in adult animals[184] with the exception of testes where it is low until 15 days after birth and then increases to reach the adult level after approximately 30 days[184]. We can thus suggest that BCG might have evolved to enable cells to chelate this metal and prevent ROS mediated damage in rapidly dividing cells. The idea that BCG serves as an iron chelator is also supported by considering its structural similarity to already known naturally occuring iron chelators, e.g. rhizoferrin or staphylopherrin A[186,187]. Furthermore, the highest levels of BCG are found there where the BCG synthesizing enzyme NAAGS-I (gene RIMKLB) is expressed (CNS and testes[99]), so we can speculate that BCG in tandem with GCPIII (expressed presumably at cells' surface) might serve to establish a directed flow of residual iron out cells by being cleaved by GCPIII. For such a purpose, a tight binding chelator like BCG is a prerequisite. Such a proposed iron-pumping function would be very similar to what is observed e.g. in *Escherichia coli* which employs the iron binding chelator enterobactin[188] to extract iron from its environment.

In the CNS, there are "gluzincergic" neurons which are speculated to use zinc as an orthograde, transcellular messenger [189]. Because GCPIII is probably present rather on neurons (see 1.3.2), and because it hydrolyzes BCG in a zinc-dependent manner, it should be found out whether zincergy in CNS can inhibit GCPIII (the same way as $FolGlu_1$ hydrolysis is inhibited by $Ca^{2+}$, see 4.2.4.3.1) and whether it could have some physiological function or consequences.

Our work also reveals kinetic parameters of the hydrolysis of N-acetyl-L-aspartyl-L-glutamyl-L-glutamate (NAAG2) by both human GCPII and GCPIII. Because the activity of GCPIII was relatively low, and because GCPIII is likely half-saturated by very low concentrations of zinc (around 6 μM, discussed above) we measured the NAAG2- and NAAG-hydrolyzing activity of GCPIII only in 0.10 mM $Zn^{2+}$. To complement our enzymologic data on the hydrolysis of NAAG2 with structural data, we attempted to analyze the binding of this novel substrate to GCPII by X-ray crystallography. We used the inactive mutant of GCPII (Glu424Ala) and obtained a 1.9 Å resolution structure. However, the low electron density of the substrate, which was probably present in two different conformations in the active site, did not allow us to appropriately refine the structure (data not shown).

After finding out what is the probable structural basis of the difference between specificities of GCPII and GCPIII (see 4.3.2), we designed and tested a GCPIII-selective inhibitor. The

compound, based on the structure of BCG, is indeed a specific inhibitor of GCPIII: however, its activity is in low micromolar values and the selectivity ratio just 3.8 (see 4.7). One way of utilizing this compound could be the exploitation of the avidity effect of multiple inhibitor moieties attached to a macromolecular scaffold (an approach demonstrated to work by *Sacha et al*[190]. earlier this year, using GCPII-specific inhibitors). If successful, this approach might lead to the development of specific anti-GCPIII macromolecules that could be used for the visualisation and imaging of GCPIII in animal tissues.

Taken together, we present a very detailed structural and enzymologic comparison of an important diagnostic and therapeutic target (GCPII) with its cosest human homolog (GCPIII). By the identification and analysis of a specific substrate for GCPIII we developer a tool for the further analysis of the distribution and activity of this enigmatic enzyme and thus for the elucidation of its physiologic role.

# 6. SUMMARY

- The mode of binding of $FolGlu_n$ substrates and β-citryl-L-glutamate to GCPII has been characterized by X-ray crystallography.
- We grew the biochemical and structural body of knowledge about the arene-binding site of GCPII.
- A highly specific substrate of human GCPIII has been identified.
- All substrates of GCPII and GCPIII have been characterized from the kinetic point of view.
- The plausible structural reason for the distinct substrate specificities of GCPII and GCPIII has been proposed, based on QM/MM and other biochemical data.
- $FolGlu_n$-hydrolyzing activity of wild-type GCPII and the polymorphic variant His475Tyr has been quantified and found to be virtually the same.
- Structure of GCPII His475Tyr has been found to be equivalent to the wild type.
- Tissue distribution of human GCPIII has been determined at the protein and mRNA level.
- NAAG2-hydrolyzing activity of human GCPII and GCPIII has been characterized.
- More lipophilic inhibitors of GCPII have been identified and biochemically and structurally characterized.
- The first GCPIII-selective inhibitor has been identified.

# 7. FUTURE PERSPECTIVES

Much of the future perspectives are already implicitly mentioned in the Discussion. However, a list of urgent issues, which require attention, is below in this section. These future perspectives include:

- Finding out whether GCPIII is expressed on the cell surface and whether it serves there to cleave BCG, thus establishing an efflux of iron which it is proposed to chelate.
- Finding out whether GCPIII knockout mice are more prone to brain or testicular cancers in adulthood or prenatal brain tumors. If they would be, it would be straightforward to test how this phenotype is influenced by iron overload, and how well they absorb dietary iron.
- Finding out whether the relatively high expression of GCPIII in lungs serves also to chelate and remove excessive iron and to possibly protect them from higher exposition to oxygen.

# 8. REFERENCES


1. Robinson, M. B., Blakely, R. D., Couto, R. & Coyle, J. T. Hydrolysis of the brain dipeptide N-acetyl-L-aspartyl-L-glutamate. Identification and characterization of a novel N-acetylated alpha-linked acidic dipeptidase activity from rat brain. *J Biol Chem* **262,** 14498–506 (1987).
2. Israeli, R. S., Powell, C. T., Fair, W. R. & Heston, W. D. Molecular cloning of a complementary DNA encoding a prostate-specific membrane antigen. *Cancer Res* **53,** 227–30 (1993).
3. Israeli, R. S., Powell, C. T., Corr, J. G., Fair, W. R. & Heston, W. D. W. Expression of the Prostate-Specific Membrane Antigen. *Cancer Res.* **54,** 1807–1811 (1994).
4. Carter, R. E., Feldman, A. R. & Coyle, J. T. Prostate-specific membrane antigen is a hydrolase with substrate and pharmacologic characteristics of a neuropeptidase. *Proc. Natl. Acad. Sci. U. S. A.* **93,** 749–753 (1996).
5. Pinto, J. T., Suffoletto, B. P., Berzin, T. M., Qiao, C. H., Lin, S., Tong, W. P., May, F., Mukherjee, B. & Heston, W. D. Prostate-specific membrane antigen: a novel folate hydrolase in human prostatic carcinoma cells. *Clin Cancer Res* **2,** 1445–51 (1996).
6. Chandler, C. J., Wang, T. T. Y. & Halsted, C. H. Pteroylpolyglutamate Hydrolase from Human Jejunal Brush-Borders - Purification and Characterization. *J Biol Chem* **261,** 928–933 (1986).
7. Miyake, M., Innami, T. & Kakimoto, Y. A beta-citryl-L-glutamate-hydrolysing enzyme in rat testes. *Biochim Biophys Acta* **760,** 206–14 (1983).
8. Collard, F., Vertommen, D., Constantinescu, S., Buts, L. & Van Schaftingen, E. Molecular Identification of beta-Citrylglutamate Hydrolase as Glutamate Carboxypeptidase 3. *J Biol Chem* **286,** 38220–38230 (2011).
9. Leek, J., Lench, N., Maraj, B., Bailey, A., Carr, I. M., Andersen, S., Cross, J., Whelan, P., MacLennan, K. A., Meredith, D. M. & et al. Prostate-specific membrane antigen: evidence for the existence of a second related human gene. *Br J Cancer* **72,** 583–8 (1995).
10. O'Keefe, D. S., Su, S. L., Bacich, D. J., Horiguchi, Y., Luo, Y., Powell, C. T., Zandvliet, D., Russell, P. J., Molloy, P. L., Nowak, N. J., Shows, T. B., Mullins, C., Vonder Haar, R. A., Fair,

W. R. & Heston, W. D. W. Mapping, genomic organization and promoter analysis of the human prostate-specific membrane antigen gene. *Biochim. Biophys. Acta-Gene Struct. Expr.* **1443,** 113–127 (1998).

11. Watt, F., Martorana, A., Brookes, D. E., Ho, T., Kingsley, E., O'Keefe, D. S., Russell, P. J., Heston, W. D. W. & Molloy, P. L. A tissue-specific enhancer of the prostate-specific membrane antigen gene, FOLH1. *Genomics* **73,** 243–254 (2001).
12. Navrátil, V. Lidská glutamátkarboxypeptidasa II a její paralogy. (2007).
13. Cunha, A. C., Weigle, B., Kiessling, A., Bachmann, M. & Rieber, E. P. Tissue-specificity of prostate specific antigens: Comparative analysis of transcript levels in prostate and non-prostatic tissues. *Cancer Lett.* **236,** 229–238 (2006).
14. Hlouchova, K., Navratil, V., Tykvart, J., Sacha, P. & Konvalinka, J. GCPII Variants, Paralogs and Orthologs. *Curr. Med. Chem.* **19,** 1316–1322 (2012).
15. Bařinka, C. Glutamate carboxypeptidase II. (2003).
16. Klusak, V., Barinka, C., Plechanovova, A., Mlcochova, P., Konvalinka, J., Rulisek, L. & Lubkowski, J. Reaction mechanism of glutamate carboxypeptidase II revealed by mutagenesis, X-ray crystallography, and computational methods. *Biochemistry (Mosc.)* **48,** 4126–38 (2009).
17. Barinka, C., Rinnova, M., Sacha, P., Rojas, C., Majer, P., Slusher, B. S. & Konvalinka, J. Substrate specificity, inhibition and enzymological analysis of recombinant human glutamate carboxypeptidase II. *J Neurochem* **80,** 477–87 (2002).
18. Tykvart, J., Sacha, P., Barinka, C., Knedlik, T., Starkova, J., Lubkowski, J. & Konvalinka, J. Efficient and versatile one-step affinity purification of in vivo biotinylated proteins: Expression, characterization and structure analysis of recombinant human glutamate carboxypeptidase II. *Protein Protein Expres Purif* **82,** 106–115 (2012).
19. Schulke, N., Varlamova, O. A., Donovan, G. P., Ma, D. S., Gardner, J. P., Morrissey, D. M., Arrigale, R. R., Zhan, C. C., Chodera, A. J., Surowitz, K. G., Maddon, P. J., Heston, W. D. W. &

Olson, W. C. The homodimer of prostate-specific membrane antigen is a functional target for cancer therapy. *Proc. Natl. Acad. Sci. U. S. A.* **100,** 12590–12595 (2003).

20. Lodder-Gadaczek, J., Becker, I., Gieselmann, V., Wang-Eckhardt, L. & Eckhardt, M. N-Acetylaspartylglutamate Synthetase II Synthesizes N-Acetylaspartylglutamylglutamate. *J Biol Chem* **286,** 16693–16706 (2011).

21. Schmittgen, T. D., Tiske, S., Vessella, R. L., True, L. D. & Zakrajsek, B. A. Expression of prostate specific membrane antigen and three alternatively spliced variants of PSMA in prostate cancer patients. *Int. J. Cancer* **107,** 323–329 (2003).

22. O'Keefe, D. S. & Heston, W. D. W. Clearing up the confusion over the glutamate carboxypeptidase II gene. *Am. J. Med. Genet. A.* **130A,** 327–328 (2004).

23. Mlcochova, P., Plechanovova, A., Barinka, C., Mahadevan, D., Saldanha, J. W., Rulisek, L. & Konvalinka, J. Mapping of the active site of glutamate carboxypeptidase II by site-directed mutagenesis. *FEBS J* **274,** 4731–41 (2007).

24. Tiffany, C. W. & Slusher, B. S. Measurement of glutamate carboxypeptidase II (NAALADase) enzyme activity by the hydrolysis of [(3)H]-N-acetylaspartylglutamate (NAAG). *Curr Protoc Pharmacol* **Chapter 3,** Unit3 10 (2002).

25. Rojas, C., Frazier, S. T., Flanary, J. & Slusher, B. S. Kinetics and inhibition of glutamate carboxypeptidase II using a microplate assay. *Anal. Biochem.* **310,** 50–54 (2002).

26. Hlouchova, K., Barinka, C., Klusak, V., Sacha, P., Mlcochova, P., Majer, P., Rulisek, L. & Konvalinka, J. Biochemical characterization of human glutamate carboxypeptidase III. *J. Neurochem.* **101,** 682–696 (2007).

27. Holm, R. H., Kennepohl, P. & Solomon, E. I. Structural and Functional Aspects of Metal Sites in Biology. *Chem. Rev.* **96,** 2239–2314 (1996).

28. Curatolo, A., Darcange.P, Lino, A. & Brancati, A. Distribution of N-Acetyl-Aspartic and N-Acetyl-Aspartyl-Glutamic Acids in Nervous Tissue. *J. Neurochem.* **12,** 339- (1965).

29. Lodder-Gadaczek, J. A. K. The biosynthesis and transport of N-Acetylaspartylglutamate und N-Acetylaspartylglutamylglutamate. (2013).

30. Miyake, M., Kakimoto, Y. & Sorimachi, M. Isolation and Identification of Beta-Citryl-L-Glutamic Acid from Newborn Rat-Brain. *Biochim. Biophys. Acta* **544,** 656–666 (1978).

31. Choy, C. J., Fulton, M. D., Davis, A. L., Hopkins, M., Choi, J. K., Anderson, M. O. & Berkman, C. E. Rationally Designed Sulfamides as Glutamate Carboxypeptidase II Inhibitors. *Chem. Biol. Drug Des.* **82,** 612–619 (2013).

32. Tsukamoto, T., Wozniak, K. M. & Slusher, B. S. Progress in the discovery and development of glutamate carboxypeptidase II inhibitors. *Drug Discov. Today* **12,** 767–776 (2007).

33. Novakova, Z., Cerny, J., Choy, C. J., Nedrow, J. R., Choi, J. K., Lubkowski, J., Berkman, C. E. & Barinka, C. Design of composite inhibitors targeting glutamate carboxypeptidase II: the importance of effector functionalities. *FEBS J.* **283,** 130–143 (2016).

34. Barinka, C., Rojas, C., Slusher, B. & Pomper, M. Glutamate Carboxypeptidase II in Diagnosis and Treatment of Neurologic Disorders and Prostate Cancer. *Curr. Med. Chem.* **19,** 856–870 (2012).

35. Davis, M. I., Bennett, M. J., Thomas, L. M. & Bjorkman, P. J. Crystal structure of prostate-specific membrane antigen, a tumor marker and peptidase. *Proc. Natl. Acad. Sci. U. S. A.* **102,** 5981–5986 (2005).

36. Mesters, J. R., Barinka, C., Li, W. X., Tsukamoto, T., Majer, P., Slusher, B. S., Konvalinka, J. & Hilgenfeld, R. Structure of glutamate carboxypeptidase II, a drug target in neuronal damage and prostate cancer. *Embo J* **25,** 1375–1384 (2006).

37. Mesters, J. R., Henning, K. & Hilgenfeld, R. Human glutamate carboxypeptidase II inhibition: structures of GCPII in complex with two potent inhibitors, quisqualate and 2-PMPA. *Acta Crystallogr. Sect. -Biol. Crystallogr.* **63,** 508–513 (2007).

38. Barinka, C., Starkova, J., Konvalinka, J. & Lubkowski, J. A high-resolution structure of ligand-free human glutamate carboxypeptidase II. *Acta Crystallogr. Sect. F-Struct. Biol. Cryst. Commun.* **63,** 150–153 (2007).

39. Barinka, C., Rovenska, M., Mlcochova, P., Hlouchova, K., Plechanovova, A., Majer, P., Tsukamoto, T., Slusher, B. S., Konvalinka, J. & Lubkowski, J. Structural insight into the pharmacophore pocket of human glutamate carboxypeptidase II. *J. Med. Chem.* **50,** 3267–3273 (2007).

40. Barinka, C., Hlouchova, K., Rovenska, M., Majer, P., Dauter, M., Hin, N., Ko, Y. S., Tsukamoto, T., Slusher, B. S., Konvalinka, J. & Lubkowski, J. Structural basis of interactions between human glutamate carboxypeptidase II and its substrate analogs. *J. Mol. Biol.* **376,** 1438–1450 (2008).

41. Barinka, C., Byun, Y., Dusich, C. L., Banerjee, S. R., Chen, Y., Castanares, M., Kozikowski, A. P., Mease, R. C., Pomper, M. G. & Lubkowski, J. Interactions between Human Glutamate Carboxypeptidase II and Urea-Based Inhibitors: Structural Characterization. *J. Med. Chem.* **51,** 7737–7743 (2008).

42. Wang, H. F., Byun, Y., Barinka, C., Pullambhatla, M., Bhang, H. E. C., Fox, J. J., Lubkowski, J., Mease, R. C. & Pomper, M. G. Bioisosterism of urea-based GCPII inhibitors: Synthesis and structure-activity relationship studies. *Bioorg. Med. Chem. Lett.* **20,** 392–397 (2010).

43. Zhang, A. X., Murelli, R. P., Barinka, C., Michel, J., Cocleaza, A., Jorgensen, W. L., Lubkowski, J. & Spiegel, D. A. A Remote Arene-Binding Site on Prostate Specific Membrane Antigen Revealed by Antibody-Recruiting Small Molecules. *J. Am. Chem. Soc.* **132,** 12711–12716 (2010).

44. Tykvart, J., Schimer, J., Barinkova, J., Pachl, P., Postova-Slavetinska, L., Majer, P., Konvalinka, J. & Sacha, P. Rational design of urea-based glutamate carboxypeptidase II (GCPII)

inhibitors as versatile tools for specific drug targeting and delivery. *Bioorg. Med. Chem.* **22,** 4099–4108 (2014).

45. Pavlicek, J., Ptacek, J., Cerny, J., Byun, Y., Skultetyova, L., Pomper, M. G., Lubkowski, J. & Barinka, C. Structural characterization of P1 ’-diversified urea-based inhibitors of glutamate carboxypeptidase II. *Bioorg. Med. Chem. Lett.* **24,** 2340–2345 (2014).

46. DeLano, W. L. Use of PYMOL as a communications tool for molecular science. *Abstr. Pap. Am. Chem. Soc.* **228,** U313–U314 (2004).

47. Jackson, P. F., Cole, D. C., Slusher, B. S., Stetz, S. L., Ross, L. E., Donzanti, B. A. & Trainor, D. A. Design, synthesis, and biological activity of a potent inhibitor of the neuropeptidase N-acetylated alpha-linked acidic dipeptidase. *J. Med. Chem.* **39,** 619–622 (1996).

48. Youn, S., Kim, K. I., Ptacek, J., Ok, K., Novakova, Z., Kim, Y., Koo, J., Barinka, C. & Byun, Y. Carborane-containing urea-based inhibitors of glutamate carboxypeptidase II: Synthesis and structural characterization. *Bioorg. Med. Chem. Lett.* **25,** 5232–5236 (2015).

49. Tykvart, J., Schimer, J., Jančařík, A., Bařinková, J., Navrátil, V., Starková, J., Šrámková, K., Konvalinka, J., Majer, P. & Šácha, P. Design of Highly Potent Urea-Based, Exosite-Binding Inhibitors Selective for Glutamate Carboxypeptidase II. *J. Med. Chem.* **58,** 4357–4363 (2015).

50. Rajasekaran, A. K. Is prostate-specific membrane antigen a multifunctional protein? *AJP Cell Physiol.* **288,** C975–C981 (2005).

51. Neale, J. H., Bzdega, T. & Wroblewska, B. N-acetylaspartylglutamate: The most abundant peptide neurotransmitter in the mammalian central nervous system. *J. Neurochem.* **75,** 443–452 (2000).

52. Halsted, C. H., Ling, E. H., Luthi-Carter, R., Villanueva, J. A., Gardner, J. M. & Coyle, J. T. Folylpoly-gamma-glutamate carboxypeptidase from pig jejunum - Molecular characterization and relation to glutamate carboxypeptidase II. *J. Biol. Chem.* **273,** 20417–20424 (1998).

53. Berger, U. V., Luthi-Carter, R., Passani, L. A., Elkabes, S., Black, I., Konradi, C. & Coyle, J. T. Glutamate carboxypeptidase II is expressed by astrocytes in the adult rat nervous system. *J. Comp. Neurol.* **415,** 52–64 (1999).

54. Sacha, P., Zamecnik, J., Barinka, C., Hlouchova, K., Vicha, A., Mlcochova, P., Hilgert, I., Eckschlager, T. & Konvalinka, J. Expression of glutamate carboxypeptidase II in human brain. *Neuroscience* **144,** 1361–1372 (2007).

55. Baslow, M. H. Functions of N-acetyl-L-aspartate and N-acetyl-L-aspartylglutamate in the vertebrate brain: Role in glial cell-specific signaling. *J. Neurochem.* **75,** 453–459 (2000).

56. Wroblewska, B., Wroblewski, J. T., Saab, O. H. & Neale, J. H. N-Acetylaspartylglutamate Inhibits Forskolin-Stimulated Cyclic-Amp Levels Via a Metabotropic Glutamate-Receptor in Cultured Cerebellar Granule Cells. *J. Neurochem.* **61,** 943–948 (1993).

57. Wroblewska, B., Wroblewski, J. T., Pshenichkin, S., Surin, A., Sullivan, S. E. & Neale, J. H. N-acetylaspartylglutamate selectively activates mGluR3 receptors in transfected cells. *J. Neurochem.* **69,** 174–181 (1997).

58. Corti, C., Battaglia, G., Molinaro, G., Riozzi, B., Pittaluga, A., Corsi, M., Mugnaini, M., Nicoletti, F. & Bruno, V. The use of knock-out mice unravels distinct roles for mGlu2 and mGlu3 metabotropic glutamate receptors in mechanisms of neurodegeneration/neuroprotection. *J. Neurosci.* **27,** 8297–8308 (2007).

59. Schweitzer, C., Kratzeisen, C., Adam, G., Lundstrom, K., Malherbe, P., Ohresser, S., Stadler, H., Wichmann, J., Woltering, T. & Mutel, V. Characterization of [3H]-LY354740 binding to rat mGlu2 and mGlu3 receptors expressed in CHO cells using Semliki Forest virus vectors. *Neuropharmacology* **39,** 1700–1706 (2000).

60. Sanabria, E. R. G., Wozniak, K. M., Slusher, B. S. & Keller, A. GCP II (NAALADase) inhibition suppresses mossy fiber-CA3 synaptic neurotransmission by a presynaptic mechanism. *J. Neurophysiol.* **91,** 182–193 (2004).

61. Slusher, B. S., Vornov, J. J., Thomas, A. G., Hurn, P. D., Harukuni, I., Bhardwaj, A., Traystman, R. J., Robinson, M. B., Britton, P., Lu, X. C. M., Tortella, F. C., Wozniak, K. M., Yudkoff, M., Potter, B. M. & Jackson, P. F. Selective inhibition of NAALADase, which converts NAAG to glutamate, reduces ischemic brain injury. *Nat. Med.* **5,** 1396–1402 (1999).

62. Coyle, J. T. Glutamate and Schizophrenia: Beyond the Dopamine Hypothesis. *Cell. Mol. Neurobiol.* **26,** 363–382 (2006).

63. Xi, Z.-X. Group II Metabotropic Glutamate Receptors Modulate Extracellular Glutamate in the Nucleus Accumbens. *J. Pharmacol. Exp. Ther.* **300,** 162–171 (2002).

64. Lin, C.-H., Lane, H.-Y. & Tsai, G. E. Glutamate signaling in the pathophysiology and therapy of schizophrenia. *Pharmacol. Biochem. Behav.* **100,** 665–677 (2012).

65. Meldrum, B. S. Glutamate as a neurotransmitter in the brain: Review of physiology and pathology. *J. Nutr.* **130,** 1007s–1015s (2000).

66. Pouwels, P. J. W. & Frahm, J. Differential distribution of NAA and NAAG in human brain as determined by quantitative localized protein MRS. *Nmr Biomed.* **10,** 73–78 (1997).

67. Neale, J. H., Olszewski, R. T., Zuo, D. Y., Janczura, K. J., Profaci, C. P., Lavin, K. M., Madore, J. C. & Bzdega, T. Advances in understanding the peptide neurotransmitter NAAG and appearance of a new member of the NAAG neuropeptide family. *J. Neurochem.* **118,** 490–498 (2011).

68. Carpenter, K. J. & Dickenson, A. H. Amino acids are still as exciting as ever. *Curr Opin Pharmacol* **1,** 57–61 (2001).

69. Niswender, C. M. & Conn, P. J. Metabotropic Glutamate Receptors: Physiology, Pharmacology, and Disease. *Annu. Rev. Pharmacol. Toxicol.* **50,** 295–322 (2010).

70. Nicoletti, E., Bockaert, J., Collingridge, G. L., Conn, P. J., Ferraguti, F., Schoepp, D. D., Wroblewski, J. T. & Pin, J. P. Metabotropic glutamate receptors: From the workbench to the bedside. *Neuropharmacology* **60,** 1017–1041 (2011).

71. Conn, P. J. & Pin, J. P. Pharmacology and functions of metabotropic glutamate receptors. *Annu. Rev. Pharmacol. Toxicol.* **37,** 205–237 (1997).

72. Doumazane, E., Scholler, P., Zwier, J. M., Trinquet, E., Rondard, P. & Pin, J. P. A new approach to analyze cell surface protein complexes reveals specific heterodimeric metabotropic glutamate receptors. *Faseb J.* **25,** 66–77 (2011).

73. Kuffler, S. W. & Edwards, C. Mechanism of Gamma Aminobutyric Acid (Gaba) Action and Its Relation to Synaptic Inhibition. *J. Neurophysiol.* **21,** 589–610 (1958).

74. Barnard, E. A., Skolnick, P., Olsen, R. W., Mohler, H., Sieghart, W., Biggio, G., Braestrup, C., Bateson, A. N. & Langer, S. Z. International Union of Pharmacology. XV. Subtypes of gamma-aminobutyric acid(A) receptors: Classification on the basis of subunit structure and receptor function. *Pharmacol. Rev.* **50,** 291–313 (1998).

75. Olsen, R. W. & Sieghart, W. International union of pharmacology. LXX. Subtypes of gamma-aminobutyric Acid(A) receptors: Classification on the basis of subunit composition, pharmacology, and function. Update. *Pharmacol. Rev.* **60,** 243–260 (2008).

76. Pin, J. P. & Duvoisin, R. The Metabotropic Glutamate Receptors - Structure and Functions. *Neuropharmacology* **34,** 1–26 (1995).

77. Bacich, D. J., Wozniak, K. M., Lu, X. C. M., O'Keefe, D. S., Callizot, N., Heston, W. D. W. & Slusher, B. S. Mice lacking glutamate carboxypeptidase II are protected from peripheral neuropathy and ischemic brain injury. *J. Neurochem.* **95,** 314–323 (2005).

78. Neale, J. H., Olszewski, R. T., Gehl, L. M., Wroblewska, B. & Bzdega, T. The neurotransmitter N-acetylaspartylglutamate in models of pain, ALS, diabetic neuropathy, CNS injury and schizophrenia. *Trends Pharmacol. Sci.* **26,** 477–484 (2005).

79. Wright, R. A., Arnold, M. B., Wheeler, W. J., Ornstein, P. L. & Schoepp, D. D. Binding of [H-3] (2S,1 â ™ S,2 â ™ S)-2-(9-xanthylmethyl)-2-(2 '-carboxycycloprophyl) glycine ([H-3]LY341495) to cell membranes expressing recombinant human group III metabotropic glutamate receptor subtypes. *Naunyn. Schmiedebergs Arch. Pharmacol.* **362,** 546–554 (2000).

80. Chopra, M., Yao, Y., Blake, T. J., Hampson, D. R. & Johnson, E. C. The Neuroactive Peptide N-Acetylaspartylglutamate Is Not an Agonist at the Metabotropic Glutamate Receptor Subtype 3 of Metabotropic Glutamate Receptor. *J. Pharmacol. Exp. Ther.* **330,** 212–219 (2009).

81. Smith, Q. R. Transport of glutamate and other amino acids at the blood-brain barrier. *J. Nutr.* **130,** 1016s–1022s (2000).

82. Cartmell, J., Adam, G., Chaboz, S., Henningsen, R., Kemp, J. A., Klingelschmidt, A., Metzler, V., Monsma, F., Schaffhauser, H., Wichmann, J. & Mutel, V. Characterization of [3H]-(2S,2'R,3'R)-2-(2',3'-dicarboxy-cyclopropyl)glycine ([3H]-DCG IV) binding to metabotropic mGlu2 receptor-transfected cell membranes. *Br J Pharmacol* **123,** 497–504 (1998).

83. Baslow, M. H. N-acetylaspartate in the vertebrate brain: Metabolism and function. *Neurochem. Res.* **28,** 941–953 (2003).

84. Tsai, S. J. Central N-acetyl aspartylglutamate deficit: a possible pathogenesis of schizophrenia. *Med. Sci. Monit.* **11,** Hy39-Hy45 (2005).

85. Moreno, A., Ross, B. D. & Bluml, S. Direct determination of the N-acetyl-L-aspartate synthesis rate in the human brain by C-13 MRS and [1-C-13]glucose infusion. *J. Neurochem.* **77,** 347–350 (2001).

86. Moffett, J. R., Ross, B., Arun, P., Madhavarao, C. N. & Namboodiri, A. M. A. N-acetylaspartate in the CNS: From neurodiagnostics to neurobiology. *Prog. Neurobiol.* **81,** 89–131 (2007).

87. Tsai, G. C. & Coyle, J. T. N-Acetylaspartate in Neuropsychiatric Disorders. *Prog. Neurobiol.* **46,** 531–540 (1995).

88. Tsai, G., Cork, L. C., Slusher, B. S., Price, D. & Coyle, J. T. Abnormal Acidic Amino-Acids and N-Acetylaspartylglutamate in Hereditary Canine Motoneuron Disease. *Brain Res.* **629,** 305–309 (1993).

89. Jung, R. E., Gasparovic, C., Chavez, R. S., Caprihan, A., Barrow, R. & Yeo, R. A. Imaging intelligence with proton magnetic resonance spectroscopy. *Intelligence* **37,** 192–198 (2009).

90. Urrila, A. S. Sleep deprivation and brain energy metabolism. (2007).

91. Border, W. A. & Ruoslahti, E. Transforming Growth-Factor-Beta in Disease - the Dark Side of Tissue-Repair. *J. Clin. Invest.* **90,** 1–7 (1992).

92. Bruno, V., Battaglia, G., Casabona, G., Copani, A., Caciagli, F. & Nicoletti, F. Neuroprotection by glial metabotropic glutamate receptors is mediated by transforming growth factor-beta. *J. Neurosci.* **18,** 9594–9600 (1998).

93. Thomas, A. G., Liu, W. L., Olkowski, J. L., Tang, Z. C., Lin, Q., Lu, X. C. M. & Slusher, B. S. Neuroprotection mediated by glutamate carboxypeptidase II (NAALADase) inhibition requires TGF-beta. *Eur. J. Pharmacol.* **430,** 33–40 (2001).

94. Ruocco, A., Nicole, O., Docagne, F., Ali, C., Chazalviel, L., Komesli, S., Yablonsky, F., Roussel, S., MacKenzie, E. T., Vivien, D. & Buisson, A. A transforming growth factor-beta antagonist unmasks the neuroprotective role of this endogenous cytokine in excitotoxic and ischemic brain injury. *J. Cereb. Blood Flow Metab.* **19,** 1345–1353 (1999).

95. Pouwels, P. J. W. & Frahm, J. Regional metabolite concentrations in human brain as determined by quantitative localized proton MRS. *Magn. Reson. Med.* **39,** 53–60 (1998).

96. Moffett, J. R., Namboodiri, M. A. A. & Neale, J. H. Enhanced Carbodiimide Fixation for Immunohistochemistry - Application to the Comparative Distributions of N-Acetylaspartylglutamate and N-Acetylaspartate Immunoreactivities in Rat-Brain. *J. Histochem. Cytochem.* **41,** 559–570 (1993).

97. Lodder-Gadaczek, J., Gieselmann, V. & Eckhardt, M. Vesicular uptake of N-acetylaspartylglutamate is catalysed by sialin (SLC17A5). *Biochem. J.* **454,** 31–38 (2013).

98. Becker, I., Lodder, J., Gieselmann, V. & Eckhardt, M. Molecular Characterization of N-Acetylaspartylglutamate Synthetase. *J. Biol. Chem.* **285,** 29156–29164 (2010).

99. Collard, F., Stroobant, V., Lamosa, P., Kapanda, C. N., Lambert, D. M., Muccioli, G. G., Poupaert, J. H., Opperdoes, F. & Van Schaftingen, E. Molecular Identification of N-

Acetylaspartylglutamate Synthase and beta-Citrylglutamate Synthase. *J. Biol. Chem.* **285,** 29826–29833 (2010).

100. Passani, L., Elkabes, S. & Coyle, J. T. Evidence for the presence of N-acetylaspartylglutamate in cultured oligodendrocytes and LPS activated microglia. *Brain Res.* **794,** 143–145 (1998).

101. Hecker, S. J. & Erion, M. D. Prodrugs of phosphates and phosphonates. *J. Med. Chem.* **51,** 2328–2345 (2008).

102. Olszewski, R. T., Bukhari, N., Zhou, J., Kozikowski, A. P., Wroblewski, J. T., Shamimi-Noori, S., Wroblewska, B., Bzdega, T., Vicini, S., Barton, F. B. & Neale, J. H. NAAG peptidase inhibition reduces locomotor activity and some stereotypes in the PCP model of schizophrenia via group II mGluR. *J. Neurochem.* **89,** 876–885 (2004).

103. Feng, J. F., Van, K. C., Gurkoff, G. G., Kopriva, C., Olszewski, R. T., Song, M., Sun, S. F., Xue, M., Neale, J. H., Yuen, P. W., Lowe, D. A., Zhou, J. & Lyeth, B. G. Post-injury administration of NAAG peptidase inhibitor prodrug, PGI-02776, in experimental TBI. *Brain Res.* **1395,** 62–73 (2011).

104. Zhong, C., Zhao, X., Sarva, J., Kozikowski, A., Neale, J. H. & Lyeth, B. G. NAAG peptidase inhibitor reduces acute neuronal degeneration and astrocyte damage following lateral fluid percussion TBI in rats. *J Neurotrauma* **22,** 266–76 (2005).

105. Zhong, C., Zhao, X., Van, K. C., Bzdega, T., Smyth, A., Zhou, J., Kozikowski, A. P., Jiang, J., O'Connor, W. T., Berman, R. F., Neale, J. H. & Lyeth, B. G. NAAG peptidase inhibitor increases dialysate NAAG and reduces glutamate, aspartate and GABA levels in the dorsal hippocampus following fluid percussion injury in the rat. *J Neurochem* **97,** 1015–25 (2006).

106. Feng, J. F., Gurkoff, G. G., Van, K. C., Song, M., Lowe, D. A., Zhou, J. & Lyeth, B. G. NAAG peptidase inhibitor reduces cellular damage in a model of TBI with secondary hypoxia. *Brain Res.* **1469,** 144–152 (2012).

107. Bruno, V., Copani, A., Battaglia, G., Raffaele, R., Shinozaki, H. & Nicoletti, F. Protective Effect of the Metabotropic Glutamate-Receptor Agonist, Dcg-Iv, against Excitotoxic Neuronal Death. *Eur. J. Pharmacol.* **256,** 109–112 (1994).

108. Yi, J. H. & Hazell, A. S. Excitotoxic mechanisms and the role of astrocytic glutamate transporters in traumatic brain injury. *Neurochem. Int.* **48,** 394–403 (2006).

109. Lau, A. & Tymianski, M. Glutamate receptors, neurotoxicity and neurodegeneration. *Pflugers Arch.-Eur. J. Physiol.* **460,** 525–542 (2010).

110. Arundine, M. & Tymianski, M. Molecular mechanisms of glutamate-dependent neurodegeneration in ischemia and traumatic brain injury. *Cell. Mol. Life Sci.* **61,** 657–668 (2004).

111. Olszewski, R. T., Janczura, K. J., Ball, S. R., Madore, J. C., Lavin, K. M., Lee, J. C. M., Lee, M. J., Der, E. K., Hark, T. J., Farago, P. R., Profaci, C. P., Bzdega, T. & Neale, J. H. NAAG peptidase inhibitors block cognitive deficit induced by MK-801 and motor activation induced by d-amphetamine in animal models of schizophrenia. *Transl. Psychiatry* **2,** (2012).

112. Carter, C. J. Schizophrenia susceptibility genes converge on interlinked pathways related to glutamatergic transmission and long-term potentiation, oxidative stress and oligodendrocyte viability. *Schizophr. Res.* **86,** 1–14 (2006).

113. Lisman, J. E., Coyle, J. T., Green, R. W., Javitt, D. C., Benes, F. M., Heckers, S. & Grace, A. A. Circuit-based framework for understanding neurotransmitter and risk gene interactions in schizophrenia. *Trends Neurosci.* **31,** 234–242 (2008).

114. Xi, Z. X., Kiyatkin, M., Li, X., Peng, X. Q., Wiggins, A., Spiller, K., Li, J. & Gardner, E. L. N-acetylaspartylglutamate (NAAG) inhibits intravenous cocaine self-administration and cocaine-enhanced brain-stimulation reward in rats. *Neuropharmacology* **58,** 304–313 (2010).

115. Lu, L., Uejima, J. L., Gray, S. M., Bossert, J. M. & Shaham, Y. Systemic and central amygdala injections of the mGluR(2/3) agonist LY379268 attenuate the expression of incubation of cocaine craving. *Biol. Psychiatry* **61,** 591–598 (2007).

116. Berkovic, S. F., Mulley, J. C., Scheffer, I. E. & Petrou, S. Human epilepsies: interaction of genetic and acquired factors. *Trends Neurosci.* **29,** 391–397 (2006).

117. Rothstein, J. D., DykesHoberg, M., Pardo, C. A., Bristol, L. A., Jin, L., Kuncl, R. W., Kanai, Y., Hediger, M. A., Wang, Y. F., Schielke, J. P. & Welty, D. F. Knockout of glutamate transporters reveals a major role for astroglial transport in excitotoxicity and clearance of glutamate. *Neuron* **16,** 675–686 (1996).

118. Annegers, J. F., Hauser, W. A., Coan, S. P. & Rocca, W. A. A population-based study of seizures after traumatic brain injuries. *N. Engl. J. Med.* **338,** 20–24 (1998).

119. Hauser, W. A. Seizure Disorders - the Changes with Age. *Epilepsia* **33,** S6–S14 (1992).

120. Brodie, M. J., Elder, A. T. & Kwan, P. Epilepsy in later life. *Lancet Neurol.* **8,** 1019–1030 (2009).

121. Costello, D. J. & Delanty, N. Oxidative injury in epilepsy: potential for antioxidant therapy? *Expert Rev. Neurother.* **4,** 541–553 (2004).

122. Witkin, J. M., Gasior, M., Schad, C., Zapata, A., Shippenberg, T., Hartman, T. & Slusher, B. S. NAALADase (GCP II) inhibition prevents cocaine-kindled seizures. *Neuropharmacology* **43,** 348–356 (2002).

123. Yamamoto, T., Hirasawa, S., Wroblewska, B., Grajkowska, E., Zhou, J., Kozikowski, A., Wroblewski, J. & Neale, J. H. Antinociceptive effects of N-acetylaspartylglutamate (NAAG) peptidase inhibitors ZJ-11, ZJ-17 and ZJ-43 in the rat formalin test and in the rat neuropathic pain model. *Eur. J. Neurosci.* **20,** 483–494 (2004).

124. Potter, M. C., Wozniak, K. M., Callizot, N. & Slusher, B. S. Glutamate Carboxypeptidase II Inhibition Behaviorally and Physiologically Improves Pyridoxine-Induced Neuropathy in Rats. *PLoS ONE* **9,** e102936 (2014).

125. Wozniak, K. M., Wu, Y., Vornov, J. J., Lapidus, R., Rais, R., Rojas, C., Tsukamoto, T. & Slusher, B. S. The Orally Active Glutamate Carboxypeptidase II Inhibitor E2072 Exhibits

Sustained Nerve Exposure and Attenuates Peripheral Neuropathy. *J. Pharmacol. Exp. Ther.* **343,** 746–754 (2012).

126. Muly, E. C., Mania, I., Guo, J. D. & Rainnie, D. G. Group II metabotropic glutamate receptors in anxiety circuitry: Correspondence of physiological response and subcellular distribution. *J. Comp. Neurol.* **505,** 682–700 (2007).

127. Jung, R. E., Haier, R. J., Yeo, R. A., Rowland, L. M., Petropoulos, H., Levine, A. S., Sibbitt, W. L. & Brooks, W. M. Sex differences in N-acetylaspartate correlates of general intelligence: An H-1-MRS study of normal human brain. *Neuroimage* **26,** 965–972 (2005).

128. Pfleiderer, B., Ohrmann, P., Suslow, T., Wolgast, M., Gerlach, A. L., Heindel, W. & Michael, N. N-acetylaspartate levels of left frontal cortex are associated with verbal intelligence in women but not in men: a proton magnetic resonance spectroscopy study. *Neuroscience* **123,** 1053–8 (2004).

129. Rahn, K. A., Watkins, C. C., Alt, J., Rais, R., Stathis, M., Grishkan, I., Crainiceau, C. M., Pomper, M. G., Rojas, C., Pletnikov, M. V., Calabresi, P. A., Brandt, J., Barker, P. B., Slusher, B. S. & Kaplin, A. I. Inhibition of Glutamate Carboxypeptidase II (GCPII) activity as a treatment for cognitive impairment in multiple sclerosis. *Proc. Natl. Acad. Sci.* **109,** 20101–20106 (2012).

130. Hollinger, K. R., Alt, J., Riehm, A. M., Slusher, B. S. & Kaplin, A. I. Dose-dependent inhibition of GCPII to prevent and treat cognitive impairment in the EAE model of multiple sclerosis. *Brain Res.* **1635,** 105–112 (2016).

131. Wolf, N. I., Willemsen, M. A. A. P., Engelke, U. F., van der Knaap, M. S., Pouwels, P. J. W., Harting, I., Zschocke, J., Sistermans, E. A., Rating, D. & Wevers, R. A. Severe hypomyelination associated with increased levels of N-acetylaspartylglutamate in CSF. *Neurology* **62,** 1503–1508 (2004).

132. Monn, J. A., Prieto, L., Taboada, L., Pedregal, C., Hao, J., Reinhard, M. R., Henry, S. S., Goldsmith, P. J., Beadle, C. D., Walton, L., Man, T., Rudyk, H., Clark, B., Tupper, D., Baker, S. R., Lamas, C., Montero, C., Marcos, A., Blanco, J., Bures, M., Clawson, D. K., Atwell, S., Lu,

F., Wang, J., Russell, M., Heinz, B. A., Wang, X., Carter, J. H., Xiang, C., Catlow, J. T., Swanson, S., Sanger, H., Broad, L. M., Johnson, M. P., Knopp, K. L., Simmons, R. M., Johnson, B. G., Shaw, D. B. & McKinzie, D. L. Synthesis and Pharmacological Characterization of C4-Disubstituted Analogs of 1S,2S,5R,6S-2-Aminobicyclo[3.1.0]hexane-2,6-dicarboxylate: Identification of a Potent, Selective Metabotropic Glutamate Receptor Agonist and Determination of Agonist-Bound Human mGlu2 and mGlu3 Amino Terminal Domain Structures. *J Med Chem* **58,** 1776–94 (2015).

133. Wright, G. L., Grob, B. M., Haley, C., Grossman, K., Newhall, K., Petrylak, D., Troyer, J., Konchuba, A., Schellhammer, P. F. & Moriarty, R. Upregulation of prostate-specific membrane antigen after androgen-deprivation therapy. *Urology* **48,** 326–334 (1996).

134. Labrie, F. Endocrine therapy for prostate cancer. *Endocrinol. Metab. Clin. North Am.* **20,** 845–72 (1992).

135. Afshar-Oromieh, A., Haberkorn, U., Schlemmer, H. P., Fenchel, M., Eder, M., Eisenhut, M., Hadaschik, B. A., Kopp-Schneider, A. & Rothke, M. Comparison of PET/CT and PET/MRI hybrid systems using a Ga-68-labelled PSMA ligand for the diagnosis of recurrent prostate cancer: initial experience. *Eur. J. Nucl. Med. Mol. Imaging* **41,** 887–897 (2014).

136. Afshar-Oromieh, A., Zechmann, C. M., Malcher, A., Eder, M., Eisenhut, M., Linhart, H. G., Holland-Letz, T., Hadaschik, B. A., Giesel, F. L., Debus, J. & Haberkorn, U. Comparison of PET imaging with a Ga-68-labelled PSMA ligand and F-18-choline-based PET/CT for the diagnosis of recurrent prostate cancer. *Eur. J. Nucl. Med. Mol. Imaging* **41,** 11–20 (2014).

137. Mease, R. C., Foss, C. A. & Pomper, M. G. PET Imaging in Prostate Cancer: Focus on Prostate-Specific Membrane Antigen. *Curr. Top. Med. Chem.* **13,** 951–962 (2013).

138. Barwe, S. P., Maul, R. S., Christiansen, J. J., Anilkumar, G., Cooper, C. R., Kohn, D. B. & Rajasekaran, A. K. Preferential association of prostate cancer cells expressing prostate specific membrane antigen to bone marrow matrix. *Int. J. Oncol.* **30,** 899–904 (2007).

139. Troyer, J. K., Feng, Q., Beckett, M. L. & Wright, G. L., Jr. Biochemical characterization and mapping of the 7E11-C5.3 epitope of the prostate-specific membrane antigen. *Urol Oncol* **1,** 29–37 (1995).

140. Silver, D. A., Pellicer, I., Fair, W. R., Heston, W. D. W. & CordonCardo, C. Prostate-specific membrane antigen expression in normal and malignant human tissues. *Clin. Cancer Res.* **3,** 81–85 (1997).

141. Conway, R. E., Petrovic, N., Li, Z., Heston, W., Wu, D. & Shapiro, L. H. Prostate-specific membrane antigen regulates angiogenesis by modulating integrin signal transduction. *Mol Cell Biol* **26,** 5310–24 (2006).

142. Devlin, A. M., Ling, E. H., Peerson, J. M., Fernando, S., Clarke, R., Smith, A. D. & Halsted, C. H. Glutamate carboxypeptidase II: a polymorphism associated with lower levels of serum folate and hyperhomocysteinemia. *Hum. Mol. Genet.* **9,** 2837–2844 (2000).

143. Vargas-Martinez, C., Ordovas, J. M., Wilson, P. W. & Selhub, J. The glutamate carboxypeptidase gene II (C>T) polymorphism does not affect folate status in the Framingham Offspring cohort. *J Nutr* **132,** 1176–9 (2002).

144. Chen, J., Kyte, C., Valcin, M., Chan, W., Wetmur, J. G., Selhub, J., Hunter, D. J. & Ma, J. Polymorphisms in the one-carbon metabolic pathway, plasma folate levels and colorectal cancer in a prospective study. *Int J Cancer* **110,** 617–20 (2004).

145. Devlin, A. M., Clarke, R., Birks, J., Evans, J. G. & Halsted, C. H. Interactions among polymorphisms in folate-metabolizing genes and serum total homocysteine concentrations in a healthy elderly population. *Am J Clin Nutr* **83,** 708–13 (2006).

146. Halsted, C. H., Wong, D. H., Peerson, J. M., Warden, C. H., Refsum, H., Smith, A. D., Nygard, O. K., Ueland, P. M., Vollset, S. E. & Tell, G. S. Relations of glutamate carboxypeptidase II (GCPII) polymorphisms to folate and homocysteine concentrations and to scores of cognition, anxiety, and depression in a homogeneous Norwegian population: the Hordaland Homocysteine Study. *Am J Clin Nutr* **86,** 514–21 (2007).

147. Ye, X., Lai, C.-Q., Crott, J. W., Troen, A. M., Ordovas, J. M. & Tucker, K. L. The Folate Hydrolase 1561C-T Polymorphism Is Associated With Depressive Symptoms in Puerto Rican Adults. *Psychosom. Med.* **73,** 385–392 (2011).

148. Tykvart, J., Barinka, C., Svoboda, M., Navratil, V., Soucek, R., Hubalek, M., Hradilek, M., Sacha, P., Lubkowski, J. & Konvalinka, J. Structural and Biochemical Characterization of a Novel Aminopeptidase from Human Intestine. *J Biol Chem* (2015). doi:10.1074/jbc.M114.628149

149. Whitaker, H. C., Shiong, L. L., Kay, J. D., Gronberg, H., Warren, A. Y., Seipel, A., Wiklund, F., Thomas, B., Wiklund, P., Miller, J. L., Menon, S., Ramos-Montoya, A., Vowler, S. L., Massie, C., Egevad, L. & Neal, D. E. N-acetyl-L-aspartyl-L-glutamate peptidase-like 2 is overexpressed in cancer and promotes a pro-migratory and pro-metastatic phenotype. *Oncogene* **33,** 5274–5287 (2014).

150. Knedlik, T., Navratil, V., Vik, V., Pacik, D., Sacha, P. & Konvalinka, J. Detection and quantitation of glutamate carboxypeptidase II in human blood. *Prostate* **74,** 768–780 (2014).

151. Bzdega, T., Crowe, S. L., Ramadan, E. R., Sciarretta, K. H., Olszewski, R. T., Ojeifo, O. A., Rafalski, V. A., Wroblewska, B. & Neale, J. H. The cloning and characterization of a second brain enzyme with NAAG peptidase activity. *J. Neurochem.* **89,** 627–635 (2004).

152. Pangalos, M. N., Neefs, J. M., Somers, M., Verhasselt, P., Bekkers, M., van der Helm, L., Fraiponts, E., Ashton, D. & Gordon, R. D. Isolation and expression of novel human glutamate carboxypeptidases with N-acetylated alpha-linked acidic dipeptidase and dipeptidyl peptidase IV activity. *J. Biol. Chem.* **274,** 8470–8483 (1999).

153. Hlouchova, K., Barinka, C., Konvalinka, J. & Lubkowski, J. Structural insight into the evolutionary and pharmacologic homology of glutamate carboxypeptidases II and III. *Febs J.* **276,** 4448–4462 (2009).

154. Bacich, D. J., Ramadan, E., O'Keefe, D. S., Bukhari, N., Wegorzewska, I., Ojeifo, O., Olszewski, R., Wrenn, C. C., Bzdega, T., Wroblewska, B., Heston, W. D. W. & Neale, J. H.

Deletion of the glutamate carboxypeptidase II gene in mice reveals a second enzyme activity that hydrolyzes N-acetylaspartylglutamate. *J. Neurochem.* **83,** 20–29 (2002).

155. Tykvart, J., Navratil, V., Sedlak, F., Corey, E., Colombatti, M., Fracasso, G., Koukolik, F., Barinka, C., Sacha, P. & Konvalinka, J. Comparative analysis of monoclonal antibodies against prostate-specific membrane antigen (PSMA). *Prostate* **74,** 1674–1690 (2014).

156. Dundas, J., Ouyang, Z., Tseng, J., Binkowski, A., Turpaz, Y. & Liang, J. CASTp: computed atlas of surface topography of proteins with structural and topographical mapping of functionally annotated residues. *Nucleic Acids Res.* **34,** W116–W118 (2006).

157. Chovancova, E., Pavelka, A., Benes, P., Strnad, O., Brezovsky, J., Kozlikova, B., Gora, A., Sustr, V., Klvana, M., Medek, P., Biedermannova, L., Sochor, J. & Damborsky, J. CAVER 3.0: A Tool for the Analysis of Transport Pathways in Dynamic Protein Structures. *PLoS Comput. Biol.* **8,** (2012).

158. Dodson, E. J., Winn, M. & Ralph, A. Collaborative Computational Project, number 4: providing programs for protein crystallography. *Methods Enzym.* **277,** 620–33 (1997).

159. Bailey, S. The Ccp4 Suite - Programs for Protein Crystallography. *Acta Crystallogr. Sect. - Biol. Crystallogr.* **50,** 760–763 (1994).

160. Winn, M. D., Ballard, C. C., Cowtan, K. D., Dodson, E. J., Emsley, P., Evans, P. R., Keegan, R. M., Krissinel, E. B., Leslie, A. G. W., McCoy, A., McNicholas, S. J., Murshudov, G. N., Pannu, N. S., Potterton, E. A., Powell, H. R., Read, R. J., Vagin, A. & Wilson, K. S. Overview of the CCP4 suite and current developments. *Acta Crystallogr. D Biol. Crystallogr.* **67,** 235–242 (2011).

161. Ryde, U. & Olsson, M. H. M. Structure, strain, and reorganization energy of blue copper models in the protein. *Int. J. Quantum Chem.* **81,** 335–347 (2001).

162. Vagin, A. & Teplyakov, A. An approach to multi-copy search in molecular replacement. *Acta Crystallogr. D Biol. Crystallogr.* **56,** 1622–1624 (2000).

163. McCoy, A. J., Grosse-Kunstleve, R. W., Adams, P. D., Winn, M. D., Storoni, L. C. & Read, R. J. Phaser crystallographic software. *J Appl Crystallogr* **40,** 658–674 (2007).

164. Adams, P. D., Afonine, P. V., Bunkoczi, G., Chen, V. B., Davis, I. W., Echols, N., Headd, J. J., Hung, L. W., Kapral, G. J., Grosse-Kunstleve, R. W., McCoy, A. J., Moriarty, N. W., Oeffner, R., Read, R. J., Richardson, D. C., Richardson, J. S., Terwilliger, T. C. & Zwart, P. H. PHENIX: a comprehensive Python-based system for macromolecular structure solution. *Acta Crystallogr Biol Crystallogr* **66,** 213–21 (2010).

165. Murshudov, G. N., Vagin, A. A. & Dodson, E. J. Refinement of macromolecular structures by the maximum-likelihood method. *Acta Crystallogr Biol Crystallogr* **53,** 240–55 (1997).

166. Murshudov, G. N., Skubak, P., Lebedev, A. A., Pannu, N. S., Steiner, R. A., Nicholls, R. A., Winn, M. D., Long, F. & Vagin, A. A. REFMAC5 for the refinement of macromolecular crystal structures. *Acta Crystallogr Biol Crystallogr* **67,** 355–67 (2011).

167. Ahlrichs, R., Bär, M., Häser, M., Horn, H. & Kölmel, C. Electronic structure calculations on workstation computers: The program system turbomole. *Chem. Phys. Lett.* **162,** 165–169 (1989).

168. Emsley, P., Lohkamp, B., Scott, W. G. & Cowtan, K. Features and development of Coot. *Acta Crystallogr. D Biol. Crystallogr.* **66,** 486–501 (2010).

169. Kabsch, W. Xds. *Acta Crystallogr Biol Crystallogr* **66,** 125–132 (2010).

170. Krug, M., Weiss, M. S., Heinemann, U. & Mueller, U. XDSAPP: a graphical user interface for the convenient processing of diffraction data using XDS. *J. Appl. Crystallogr.* **45,** 568–572 (2012).

171. Sambrook, J. & Russell, D. W. *Molecular Cloning: A Laboratory Manual*. (Cold Spring Harbor Laboratory Press, 2001).

172. Sanger, F., Nicklen, S. & Coulson, A. R. DNA sequencing with chain-terminating inhibitors. *Proc. Natl. Acad. Sci.* **74,** 5463–5467 (1977).

173. Laemmli, U. K. Cleavage of Structural Proteins during the Assembly of the Head of Bacteriophage T4. *Nature* **227,** 680–685 (1970).

174. Navratil, M., Ptacek, J., Sacha, P., Starkova, J., Lubkowski, J., Barinka, C. & Konvalinka, J. Structural and biochemical characterization of the folyl-poly-gamma-L-glutamate hydrolyzing activity of human glutamate carboxypeptidase II. *Febs J* **281,** 3228–3242 (2014).

175. Ericsson, U. B., Hallberg, B. M., DeTitta, G. T., Dekker, N. & Nordlund, P. Thermofluor-based high-throughput stability optimization of proteins for structural studies. *Anal. Biochem.* **357,** 289–298 (2006).

176. Niesen, F. H., Berglund, H. & Vedadi, M. The use of differential scanning fluorimetry to detect ligand interactions that promote protein stability. *Nat. Protoc.* **2,** 2212–2221 (2007).

177. Plechanovova, A., Byun, Y., Alquicer, G., Skultetyova, L., Mlcochova, P., Nemcova, A., Kim, H. J., Navratil, M., Mease, R., Lubkowski, J., Pomper, M., Konvalinka, J., Rulisek, L. & Barinka, C. Novel Substrate-Based Inhibitors of Human Glutamate Carboxypeptidase II with Enhanced Lipophilicity. *J. Med. Chem.* **54,** 7535–7546 (2011).

178. Kelleher, S. L., McCormick, N. H., Velasquez, V. & Lopez, V. Zinc in specialized secretory tissues: roles in the pancreas, prostate, and mammary gland. *Adv Nutr* **2,** 101–11 (2011).

179. Magneson, G. R., Puvathingal, J. M. & Ray, W. J. The concentrations of free Mg2+ and free Zn2+ in equine blood plasma. *J. Biol. Chem.* **262,** 11140–11148 (1987).

180. Costello, L. C. & Franklin, R. B. Novel role of zinc in the regulation of prostate citrate metabolism and its implications in prostate cancer. *Prostate* **35,** 285–296 (1998).

181. Hamada-Kanazawa, M., Kouda, M., Odani, A., Matsuyama, K., Kanazawa, K., Hasegawa, T., Narahara, M. & Miyake, M. beta-Citryl-L-glutamate Is an Endogenous Iron Chelator That Occurs Naturally in the Developing Brain. *Biol. Pharm. Bull.* **33,** 729–737 (2010).

182. Hamada-Kanazawa, M., Narahara, M., Takano, M., Min, K. S., Tanaka, K. & Miyake, M. beta-Citryl-L-glutamate Acts as an Iron Carrier to Activate Aconitase Activity. *Biol. Pharm. Bull.* **34,** 1455–1464 (2011).

183. Stohs, S. J. & Bagchi, D. Oxidative Mechanisms in the Toxicity of Metal-Ions. *Free Radic. Biol. Med.* **18,** 321–336 (1995).

184. Miyake, M., Kume, S. & Kakimoto, Y. Correlation of the level of beta-citryl-L-glutamic acid with spermatogenesis in rat testes. *Biochim Biophys Acta* **719,** 495–500 (1982).

185. Miyake, M. & Kakimoto, Y. Developmental-Changes of N-Acetyl-L-Aspartic Acid, N-Acetyl-Alpha-Aspartylglutamic Acid and Beta-Citryl-L-Glutamic Acid in Different Brain-Regions and Spinal Cords of Rat and Guinea Pig. *J. Neurochem.* **37,** 1064–1067 (1981).

186. Konetschnyrapp, S., Jung, G., Meiwes, J. & Zahner, H. Staphyloferrin-a - a Structurally New Siderophore from Staphylococci. *Eur. J. Biochem.* **191,** 65–74 (1990).

187. Drechsel, H., Metzger, J., Freund, S., Jung, G., Boelaert, J. R. & Winkelmann, G. Rhizoferrin - a Novel Siderophore from the Fungus Rhizopus-Microsporus Var Rhizopodiformis. *Biol. Met.* **4,** 238–243 (1991).

188. Raymond, K. N., Dertz, E. A. & Kim, S. S. Enterobactin: An archetype for microbial iron transport. *Proc. Natl. Acad. Sci. U. S. A.* **100,** 3584–3588 (2003).

189. Frederickson, C. J., Suh, S. W., Silva, D., Frederickson, C. J. & Thompson, R. B. Importance of zinc in the central nervous system: The zinc-containing neuron. *J. Nutr.* **130,** 1471s–1483s (2000).

190. Šácha, P., Knedlík, T., Schimer, J., Tykvart, J., Parolek, J., Navrátil, V., Dvořáková, P., Sedlák, F., Ulbrich, K., Strohalm, J., Majer, P., Šubr, V. & Konvalinka, J. iBodies: Modular Synthetic Antibody Mimetics Based on Hydrophilic Polymers Decorated with Functional Moieties. *Angew. Chem. Int. Ed.* **55,** 2356–2360 (2016).

# PROHLÁŠENÍ

Prohlašuji, že jsem tuto práci ani její podstatnou část nepředložila k získání jiného nebo stejného akademického titulu.

_____

Michal Navrátil

V _____ dne _____